

Alma Mater Studiorum – Università di Bologna

**DOTTORATO DI RICERCA IN
Scienze Farmaceutiche**

Ciclo XXIV

Settore Concorsuale di afferenza: 03/D1

Settore Scientifico disciplinare: CHIM/08

TITOLO TESI

**Small Molecules as Modulators of Different Targets Involved
in Tumor Progression**

Presentata da: Claudia Ferroni

Coordinatore Dottorato

Prof. Maurizio Recanatini

Relatore

Prof.ssa Alessandra Bisi

Co-Relatore

Dott.ssa Greta Varchi

Esame finale anno 2012

Index

SECTION A: CHALCONES AS POTENTIAL Hsp90 INHIBITORS IN CANCER THERAPY

1. Introduction	2
1.1. Flavonoids	2
1.1.1. Nomenclature and Classification	3
1.1.2. Biochemical and Pharmacological Effects	5
1.1.2.1. Antioxidant Effect	6
1.1.2.2. Antiatherosclerotic Effect	7
1.1.2.3. Antiulcer and Hepatoprotective Effects	7
1.1.2.4. Antimicrobial Effect	7
1.1.2.5. Anti-Inflammatory Effect	8
1.1.2.6. Effect on Blood Vessel	8
1.1.2.7. Antineoplastic Effect	8
1.1.2.8. Effect on Heat Shock Proteins	8
1.2. Chalcones	9
1.2.1. Biochemical and Pharmacological Effects	9
1.2.1.1. Chemoprotective Effect	9
1.2.1.2. Anti-Inflammatory Effect	11
1.2.1.3. Hypoglycemic Effect	12
1.2.1.4. Cytotoxic Effect	13
1.2.1.5. Antihepatotoxic Effect	13
1.2.1.6. Antimicrobial Effect	13
1.2.1.7. Antimalarial Effect	14
1.2.1.8. Antileishmanial Effect	14
1.2.1.9. Anti-Trypanosoma Cruzi Effect	15
1.2.2. Synthesis of Chalcones	15
1.2.2.1. The Claisen-Schmidt Reaction	15
1.2.2.2. The Suzuki Reaction	16
1.2.2.3. Synthesis of Chalcone via Ultrasound and Microwave-Assisted Methods	16
1.2.3. Physico-Chemical Properties of Chalcone	17
1.3. Heat Shock Proteins	19
1.3.1. Hsp90	19
1.3.1.1. Hsp90 Folding Mechanism	21
1.3.2. Hsp90-Dependent Client Proteins	23

1.3.3.	The Hallmarks of Cancer	24
1.3.3.1.	Self-Sufficiency in Growth Signals	26
1.3.3.2.	Insensitivity to Growth-Inhibitory (Antigrowth) Signals	26
1.3.3.3.	Evasion of Programmed Cell Death (Apoptosis)	27
1.3.3.4.	Limitless Replicative Potential	28
1.3.3.5.	Sustained Angiogenesis	28
1.3.3.6.	Tissue Invasion and Metastasis	29
1.3.4.	Hsp90 Inhibitors	29
1.3.4.1.	Inhibitors of the N-terminal ATP Binding Domain	30
1.3.4.2.	Other Hsp90 Inhibitors	37
2.	Aim of the Thesis	41
3.	Results Discussion and Conclusion	45
3.1.	Drugs and Treatment Conditions	45
3.1.1.	Antiproliferative Assay	45
3.1.2.	Western Blot Analysis	46
3.2.	Results and Conclusion	46
3.2.1.	Antiproliferative Assay	46
3.2.2.	Western Blot Analysis	49
4.	Experimental Section	51
4.1.	Acetophenones Synthesis	51
4.2.	Aldehydes Synthesis	52
4.3.	Aldol Condensation	52
4.4.	Cyclisation	52
4.5.	Experimental Section	53
4.5.1.	Acetylation	53
4.5.2.	Fries Rearrangement	54
4.5.3.	Chlorination	54
4.5.4.	Radical Bromination	55
4.5.5.	Amination	56
4.5.6.	Reduction of Nitrile to Aldehyde	58
4.5.7.	Aldehyde protection	60
4.5.8.	Reduction of Nitrile to Amine	61
4.5.9.	Coupling with Sulfone	63
4.5.10.	Aldehyde Deprotection	65
4.5.11.	4-Chloro-2-Hydroxybenzaldehyde Synthesis	67
4.5.12.	Williamson Reaction	67
4.5.13.	Aldol Condensation	70
4.5.14.	Cyclisation	85
5.	References	86

SECTION B: SYNTHESIS OF A NEW CLASS OF POTENTIAL NON- STEROIDAL ANTIANDROGENS

1. Introduction	96
1.1. The Androgen Receptor (AR)	96
1.1.1. Structure and Function of AR	96
1.1.2. Mechanism of AR Action	98
1.2. Androgens: Testosterone Biosynthesis	99
1.3. Prostate Cancer	101
1.3.1. Pathophysiology	102
1.3.2. The Development of Androgen-Independent Prostate Cancer (AIPC)	103
1.3.2.1. Hypersensitive Pathway	104
1.3.2.2. Promiscuous Pathway	105
1.3.2.3. Outlaw Pathway	105
1.3.2.4. Bypass Pathway	105
1.3.2.5. Lurker Cell Pathway	106
1.3.3. Treatment of Prostate Cancer	106
1.4. Antiandrogens	108
1.4.1. Nonsteroidal Antiandrogens	109
1.4.2. Mechanism of AR Antagonism by Bicalutamide	112
1.4.3. A New Generation of Antiandrogens: Diarylthiohydantoins	113
1.5. SARMs: Selective Androgen Receptor Modulators	116
2. Aim of the Thesis	119
3. Result Discussion and Conclusion	122
3.1. Quantitative Real-Time Reverse Transcription-Polymerase Chain Reaction	122
4. Experimental Section	126
4.1. Schemes of Reaction	126
4.2. Experimental Section	128
4.2.1. Corey-Fucks Reaction	128
4.2.2. Williamson Reaction	131
4.2.3. Click Chemistry	135
4.2.4. Direct Functionalization of 1,4-Triazoles at the 5-Position	143
4.2.5. Oxidation of Sulfur to Sulfone	144
4.2.6. Microwave-Assisted Click Chemistry	145
4.2.7. Click Chemistry with CuI	147
4.2.8. Deprotection of Methyl Ester	148

4.2.9. Coupling	150
4.2.10. Mitsunobu Reaction	153
5. References	156

*SECTION A: CHALCONES AS
POTENTIAL HSP90 INHIBITORS
IN CANCER THERAPY*

1. Introduction

1.1. Flavonoids

Flavonoids are an extensive group of about 6000 naturally occurring compounds that are ubiquitous in all vascular plants and important constituents of the

human diet. On the average the daily diet contains approximately 1 g of different flavonoids but the uptake of specific compounds may vary greatly depending on the food source.^{1,2} They contribute to the brilliant shades of blue, scarlet and orange in leaves, flowers and fruits.³



Fig. 1. Flavonoids in fruits

These polyphenolic compounds are found in fruits, vegetables, olive oil, nuts, seeds, nuts, grains, spices as well as in beverages like red wine, green tea, coffee and beer.

More specifically, flavones are common in cereal grains and aromatic herbs (parsley, rosemary, thyme), while their hydrogenated analogues are almost exclusively present in citrus fruits.^{3,4} The flavonols quercetin and kaempferol are predominant in vegetables and fruits, where they are found mainly in the skin, with the exception of onions. Isoflavones are found most often in legumes, including soybeans, black beans, green beans, and chickpeas. Alfalfa and clover

sprouts and sunflower seeds also contain isoflavones. The flavan-3-ols and their gallate esters are widely distributed in plants, although they are very rich in tealeaves. Flavan oligomers (proanthocyanidins) are present in apples, grapes, berries, persimmon, black currant, and sorghum and barley grains.⁵ Anthocyanidins and their glycosides (anthocyanins) are natural pigments and are abundant in berries and red grape.³

1.1.1. Nomenclature and Classification

The term “flavonoid” is generally used to describe a class of the polyphenols, which are characterized as containing two or more aromatics rings, each bearing at least one aromatic hydroxyl and connected with a carbon bridge.⁶ This class includes a C₆-C₃-C₆ carbon framework, composed of a chroman (C₆-C₃) nucleus (the benzo ring A and the heterocyclic ring C), with a phenyl (the aromatic ring B) substitution usually at the 2-position. Depending on the position of the linkage of the aromatic ring to the chromano moiety, this group of natural products may be divided into three classes:

- Flavonoids (2-phenylbenzopyrans) **1** (Fig. 2).
- Isoflavonoids (3-benzopyrans) **2** (Fig. 2).
- Neoflavonoids (4-benzopyrans) **3** (Fig. 2).

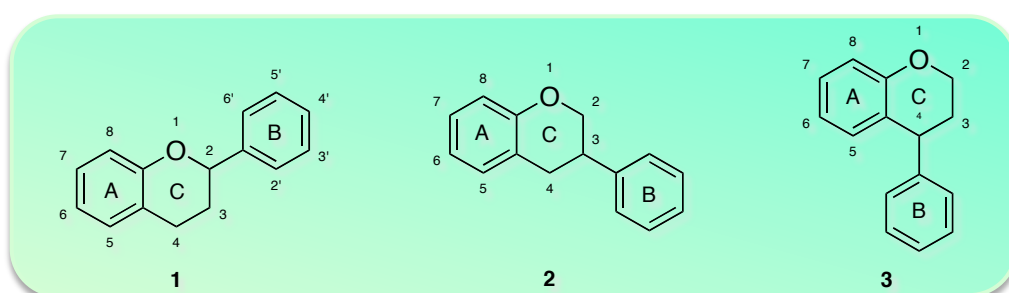


Fig. 2. Flavonoids structure

These groups usually share a common chalcone precursor, (Fig. 3) which is the basic skeleton and therefore are biogenetically and structurally related.⁷

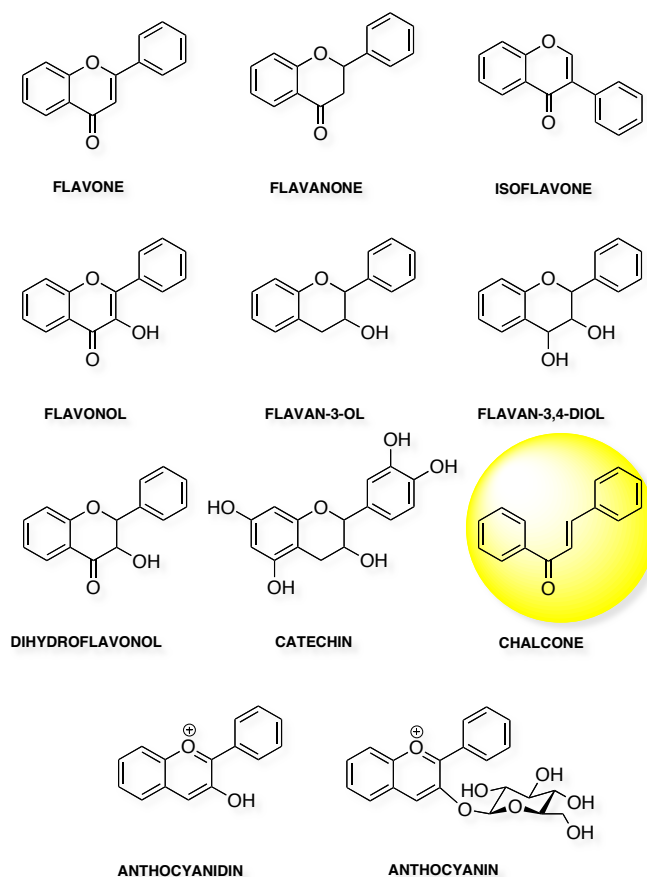


Fig. 3. The main classes of flavonoids

The biological activities of flavonoids and their metabolites depend on their chemical structure and relative orientation of various moieties on the molecule.⁸ The basic structure of the flavonoid nucleus allows for a multitude of substitution patterns in the A, B, and C rings, resulting in various subgroups. The flavonoids are further divided into subclasses according to their oxidation level on the C-ring, placement of the B ring, hydroxylation patterns, and C-glycosylation of the carbon skeleton.^{9,10} They include anthocyanidins, flavanols (catechins), flavones, flavonols, flavanones and Isoflavonoids among others (Fig. 3). Flavones and flavonols have been identified in almost all plants, the ones found most frequently being those with B-ring hydroxylation in the C-3 and C-4 positions.¹¹

In plants, they are relatively resistant to heat, oxygen, dryness, and moderate degrees of acidity but can be modified by light.¹¹ Photostability of the flavonoid molecule depends on the nature of the hydroxyl group attached to C-3 of ring C.

The absence or glycosylation of this hydroxyl group results in high photostability of the molecule.¹²

Most flavonoids are present in nature as glycosides and other conjugates (flavanols are an exception), which contribute to their complexity and the large number of individual molecules that have been identified (>5000).¹³

Many flavonoids in foods are polymerized into large molecules, which are called tannins. There are several subclasses of tannins, three of which are important to foods and perhaps health.¹⁴

Condensed tannins or proanthocyanidins consist of monomeric units of flavans linked through carbon-carbon and ether linkages. Tannins can range from dimers through large polymers and are found in a wide variety of foods, e.g., apples, berries, chocolate, red wines and nuts.⁶

The derived tannins are formed primarily under oxidative enzymatic and atmospheric conditions during the manipulation of plants and subsequent processing into foods, e.g., oolong and black teas, red wines and coffee.¹⁴

Another class of common food tannins is the hydrolysable tannins, which consist of gallic acid or ellagic acid to which are linked to a non aromatic polyol, such as a sugar or quinic acid, is esterified.¹⁵ Although hydrolysable tannins are widespread in some plant foods, e.g., grapes and wines, and contribute important organoleptic qualities, they have received little attention in terms of their impact on human health.⁶

1.1.2. Biochemical and Pharmacological Effects

Flavonoids play different roles in the ecology of plants. Due to their attractive colors, flavones, flavonols, and anthocyanidins may act as visual signals for pollinating insects.³ Because of their astringency, catechins and other flavanols can represent a defense system against insects harmful to the plant.¹⁶ Flavonoids act as catalysts in the light phase of photosynthesis and/or as regulators of iron channels involved in phosphorylation.¹⁷ They can also function as stress protectants in plant cells by scavenging ROS produced by the photosynthetic electron transport system.¹⁸ Furthermore, because of their favorable UV-absorbing properties, flavonoids protect plants from UV radiation of sun and

scavenge UV-generated ROS.^{3,19}

Flavonoids are important components in the human diet and they are capable of modulating the activity of many enzymes and possess a remarkable spectrum of biochemical and pharmacological activities, some of which interfere with control processes in carcinogenesis.^{1,20,21} These include anti-inflammatory (against ulcers, viruses, inflammation, arthritis, osteoporosis and diarrhea) and antioxidant activities,^{22,23} the scavenging effect on activated carcinogens and mutagens,²⁴ the action on cell cycle progression²⁵ and altered gene expression.¹

1.1.2.1. Antioxidant Effect

The best-described and most useful property of almost every group of flavonoids is their capacity to act as antioxidants. The flavones and catechins seem to be the most powerful flavonoids for protecting the body against reactive oxygen species (ROS). Free radicals, including the superoxide radical ($O_2^{\cdot-}$), hydroxyl radical ($\cdot OH$), hydrogen peroxide (H_2O_2), and lipid peroxide radicals have been implicated in a number of disease process, since they can attack lipids in cell membranes, proteins in tissues or enzymes, carbohydrates, and DNA, to induce oxidations, which cause membrane damage, protein modification (including enzymes), and DNA damage. This oxidative damage is considered to play a causative role in aging and several degenerative diseases associated with it, such as cardiovascular disease, cataracts, macular degeneration, cognitive dysfunction, cancer, asthma, diabetes, gastrointestinal and liver inflammatory diseases.^{26, 27}

Flavonoids can prevent injury caused by free radicals in various ways. One way is the direct scavenging of free radicals. Flavonoids are oxidized by radicals, resulting in a more stable, less-reactive radical, according to the following reaction.³



Where FOH is flavonoid and R' is free radical and FO' is less reactive free radical.²⁸

1.1.2.2. Antiatherosclerotic Effect

Physiological function of plant polyphenols has attracted much attention in relation to the prevention of vascular diseases. Flavonoids containing diphenylpropane structure are major polyphenols present in vegetables and fruits.²⁹ In 1936, Szent-Gyorgi³⁰ first claimed that citrus flavonoids (hesperidin and rutin) reduced capillary fragility and permeability in human blood vessel, as similarly to vitamin C. In 1993, Hertog *et al*³¹ found that flavonoid intake was inversely correlated with cardiovascular heart disease (CHD) mortality in elderly men. Nowadays, epidemiological studies strongly suggest that the intake of flavonoids from diet is helpful in the prevention of atherosclerosis and its related events including CHD.²⁸ Oxidative modification of low-density lipoproteins (LDL) is believed to be an initial step for the development of atherosclerosis and coronary disease. Flavonoids seem to exert the antioxidant effect against LDL oxidation.²⁹

1.1.2.3. Antiulcer and Hepatoprotective Effects

Many flavonoids possess antiulcerogenic activity. Oral treatment with the ether fraction of the flavonoid extract demonstrated a good level of gastric protection. Quercetin, kaempferol, rutin produced an inhibitory effect on intestinal functions, and that their actions are mediated through α_2 -adrenergic and calcium systems. This result may show the beneficial effects in diarrhea (cocoa beans) and other intestinal secretions.³² Besides, many flavonoids possess hepatoprotective activity through normalizing cell phospholipid synthesis.

1.1.2.4. Antimicrobial Effect

Flavonoids and esters of phenolic acids show antibacterial, antifungal and anti viral effects against herpes simplex virus, respiratory syncytial virus, parainfluenza virus, adenovirus and immuno-deficiency virus infection.³²

1.1.2.5. Anti-Inflammatory Effect

Many flavonoids can inhibit the cyclooxygenase pathway. This inhibition reduces the release of arachidonic acid, the starting point for a general inflammatory response.²⁸

1.1.2.6. Effect on Blood Vessel

Flavonoids are used for treatment of capillary fragility and phleboscrosis. They reduce cell aggregation and protect capillary against various traumas and stresses.³²

1.1.2.7. Antineoplastic Effect

Quite number of flavonoids has exhibited antineoplastic activity. Detailed studies have revealed that quercetin exerted a dose dependent inhibition of cell growth and colony formation.³²

1.1.2.8. Effect on Heat Shock Proteins

Heat shock proteins function as molecular chaperones, guiding the transport, assembly and degradation of intracellular polypeptides. Under the influence of non-physiological conditions heat shock protein synthesis is accelerated to aid cell survival. Elevated expression of the members of the hsp70 family has been reported in high-grade malignant tumors.³² Quercetin and several other flavonoids inhibit the synthesis of hsps including hsp90, hsp70s, hsp47 and hsp28 induced by heat shock, sodium arsenite, and L-azetidine 2-carboxylic acid (Azc) in human cell lines.³³

1.2. Chalcones

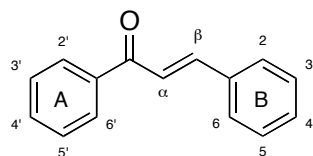


Fig. 4. Chalcone

Chalcones are 1,3-diphenyl-2-propene-1-one, in which two aromatic rings are linked by a three-carbon α , β -unsaturated carbonyl system (Fig. 4), that assume linear or near planar structure.

They possess conjugated double bonds and a completely delocalize π -electron system on both benzene rings.²⁷

Chalcones are readily synthesized in the laboratory and the literature is replete with references to structural modifications of the chalcone template. Some examples are introducing different substituents on the phenyl rings A and B, replacing the phenyl rings with heterocyclic and polyaromatic rings, saturation or substitution of the enone linking the two rings, and cyclisation of the chalcone to give conformationally restricted analogues.³⁴

In the plant arena, chalcones play a pigmentation role due to their intense yellow color. The biological activities of chalcones are equally wide ranging.

1.2.1. Biochemical and Pharmacological Effects

1.2.1.1. Chemoprotective Effect

Chemoprotection is an approach that seeks to arrest or reverse the process of carcinogenesis through the use of pharmacological agents. It may occur by various mechanism, such as inhibition of an enzyme involved in carcinogenesis (for example COX-2), inhibition of receptors that play an integrative role in modulating the activity of other receptors, induction of phase 2 enzymes like glutathione S-transferase, and scavenging of reactive oxygen species.

Chalcone bear a structural similarity to stilbene, a synthon found in several selective estrogen receptor modulators, to curcumin, a naturally occurring antioxidant and chemoprotective agent, as well as in antioxidant flavonoids like quercetin (Fig. 5).³⁴

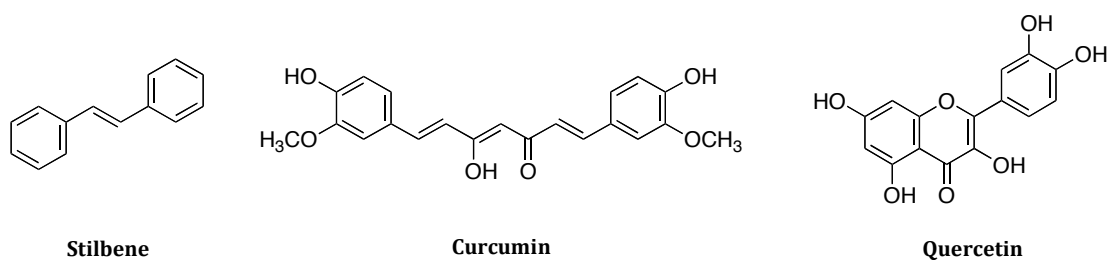


Fig. 5. Chemoprotective agents

The chemoprotective role of chalcones is usually discussed in term of their antioxidant properties that are related to different mechanisms:

- Free radical scavenging;
- Hydrogen donation singlet oxygen quenching;
- Metal ion chelation;
- Acting as substrate for free radicals.

Cytotoxic effects of antioxidant chalcones are associated with their pro-oxidant effects. Especially, the hydroxyl substituent is one of the key groups to enhance greatly the antioxidant activity of chalcone mainly due to its easy conversion to phenoxy radicals through the hydrogen atom transfer mechanism. The ortho- (i.e. catechol structure) and para-dihydroxylated benzene ring system are generally known to delocalize electrons, while meta-dihydroxylated ring is converted to unstable quinone structure (Fig. 6).²⁷

Structure Activity Relationship:

- Two hydroxyl groups on ring B are very important structural factors for the radical scavenging activity:
- 2',3'-, 3',4'- (ortho-) and 2',5'- (para) substitutions show an excellent antioxidant activities (as ascorbic acid and α -tocopherol);
- 2',4'- and 3',5'- (meta) substitutions show a very dramatic decrease in activity.

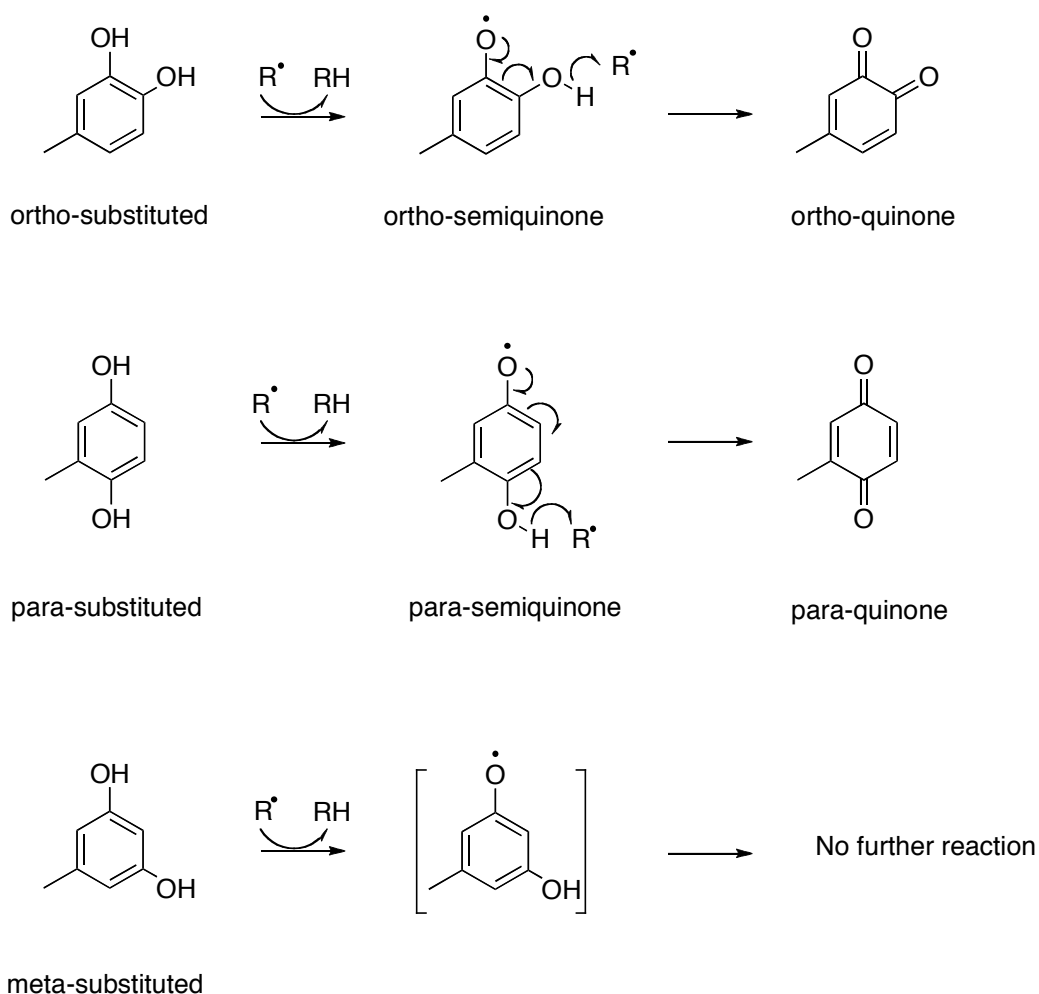


Fig. 6. Mechanism of antioxidant activity of chalcones

1.2.1.2. Anti-Inflammatory Effect

Non-steroidal anti-inflammatory drugs (NSAIDs) are therapeutically important in the treatment of rheumatic arthritis and various types of inflammatory conditions but found to be limited because of their frequently observed gastrointestinal side effects.

Being a natural origin, chalcones may be devoid of toxicity and hence beneficial for drug discovery as active compound.

Macrophages are active secretory cells, releasing nitric oxide (NO), which plays an important role in biologic activity. NO is a potent vasodilator, responsible for induction of cell growth, cytotoxicity, formation of edema leukocyte migration and cytokines production.³⁶ Thus, through their abundance, distribution, motility, and responsiveness, macrophages can influence almost every aspect of

immune and inflammatory responses.³⁷

NO reacts with a very high rate constant with superoxide radicals to give peroxynitrite. It can be directly cytotoxic and it can also decompose to give a range of products, including hydroxyl radical (OH·) and nitronium ion (NO₂⁺). Addition of peroxynitrite to biological fluids leads to nitration of aromatic aminoacid residues, and the presence of these may be a 'marker' of peroxynitrite mediated damage in vivo.³⁸

Compounds that inhibit excess production of NO by macrophages might be of benefit for the prevention and the treatment of autoimmune diseases, septic shock and different inflammatory pathologies.²⁷

From the structure–activity study, the following trends can be deduced: the trimethoxychalcone derivatives with a fluoro substituent at position C-4' were found to be better inhibitors of nitrite production than with a trifluoromethyl substituent at the same position. The presence of a trifluoromethyl group at C- 2, in dimethoxychalcone as well as in trimethoxy- chalcone derivatives, is associated with a very potent inhibition of nitrite accumulation.³⁶

Anti-inflammatory activity of 3,4,5-trimethoxychalcones is also evaluated in terms of TNF-α and IL-6 inhibitory activity.

Interestingly, several studies have demonstrated endogenous TNF-α as a tumor promoter and metastatic factor. Significant levels of TNF-α are found in tumor microenvironment of various human cancers, including those of breast, ovarian, prostate, lymphoma, melanoma and leukemia. Chalcones have dual activity as anti-inflammatory as well as more effective against cancer treatment since, it can act by two mechanisms, directly by killing tumor cells and indirectly, resolving the inflammatory environment that supports tumor development.³⁵

1.2.1.3. Hypoglycemic Effect

Non-insulin dependent diabetes mellitus (NIDDM, type-II diabetes) is a chronic metabolic disease characterizes by insulin resistance, hyperglycemia and hyperinsulinaemia.²⁷ This chronic disease is often associated with obesity, dyslipidemia, hypertension and cardiovascular risk.

Chalcones with dimethoxy and methylenedioxy groups show an important

antihyperglycemic activity. They seem to inhibit enzymes like protein tyrosine phosphatase 1B and aldose reductase, that are involved in glucose metabolism.³⁹

1.2.1.4. Cytotoxic Effect

Most of the chalcones exhibit cytotoxic activity against a variety of human cancer cell line (PC-3, MCF-7, KB and KB-VIN) in the low micromolar range. Mannich bases analogues with morpholine substitution at C₃ or C₅ and pyridyl or phenyl at C₂ substitution are found to possess good cytotoxic effect.⁴⁰

A greater effort has been made to understand how chalcones exert their effects: they can be angiogenesis inhibitors: the formation of new blood vessels from endothelial cells is a prerequisite for solid tumor growth and proliferation. Chalcones can also interfere at the transcription level by inhibiting the p-53-MDM2 interaction. The MDM2 oncogene is over-expressed in human breast cancer. It inhibits the tumor suppressor protein p53 by binding the transactivation site, leading to disregulation of the cell cycle. Many 2'-hydroxychalcones induce G2/M block and caused fragmentation of DNA that is suggestive of apoptosis.

A large number of methoxylated chalcones shows antimitotic activity against a variety of tumor cell line, in fact they interact strongly with tubulin, preventing it from polymerizing into microtubules.

Conformational restraint of chalcones generally lead to a decrease in cytotoxic activity.³⁴

1.2.1.5. Antihepatotoxic Effect

Chalcone derivatives possessing 1,4-dioxane ring system exhibit a good antihepatotoxic activity.²⁷

1.2.1.6. Antimicrobial Effect

Chalcone derivatives possessing electron releasing groups, like methoxy and hydroxy, show antibacterial activity, while compounds with dichloro and fluoro

groups show better antifungal activity.²⁷

1.2.1.7. Antimalarial Effect

Over 1,000,000 people die annually due to malaria, typically young children of resource-poor families in Africa. Increased mortality has partly been attributed to the emergence of chloroquine-resistant strains of *Plasmodium falciparum*. Chalcone derivatives interact with parasite enzyme cysteine protease, one of the key enzymes involved in hemoglobin degradation within the acid food vacuole of the intra-erythrocytic parasite. Inhibition of this enzyme proves fatal for the parasite.⁴¹

For antimalarial activity, the size characteristics of ring B (large, alkoxyated) and the electronic characteristic of ring A (electron deficient) are important.⁴² Compound containing triazole and chloro substituents, was found to be the most potent antiplasmodial derivative evaluated, suggesting that small lipophilic groups containing single or multiple nitrogen can enhance antimalarial activity in vitro.²⁷

1.2.1.8. Antileishmanial Effect

The antileishmanial activity of several chalcones has been reported in the literature. The most promising member to date is licochalcone A (Fig. 7), an oxygenated chalcone, isolated from the roots of Chinese liquorice, that inhibits fumarate reductase.⁴²

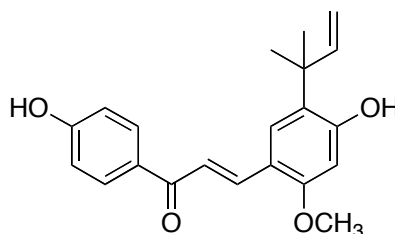


Fig. 7. Licochalcone A

Conventional structure activity relationships show that antileishmanial activity is favoured by chalcones with more hydrophilic character, with the most active

members found among 4'-hydroxychalcones.²⁷

1.2.1.9. Anti-Trypanosoma Cruzi Effect

Chagas' disease or American trypanosomiasis, caused by the vector-borne flagellate protozoan parasite *Trypanosoma Cruzi*, is an endemic tropical disease that has infected 20 million people in Central and South America and approximately between 50000 and 100000 people in the United States. Responsible for around 20000 deaths per year, Chagas' disease manifests itself as potentially fatal cardiopathy or dilations in the digestive tract. The only control intervention is chemotherapy. The antiprotozoal activity, the low toxicity and the economical, facile, and rapid synthesis of chalcones make them attractive as potential drug candidates to fight Chagas' disease.⁴³

1.2.2. Synthesis of Chalcones

There are a number of methods for the synthesis of chalcones including the classical methods of Claisen-Schmidt, Wittig Reaction and Friedel-Craft acylation.

1.2.2.1. The Claisen-Schmidt Reaction

Chalcones are readily synthesized by the base-catalyzed Claisen-Schmidt condensation of an aldehyde and an acetophenone in a polar solvent like methanol (Fig. 8). The enolate ion from acetophenone reacts with carbonyl of aldehyde to form the β -hydroxyketone, followed by dehydration to give a conjugated enone. The method is versatile and convenient, although yields may be variable, ranging from 5% to 90%.³⁴ Improved conditions using either organolithium bases in apolar solvent⁴⁴ or solid catalyst have been also described.⁴⁵

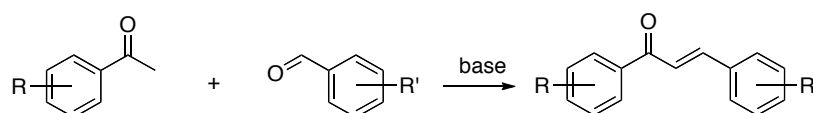


Fig. 8. The Claisen-Schmidt Reaction

1.2.2.2. The Suzuki Reaction

Eddarir and co-workers delighted that Suzuki coupling between benzoyl chloride and phenylvinylboronic acid, catalyzed by zerovalent palladium in anhydrous toluene gives the chalcones in near quantitative yield (Fig. 9).⁴⁶

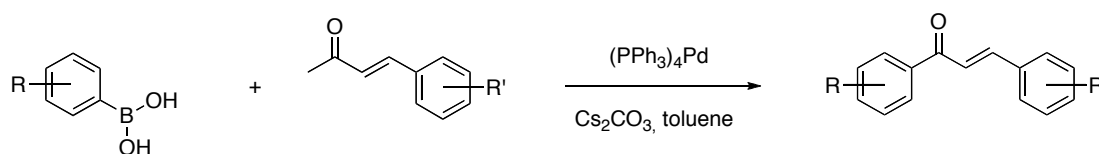


Fig. 9. The Suzuki coupling

This reaction is not affected by substituents on the acyl chloride or the phenylboronic acid.

1.2.2.3. Synthesis of Chalcone via Ultrasound and Microwave-Assisted Methods

Ultrasound and microwave-assisted methods are investigated. Claisen-Schmidt condensation in the presence of KOH or KF supported on alumina under ultrasound gives good yields under mild conditions and shorter reaction times.³⁴ The utility of microwave-assisted synthesis is investigated for 2'-hydroxychalcones, the synthesis of which is generally impeded by cyclisation to flavanones. Unfortunately, protecting the 2' hydroxyl group is not a viable option because of the ortho position of the substituent. The microwave irradiation of the reactants in 20% KOH/ethanol in a closed pressure tube gives excellent yields of 2'-hydroxylchalcones, without side products (Fig. 10).⁴⁷ The closed tube permits temperature to reach 132°C, which is presumably optimal for reaction. When the reaction is repeated in an oil bath with a temperature of about 130°C, identical yields are obtained.³⁴

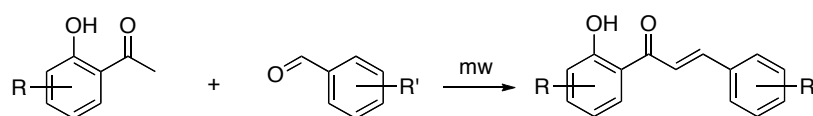


Fig. 10. Microwave-assisted synthesis

1.2.3. Physico-chemical Properties of Chalcones

Conformational analyses and X-ray structure of chalcones have confirmed the overall planarity and rigidity of the π -system. The ring A have a greater rotational flexibility, this may imply that it deviates from planarity to a greater extent than ring B. For this reason the delocalization of electrons occurs between ring B and the α,β -unsaturated double bound.

The effect of ring substituents on the planarity of the system has been also investigated. A 2'-hydroxyl group on ring A forms an intramolecular bound with the carbonyl oxygen and rises to a stable planar conformation.³⁴

The $C\alpha-C\beta$ double bound in the enone can adopt Z or E configuration. The Claisen-Schmidt preparation of chalcones predominantly generates the E-isomer, thermodynamically more stable. The Z-isomer is obtained by exposing a methanolic solution of the chalcone to normal light.⁴⁸ The Z-isomer shows more potent antitumourigenic activity than the E form.

The carbon-oxygen and carbon-carbon double bounds are in *s-cis*, but the introduction of a methyl group to the $C\alpha$ position alters the disposition in *s-trans*, leading to the lost of planarity between ring A and the enone. The α -methylchalcone has shown a greater cytotoxic activity against a human leukemia cell line than the unsubstitued analogue.

Electron delocalization along the α,β -unsaturated chain would render the β -carbon electron deficient and more susceptible to attack by weak nucleophile, like thiol, but it is too soft to interact with amino and hydroxyl groups on nucleic acids and it doesn't show mutagenic properties.

The hydroxyl substituent is widespread among chalcones from natural and synthetic sources. The hydroxyl group is a weak acid and its pKa value is dependent on its location on the chalcone. Rastelli *et al.* have determined the pKa values of 2'-hydroxyl, 4'-hydroxyl (ring A) and 4-hydroxyl (ring B) by a spectrophotometric method and concluded that 4'-hydroxyl is the most acidic (pKa 7.5) while 2'-hydroxyl (pKa 10.1) is the least acidic (Fig. 11). The greater acidity of the 4'-hydroxyl group is attributed to the stabilization of the phenolate anion by delocalization of its charge to the carbonyl oxygen.^{34,49}

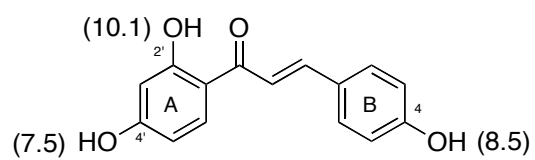


Fig. 11. pKa values of hydroxyl group in chalcones

1.3. Heat Shock Proteins

Heat shock proteins (Hsps), act as molecular chaperones, guiding nascent polypeptides through the process of folding and maturation into three-dimensional structures.⁵⁰

Hsps have been classified into six major families according to their molecular size: Hsp100 (100-110 kDa), Hsp90 (83-90 kDa), Hsp70 (66-78 kDa), Hsp60, Hsp40, and small heat shock proteins (15-30 kDa). Hsp100 (Clp family) proteins have been studied for their ability to target and unfold tagged and misfolded proteins. Hsp70 has a high-affinity bound state to unfolded proteins when bound to ADP, and a low-affinity state when bound to ATP. Hsp70s crowd an unfolded substrate stabilizing and preventing aggregation until the unfolded molecule and diffuse away. Hsp70 also acts as a mitochondrial and chloroplastic molecular chaperone in eukaryotics. Hsp60 and Hsp40 compete in the pathway of misfolding and aggregation. Within each gene family are members that are constitutively expressed, inducibly regulated, and/or targeted to different compartments.⁵¹

1.3.1. Hsp90

Hsp90 is one of the most abundant proteins in eukaryotic cells, comprising 1-2% of cellular proteins under homeostatic conditions. Cells exposed to heat shock and other stressed conditions, such as in the case of cancer, overexpress Hsp90. The full functional activity of Hsp90 is gained in concert with other co-chaperones and various “client” proteins, playing an essential role as molecular chaperones and being responsible for the conformational maturation of nascent polypeptides and the refolding of denatured proteins.⁵² These multicomponent complexes are integrally involved in cell signaling, proliferation and survival. The number of identified Hsp90 client proteins is over 100 and is still quickly increasing. They include protein kinases, transcription factors, and other signaling proteins. Many of the client proteins, such as steroid hormone receptors, epidermal growth factor receptor (EGF-R) family members, the MET

oncogene, Raf-1 kinase, AKT kinase, BCR-ABL fusion proteins in leukemia, mutant p53, cyclin dependent kinase 4 (CDK4), hypoxia-inducible factor 1 α (HIF1 α), and matrix metalloproteinase 2 (MMP2), are known to be involved in cancer signaling pathways.⁵³ Thus, Hsp90 has emerged as a promising target for cancer chemotherapy. Moreover, this molecular chaperone has exhibited exceptional neuroprotective properties due to its ability to refold aggregated proteins associated with several neurodegenerative diseases.

The Hsp90 family of chaperones is composed of four isoforms: Hsp90 α (inducible/major form) and Hsp90 β (constitutive/minor form) are found predominately in the cytosol, the 94 kDa glucose-regulated protein (GRP94) is localized to the endoplasmic reticulum, and Hsp75/tumor necrosis factor receptor associated protein 1 (TRAP-1) resides in the mitochondrial matrix.⁵⁴

An important difference between Hsp90 α and Hsp90 β is that the α form dimerizes with more efficiency. In addition they differ in the amino acid sequence of client proteins binding site.

In humans, Hsp90 exists as a homodimer, which contains three highly conserved domains:

- a 25 kDa N-terminal ATP-binding domain;
- a 35 kDa middle domain;
- a 12 kDa C-terminal dimerization domain (Fig. 12).

Inhibitors block the ability of Hsp90 to stabilize and/or fold client proteins, leading to an unproductive heteroprotein complex that is degraded by the ubiquitin-proteasome pathway. The N-terminal domain contains an ATP-binding site that also binds the natural products, as geldanamycin (GDA) and radicicol. Hsp90 function depends upon the ability of the N-terminal domain to bind and hydrolyze ATP. While the solution structure of Hsp90 exists as a continuum of C-terminally dimerized conformations, the ATP-bound state is a highly constrained structure. The formation of this structure involves coupled conformational switches to position the catalytic apparatus for ATP hydrolysis. An unstructured, highly charged linker joins the N-terminus to the middle domain.

The middle domain exhibits high affinity for co-chaperones as well as client proteins. Structural and functional analyses have demonstrated that the middle domain of Hsp90 contains a catalytic loop, which may serve as an acceptor for

the γ -phosphate of ATP, when it is bound to the N-terminus.⁵⁵

Initial studies by Csermely and co-workers suggested a second ATP-binding site located in the Hsp90 C-terminus. This C-terminal nucleotide binding pocket has been shown to not only bind ATP, but also novobiocin, cisplatin, epigallocatechin-3-gallate (EGCG) and Taxol.⁵⁶

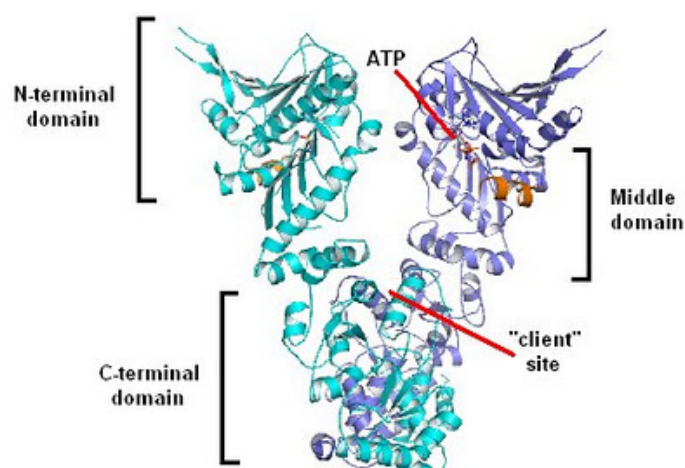


Fig. 12. Hsp90 domains

1.3.1.1. Hsp90 Folding Mechanism

After the synthesis of single-stranded polypeptides by the ribosome, the nascent polypeptides have the propensity to aggregate via interactions between amino acid side chains, unless other proteins are present to prevent this process. Aggregation is prevented by the expression of chaperones, which bind to newly formed peptides and prevent deleterious interactions. In addition to their role as protein stabilizers, chaperones also facilitate the folding of nascent polypeptides into biologically active three-dimensional structures.^{54,55}

The Hsp90 chaperon complex cycles between two major conformational states: the "open" state, where Hsp90 is nucleotide-free and able to capture client proteins, and the "closed" state. Co-chaperone, such as Hsp70, Hsp40, Hop (Hsp70-Hsp90 organizing protein) and Hip (Hsp70 interacting protein), bind to Hsp90 and are important in helping to bind client proteins. Another group of co-chaperones, Cdc37, p23 and immunophilins help Hsp90 in the process of maturation and of maintaining client proteins in their active state. The first steps of these conformational changes were elucidated recently in detail: upon ATP

binding, a short segment of the N-domain called the “ATP lid” changes its position and flaps over the binding pocket (Fig. 13, steps 2 and 3). This releases a short N-terminal segment from its original position. After lid closure, the first 24 aminoacids of each Hsp90 monomer dimerize, and the first β -strand and α -helix swap to associate with the N-domain (ND) of the other monomer. The proto-oncogenic protein Cdc37 is present in Hsp90 complexes containing protein kinase clients, but rather than being released, it remains associated with the kinase client after Hsp90’s ATP-dependent N-terminal clamping. (step 3).

These N-terminal rearrangements result in further conformational changes throughout the entire Hsp90 dimer leading to a twisted and compacted dimer, in which N- and M-domains associate and the distance between M-domains is shortened by 40 Å. The association of N- and M-domains completes the active site of this “split ATPase” (step 4). The co-chaperone p23 is also recruited to Hsp90 at this stage, which promotes ATP hydrolysis (that provides the energy necessary for conformational changes and folding of the client) and stabilization of Hsp90’s “clamped” high- affinity client-bound conformation. The ensemble of Hsp90 and its cohorts promote the folding of the bound client into its three-dimensional structure, and subsequently release the protein through an as yet uncharacterized process that appears to be stimulated by p23.⁵⁰

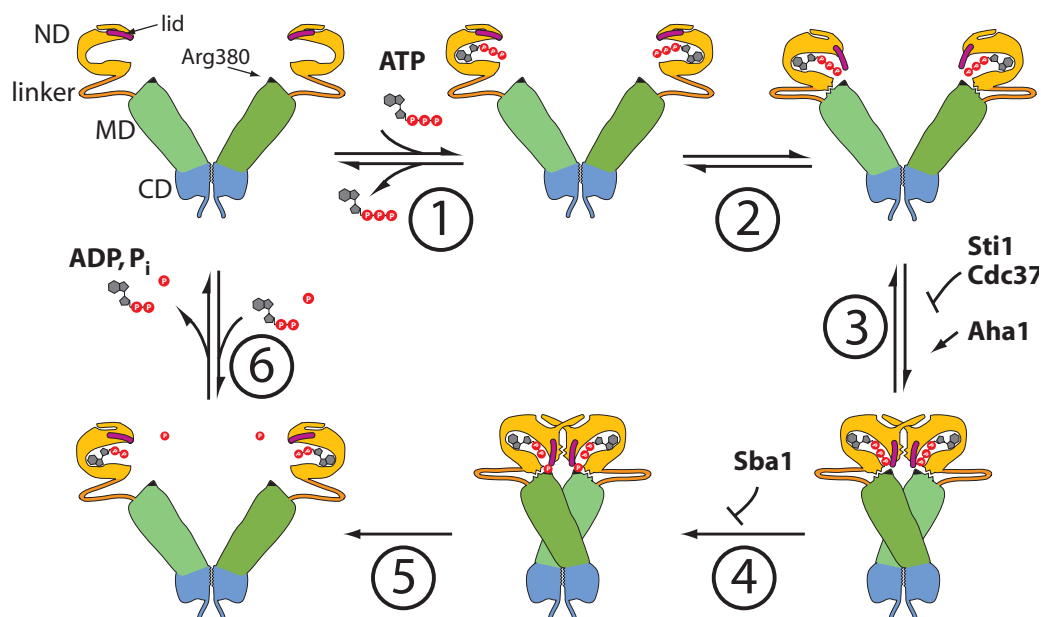


Fig. 13. ATPase cycle of Hsp90⁵⁷

After hydrolysis, the N-domain dissociates; both monomers separate N-terminally; the ATP lid opens; and after release of ADP and P_i, Hsp90 returns to the initial state (steps 5 and 6).

Interestingly, the unusual way in which Hsp90 binds ATP is perfectly mimicked by some natural compounds, such as geldanamycin and radicicol. These are highly specific and potent inhibitors of the Hsp90 ATPase, blocking the maturation of substrate proteins and eventually resulting in their degradation. As several Hsp90 substrate proteins are kinases, which can be deregulated in the development of cancer, derivatives of Hsp90 inhibitors are currently being investigated as anticancer therapeutics at the stage of clinical trials.⁵⁷

Cellular stresses, such as elevated temperatures, abnormal pH, nutrient unavailability, and malignancy, result in the denaturation of folded proteins as well as the increased synthesis of new proteins. Under these conditions, heat shock proteins (Hsps) are overexpressed to refold denatured proteins back into their biologically active conformation.

Hsp90 expression is upregulated in tumor cells and mutational analyses of Hsp90 have demonstrated eukaryotic organisms to be dependent upon Hsp90 for survival. Moreover, cancer cells have been shown to be particularly sensitive to molecules that inhibit Hsp90 function. Consequently, Hsp90 has emerged as an exciting target for the development of cancer chemotherapeutics.⁵⁴

1.3.2. Hsp90-Dependent Client Proteins

Of the more than 100 reported client proteins dependent upon the Hsp90 machinery, 48 are directly associated with oncogenesis. These Hsp90 clients rely on Hsp90 for maturation and/or stabilization and are required for continued growth in hostile tumor microenvironments resulting from hypoxia, nutrient deprivation, acidosis, and mutated/overexpressed proteins. In general, these Hsp90-dependent proteins can be separated into three main groups:

- (1) Transcription factors,
- (2) Kinases,
- (3) Other proteins that participate in multiple signal transduction cascades that ultimately contribute to cancer progression and “oncogene addiction” (Tab.1)

Under normal conditions, Hsp90 is bound to heat shock factor 1 (HSF1), which is a transcription factor responsible for induction of heat shock response. Upon incubation with Hsp90 inhibitors, the complex formed between HSF1 and Hsp90 is dismantled, and HSF1 is able to initiate the transcription of the heat shock genes that encode for Hsps, specifically Hsp70 and Hsp90. Thus, increased levels of these Hsp's are observed as concentration of drug is increased and is commonly used as a hallmark of Hsp90 inhibition.

A number of Hsp90 client proteins are used as negative controls in determining whether an inhibitor is selectively inhibiting the Hsp90 protein folding process or causing the degradation of unrelated proteins. PI3 kinase (p85 unit), b-actin, and tubulin are three commonly used protein controls to verify that inhibitors of the Hsp90 process are not affecting the levels of non-Hsp90 dependent proteins.⁵⁴

Hsp90-dependent Kinases	ErbB2 (Her2), AKT, Bcr-Abl, FAK, Cdk4, Cdk6, Cdk9, RIP (Death domain kinase), MAK, MRK, MOK, c-MET, MEK, Raf-1, B-Raf, Stel, VEGFR2, pp60v-Src, c-Src, Yes, Fps, Fes, Fgr, Lck, PDK1, Pim-1, Plk1, trkB, Weel, Swel
Hsp90-dependent Transcription Factors	AR (Androgen receptor), ER (Estrogen receptor), PR (Progesterone receptor), GR (Glucocorticoid receptor), MR (Mineralcorticoid receptor), HSF-1, mutant p53, Stat3
Other Hsp90-dependent Proteins Associated with Oncogenesis	Proteasome, Telomerase, Survivin, Apaf-1, Mdm2, SV40 large T-antigen, Ral-binding protein 1

Tab. 1. Hsp90-Dependent Client Proteins Associated With Oncogenesis⁵⁴

1.3.3. The Hallmarks of Cancer

Several lines of evidence indicate that tumor genesis in humans is a multistep process and that these steps reflect genetic alterations that drive the progressive transformation of normal human cells into highly malignant derivatives. Many types of cancers are diagnosed in the human population with an age-dependent

incidence implicating four to seven rate-limiting, stochastic events. Pathological analyses of a number of organ sites reveal lesions that appear to represent the intermediate steps in a process through which cells evolve progressively from normalcy via a series of premalignant states into invasive cancers.⁵⁸

The vast catalog of cancer cell genotypes is a manifestation of six essential alterations in cell physiology that collectively dictate malignant growth (Fig. 14):

- ✚ Self-sufficiency in growth signals;
- ✚ Insensitivity to growth-inhibitory (antigrowth) signals;
- ✚ Evasion of programmed cell death (apoptosis);
- ✚ Limitless replicative potential;
- ✚ Sustained angiogenesis;
- ✚ Tissue invasion and metastasis.

Each of these physiologic changes represents the successful breaching of an anticancer defense mechanism hardwired into cells and tissues.

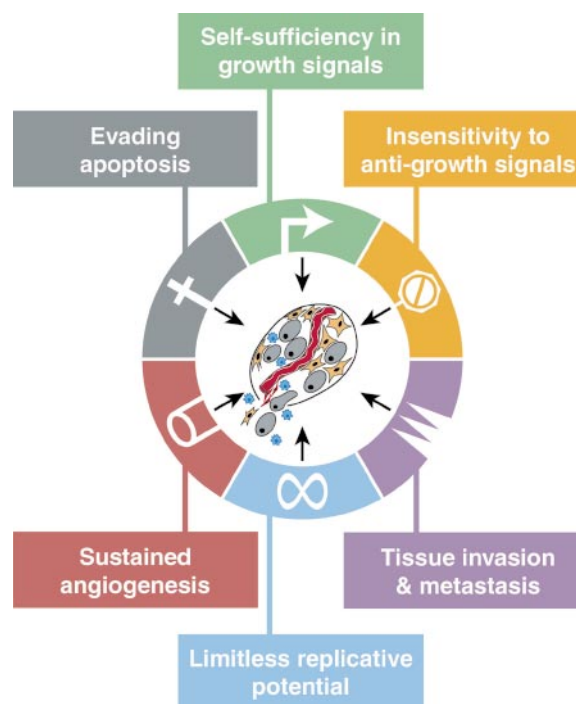


Fig. 14. The Hallmarks of Cancer⁵⁸

1.3.3.1. Self-Sufficiency in Growth Signals

Normal cells require mitogenic growth signals (GS) for moving from into an active proliferative state. These signals are transmitted into the cell by transmembrane receptors that bind distinctive classes of signaling molecules: diffusible growth factors, extracellular matrix components, and cell-to-cell adhesion/interaction molecules. Many of the oncogenes in the cancer catalog act by mimicking normal growth signaling in one way or another.

The conclusion is that tumor cells generate many of their own growth signals, thereby reducing their dependence on stimulation from their normal tissue microenvironment. This liberation from dependence on exogenously derived signals disrupts a critically important homeostatic mechanism that normally operates to ensure a proper behavior of the various cell types within a tissue.

While most soluble mitogenic growth factors (GFs) are made by one cell type in order to stimulate proliferation of another, many cancer cells acquire the ability to synthesize GFs to which they are responsive, creating a positive feedback signaling loop often termed autocrine stimulation.

GF receptors are overexpressed in many tumors and the cancer cells become hyperresponsive to ambient levels of GF that normally would not trigger proliferation. Additionally the overexpression can elicit ligand-independent receptor activation.

1.3.3.2. Insensitivity to Growth-Inhibitory (Antigrowth) Signals

Normal tissues require multiple antiproliferative signals operate to maintain cellular quiescence and tissue homeostasis (e.g. soluble growth inhibitors and immobilized inhibitors embedded in the extracellular matrix and on the surfaces of nearby cells).

Antigrowth signals can force cells out of the active proliferative cycle into the quiescent (G0) state, alternatively, cells may be induced to permanently relinquish their proliferative potential by being induced to enter into post-mitotic states, usually associated with acquisition of specific differentiation-associated traits.

Cells monitor their external environment during cell cycle and, on the basis of sensed signals, decide whether to proliferate, to be quiescent, or to enter into a post-mitotic state. At the molecular level, many and perhaps all antiproliferative signals are funneled through the retinoblastoma protein (pRb) and its two relatives, p107 and p130. When in a hypophosphorylated state, pRb blocks proliferation by sequestering and altering the function of E2F transcription factors that control the expression of banks of genes essential for progression from G1 into S phase.

Disruption of the pRb pathway liberates E2Fs and thus allows cell proliferation, rendering cells insensitive to antigrowth factors that normally operate along this pathway to block advance through the G1 phase of the cell cycle.

The pRb signaling circuit, as governed by TGF and other extrinsic factors, can be disrupted in a variety of ways in different types of human tumors.⁵⁸

1.3.3.3. Evasion of Programmed Cell Death (Apoptosis)

The ability of tumor cell populations to expand in number is determined not only by the rate of cell proliferation but also by the rate of cell attrition. The apoptotic machinery can be broadly divided into two classes of components—sensors and effectors. The sensors are responsible for monitoring the extracellular and intracellular environment for conditions of normality or abnormality that influence whether a cell should live or die. These signals regulate the second class of components, which function as effectors of apoptotic death. Many of the signals that elicit apoptosis converge on the mitochondria, which respond to proapoptotic signals by releasing cytochrome C, a potent catalyst of apoptosis. Members of the Bcl-2 family of proteins, whose members have either proapoptotic (Bax, Bak, Bid, Bim) or antiapoptotic (Bcl-2, Bcl-XL, Bcl-W) function, act in part by governing mitochondrial death signaling through cytochrome C release. The p53 tumor suppressor protein can elicit apoptosis by upregulating expression of proapoptotic Bax in response to sensing DNA damage; Bax in turn stimulates mitochondria to release cytochrome C.⁵⁸

Tumor cells evolve a variety of strategies to limit or circumvent apoptosis. Most common is the loss of TP53 tumor suppressor function, which eliminates this

critical damage sensor from the apoptosis-inducing circuitry. Alternatively, tumors may achieve similar ends by increasing expression of antiapoptotic regulators (Bcl-2, Bcl-xL) or of survival signals (Igf1/2), by downregulating proapoptotic factors (Bax, Bim, Puma), or by short-circuiting the extrinsic ligand-induced death pathway.⁵⁹

1.3.3.4. Limitless Replicative Potential

Telomerase, the specialized DNA polymerase that adds telomere repeat segments to the ends of telomeric DNA, is almost absent in non-immortalized cells but expressed at functionally significant levels in the vast majority of spontaneously immortalized cells, including human cancer cells. By extending telomeric DNA, telomerase is able to counter the progressive telomere erosion that would otherwise occur in its absence. The presence of telomerase activity, either in spontaneously immortalized cells or in the context of cells engineered to express the enzyme, is correlated with a resistance to induction of both senescence and crisis/apoptosis; conversely, suppression of telomerase activity leads to telomere shortening and to activation of one or the other of these proliferative barriers.⁵⁹

The eventual immortalization of rare variant cells that proceed to form tumors has been attributed to their ability to maintain telomeric DNA at lengths sufficient to avoid triggering senescence or apoptosis, achieved most commonly by upregulating expression of telomerase or, less frequently, via an alternative recombination-based telomere maintenance mechanism.

1.3.3.5. Sustained Angiogenesis

The oxygen and nutrients supplied by the vasculature are crucial for cell function and survival. During tumor progression the angiogenesis is almost always activated, causing the tumor growth. Almost all angiogenic regulators are signaling proteins that bind to stimulatory or inhibitory cell-surface receptors displayed by vascular endothelial cells. The well-known prototypes of angiogenesis inducers and inhibitors are vascular endothelial growth factor-A

(VEGF-A), members of fibroblast growth factor (FGF) family and thrombospondin-1 (TSP-1), respectively.

The blood vessels produced within tumors by chronically activated angiogenesis and an unbalanced mix of proangiogenic signals are typically aberrant: tumor neovasculature is marked by precocious capillary sprouting, convoluted and excessive vessel branching, distorted and enlarged vessels, erratic blood flow, microhemorrhaging, leakiness, and abnormal levels of endothelial cell proliferation and apoptosis.⁵⁹

1.3.3.6. Tissue Invasion and Metastasis

The multistep process of invasion and metastasis has been schematized as a sequence of discrete steps, often termed the invasion-metastasis cascade. This depiction envisions a succession of cell-biologic changes, beginning with local invasion, then intravasation by cancer cells into nearby blood and lymphatic vessels, transit of cancer cells through the lymphatic and hematogenous systems, followed by escape of cancer cells from the lumina of such vessels into the parenchyma of distant tissues (extravasation), the formation of small nodules of cancer cells (micrometastases), and finally the growth of micrometastatic lesions into macroscopic tumors, this last step being termed “colonization.”⁵⁹

1.3.4. Hsp90 Inhibitors

Cytotoxic inhibitors of Hsp90 are the only cancer chemotherapeutic agents known to impact all six hallmarks of cancer simultaneously, in fact the inhibition of Hsp90 function disrupts the complex and leads to degradation of client proteins in a proteasome-dependent manner. This results in simultaneous interruption of many signal transduction pathways pivotal to tumor progression and survival.

Hsp90 inhibitors may be classified by their mechanism of binding:

1. Inhibitors of the N-terminal ATP binding domain;
2. Inhibitors of the C-terminal domain.

1.3.4.1. Inhibitors of the N-terminal ATP Binding Domain

Based on the unique and therapeutically attractive action of Hsp90 inhibitors as potent anti-cancer agent and on well-tolerated side effects, extensive studies in developing Hsp90 inhibitors is rapidly increasing.

GELDANAMYCIN AND ANSAMYCIN

Geldanamycin is naturally occurring benzoquinone ansamycin that was first isolated as an antibiotic in 1970 through fermentation of *Streptomyces hygroscopicus*.⁶⁰ Its structure includes a benzoquinone ring fused to a macrocyclic ansa ring (Fig. 15).

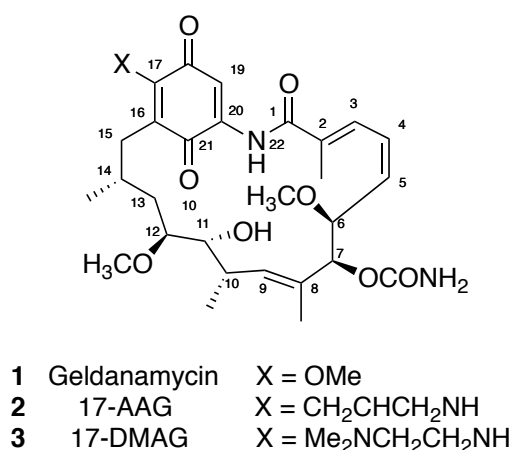


Fig. 15. Structure of Geldanamycin and related derivatives

The antitumor properties of GDA were first reported in 1986, and were initially attributed to its ability to inhibit v-Src phosphorylation in whole cells *via* Src tyrosine kinase.⁵⁰ In 1994, Whitesell and Neckers proved this relationship as a downstream effect of GDA's ability to specifically bind and antagonize Hsp90.^{61,62} Further investigation proved that GDA specifically binds to the N-terminal ATP binding domain of, facilitating destabilization and degradation of many client proteins.

The co-crystal structure of GDA with yeast Hsp90 (Fig. 16) shows that it binds tightly to the ATP pocket of the N-terminal domain. The benzoquinone ring is found near the entrance of the binding pocket and the ansa ring is directed towards the bottom of the pocket. When bound to Hsp90, GDA adopts a C-shaped

conformation similar to that of ADP, that forms five hydrogen bonding interaction with the protein.⁶³ SAR studies have shown that modifications to the carbamate group of GDA substantially decrease the potency of newly formed derivatives, as it serves to mimic the exocyclic amino and imino nitrogens of adenine. A similar loss in activity can be observed upon reduction of the 2–3 double bond, as the target-specific conformation of the macrocycle is compromised.⁵⁰

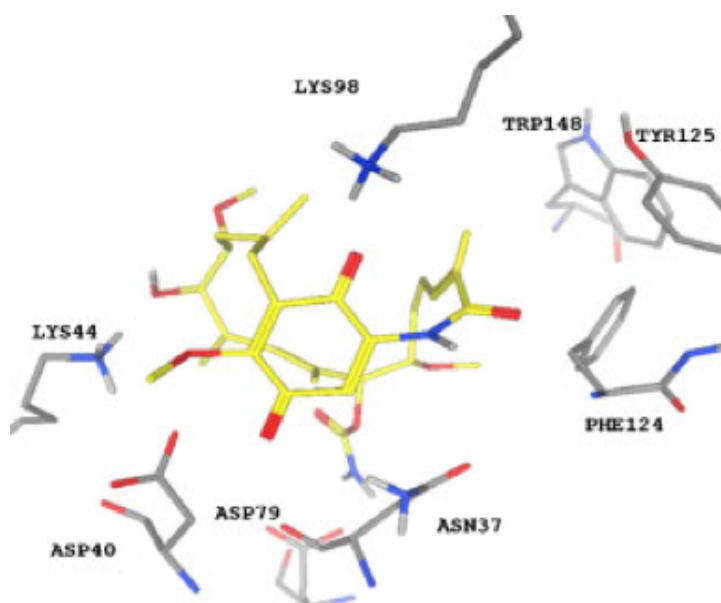


Fig. 16. Co-crystal structure of GDA (yellow) bound to yeast Hsp90⁵⁴

GDA exhibits severe hepatotoxicity, which has been associated with the benzoquinone ring and imposes strict dosing limitations. Secondly, it is metabolically and chemically unstable. Also, it has very low solubility in aqueous media resulting in formulations requiring DMSO. As a result, a substantial effort has been made in modifying its structure to improve safety, stability, potency and water solubility. Fortunately, modification of the 17-methoxy group keeps the excellent biological activity, the substitution with an electron donating group decreases toxicity by stabilizing the quinone moiety and retarding formation of the semiquinone, which is capable of reacting with molecular oxygen, and producing superoxide radicals.

The derivative 17-allylamino-17-desmethoxy-geldanamycin (17- AAG; 2; Fig. 15) has potent in vivo activity and is less toxic than GDA. 17- AAG binds to Hsp90 in

cancer cells with about 100-fold higher affinity than it does in normal cells, probably because the tumor Hsp90 is mostly in multi-protein complexes with high ATPase activity. Despite its promising activity in clinical studies, 17-AAG has several limitations that restrict its optimal clinical development. A lack or reduced activity of this agent in certain cells has been observed due to drug efflux by multidrug resistance elements or metabolic inactivation of these agents by nucleophiles, such as glutathione, or its low solubility in water which makes it difficult to formulate for high absorption and bioavailability.⁶³

A second-generation analogue of GDA, the diamine 17-(2-dimethylaminoethyl)amino-17-demethoxygeldanamycin (17-DMAG; 3; Fig. 15) is quantitatively metabolized much less and is slightly more potent in the cellular assay than 17-AAG. 17-DMAG is water-soluble and orally bioavailable and widely distributed to tissues. Clinical studies with 17-DMAG are currently underway and preliminary results are expected.⁵⁴

RADICICOL AND DERIVATIVES

Radicicol is a 14-member macrolide antibiotic isolated first from the fungus *Monosporium bonorden*. It is the most potent natural product inhibitor of Hsp90 and inhibits several oncogenic signaling pathways in mammalian cells: it depletes K-ras effector kinase, Raf-1, and intercepts k-ras dependent signal down to MAPK cascade. Radicicol also depletes v-Src kinase and inhibits v-Src dependent tyrosine phosphorylation of cellular proteins.⁶⁴

Radicicol binds the N-terminal ATP pocket, but it interacts differently when compared with GDA.

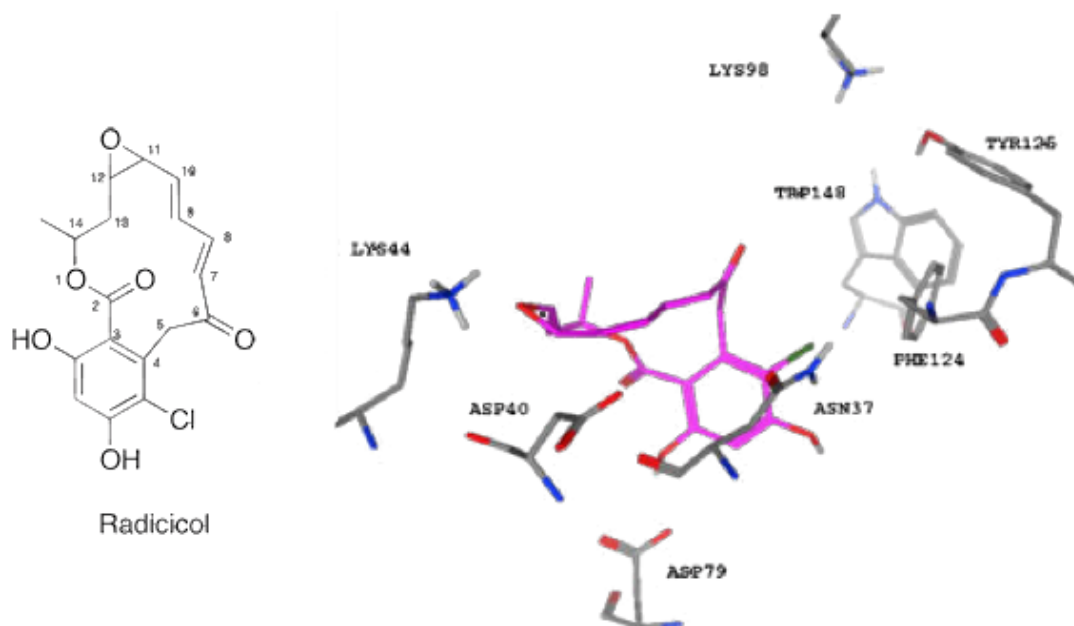


Fig. 17. Co-crystal structure of Radicicol (magenta) bound to yeast Hsp90⁵⁴

The co-crystal structure of RD with yeast Hsp90 shows that it binds tightly to the N-terminal ATP-pocket in a C-shaped conformation similar to ADP (Fig. 17). The aromatic ring is directed towards the bottom of the pocket whereas the macrocycle is at the top. The 2-hydroxyl group and 2-carbonyl bind to Asp79, primarily through a molecule of bound water and the epoxide interacts with Lys44. Occupancy of this pocket by RD disrupts its chaperone function resulting in an inactive Hsp90-protein complex, which is then degraded in a ubiquitin-dependent manner. It has cellular effects similar to ansamycins but lacks hepatotoxicity.⁶³

However, it does not manifest selectivity for the activated heteroprotein complex over the inactive form, as is the case for GDA. This can be attributed to the more rigid structure of Radicicol. No activity has been demonstrated *in vivo*, as Radicicol is rapidly converted to inactive metabolites due to the electrophilicity of the epoxide ring and $\alpha,\beta,\gamma,\delta$ -unsaturated carbonyl.

Several analogues of Radicicol have been synthesized that minimize *in vivo* metabolism by decreasing its electrophilic nature.^{65,66,67}

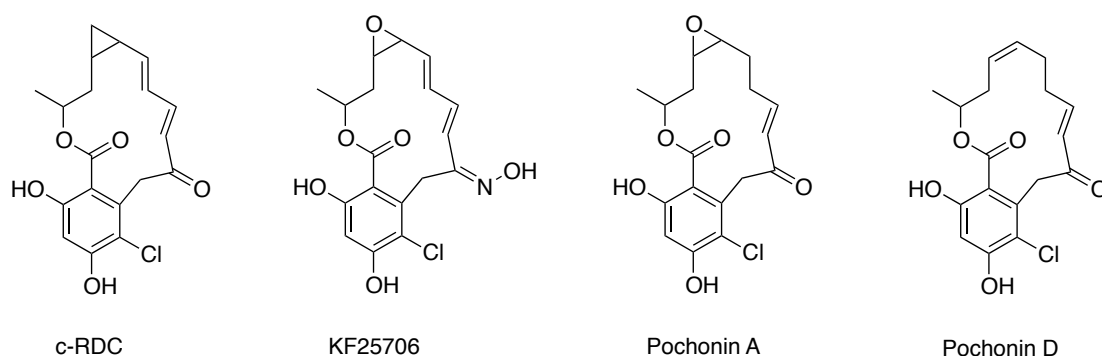


Fig. 18. Analogues of Radicicol

One approach towards enhancing *in vivo* activity has been to synthesize oxime derivatives in an effort to reduce the electrophilicity of the Michael acceptor. The oxime KF25706 (Fig. 18) is more potent than RD in inhibiting v-Src and K-Ras and it also depletes the Hsp90 client proteins Raf-1, v-Src, Her2, Cdk4 and mutated p53 in tumors. In addition, it exhibits more potent antiproliferative activity against various human tumor cell lines *in vitro* and *in vivo* and less liver toxicity than does the parent compound, Radicicol.

Efforts at further optimizing the oxime group to increase both *in vivo* antitumor activity and water solubility through the introduction of carbamoylmethyl groups result in several derivatives with enhanced activity. Generally, the introduction of hydrophobic carbamoylmethyl groups leads to enhanced activity whereas the introduction of hydrophilic groups or an aromatic ring decreases activity.⁶⁴

Another approach in enhancing *in vivo* activity of RD involves modifications to its epoxide ring. In cycloproparadicicol (c-RDC, Fig. 18) the epoxide is replaced by cyclopropane. Cycloproparadicicol degrades the oncogenic proteins Raf-1 and Her2 and retains potent cytotoxicity.⁶⁸

Isolation of the structurally similar pochonin family of natural products from *Pochonia chlamydosporia* has also shown promise in Hsp90 inhibition, particularly with Pochonin A and Pochonin D (Fig. 18). They have been shown to directly inhibit Hsp90.⁶⁹

PURINE-SCAFFOLD DERIVATIVES

Chiosis and colleagues designed and synthesized small ATP analogues, using purine as a scaffold.^{70,71} Originally, the molecule was designed to place the purine

moiety into the same spatial orientation as the adenine ring of ATP. Instead of incorporating a ribose and triphosphate appendage, they attached a 3,4,5-trimethoxy benzyl substituent at the 8-position of the adenine ring and a butyl group at the 9-position. The first molecule reported by the Chiosis laboratory was PU3⁷² (Fig. 19) and in 2004 researchers at Ribotargets reported co-crystal structures of the adenine derived inhibitors bound to Hsp90 as expected, the purine nucleus bound in the region that binds the normal substrate, ATP.⁷³

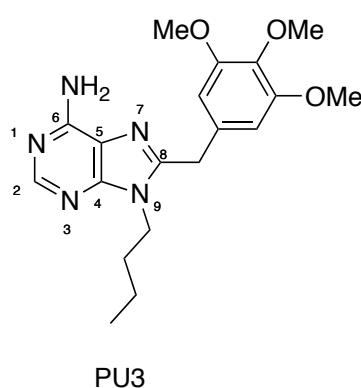


Fig. 19. Structure of PU3

Although the activity of PU3 was lower than the natural product inhibitors, its structure is amenable to extensive chemical modification in an effort to improve both potency and physical/chemical properties. Efforts were focused on probing the structure-activity relationship of the aromatic moiety on the purine at C8-position and on investigating the effects of various chains at N9-position. Additionally, the nature of the linker between the purine-scaffold and the substituted aromatic ring has also been investigated. In total, 72 compounds were prepared and upon biological testing more potent inhibitors of the purine scaffold were identified.

PYRAZOLE DERIVATIVES

From high-throughput screening against a library of 50000 compounds, Workman and co-workers identified CCT018159 as a potent Hsp90 inhibitor (Fig. 20).

It contains a dihydroxyphenylpyrazole attached to 3,4-ethylenedioxybenzene.

Crystal structure shows that CCT018159 binds yeast Hsp90 in the N-terminal

ATP pocket, the resorcinol ring binds the protein similar to the same moiety present in Radicol and the pyrazole forms hydrogen interactions. It inhibits the growth of colon, ovarian and melanoma tumor cells, depletes Hsp90 client proteins Raf-1 and Cdk4 in cancer cells and induces the expression of Hsp70.⁷⁴

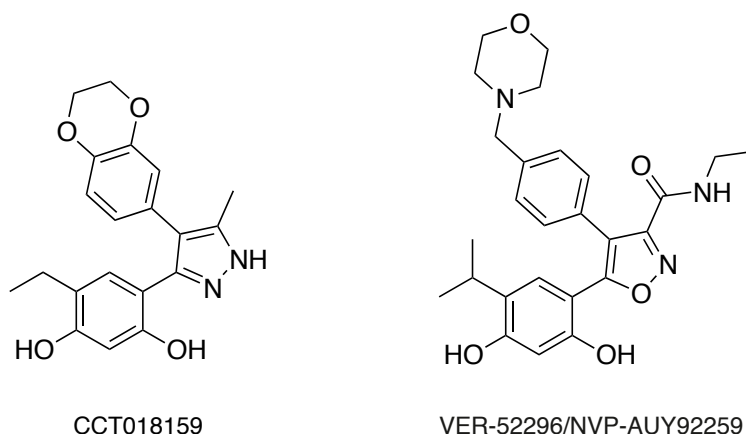


Fig. 20. Structure of pyrazole derivatives

Recently new 3, 4-diarylpyrazole class analogues have been reported.

A significant reduction of tumor growth in HCT116 colon cancer xenografts was observed with the potent Hsp90 inhibitor VER-52296/NVP-AUY92259 (Fig. 20). This compound has excellent potency against Hsp90 and inhibits proliferation in a wide range of human cancer cell lines. Treated cells show the characteristic molecular signature of Hsp90 inhibition, namely, elevation of Hsp72 and degradation of oncogenic client proteins. In addition, this compound shows excellent efficacy in a range of subcutaneous and orthotopic human tumor xenograft models covering major cancer types and diverse oncogenic profiles.⁷⁵

1.3.4.2. Other Hsp90 Inhibitors

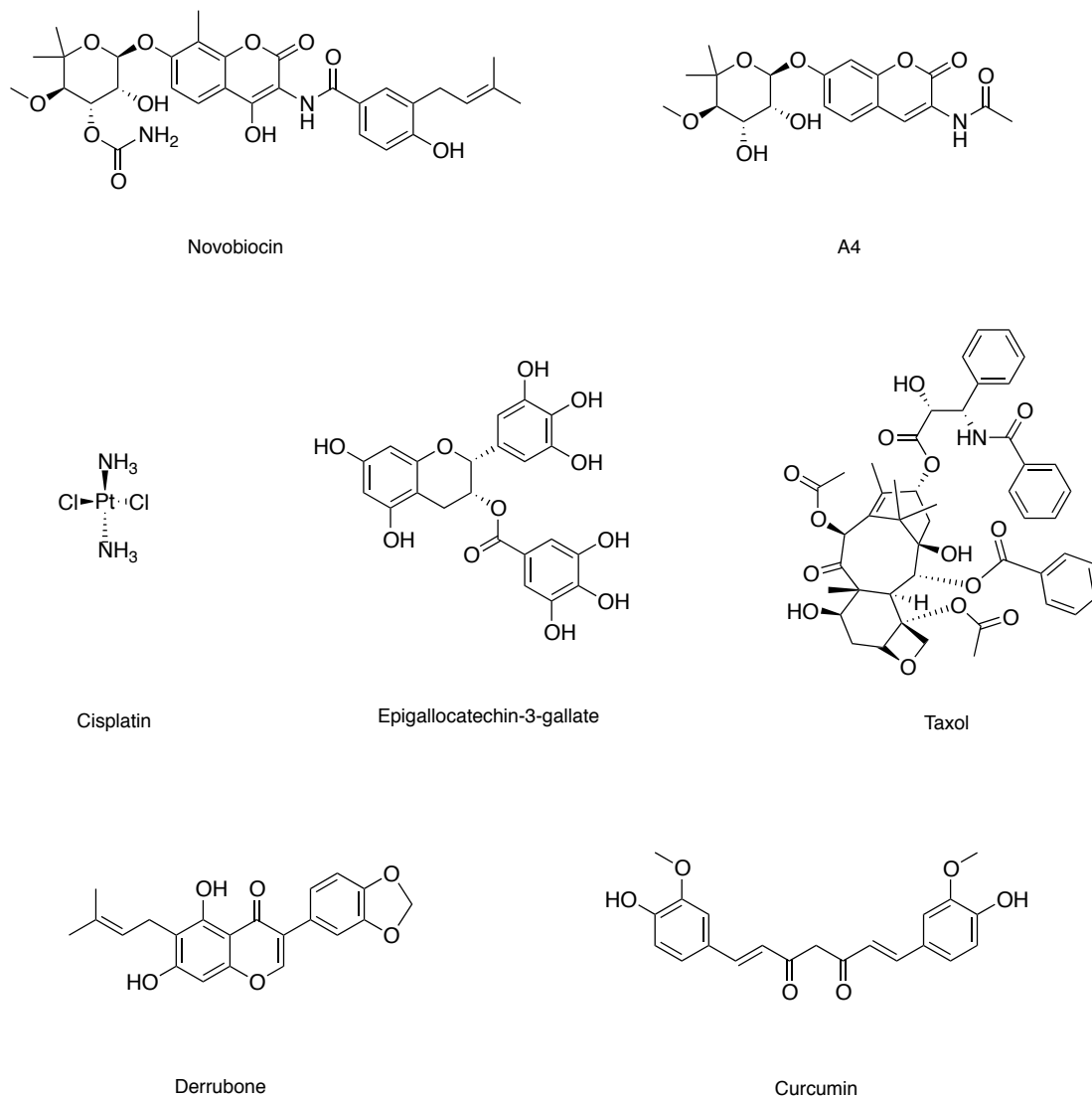


Fig. 21. Structure of other Hsp90 inhibitors

NOVOBIOCIN

Novobiocin is a coumarin antibiotic isolated from *Streptomyces* species and is recently found to be an Hsp90 inhibitor (Fig. 21). Novobiocin can competitively displace immobilized GDA bound to Hsp90, a phenomenon that is not reciprocal with N-terminal inhibitors. Further studies reveal that novobiocin binds to a previously unrecognized C-terminal binding pocket, and induce degradation of ErbB2, mutant p53 and Raf-1 in a concentration-dependent manner.⁵⁵ Yu and co-workers reported that a synthetic novobiocin derivative, A 4, has dramatically improved potency over the parent compound.⁷⁶

CISPLATIN

Cisplatin (Fig. 21) is an antineoplastic drug that coordinates to DNA bases, resulted in cross-linked DNA, thereby inhibiting cell division and tumor growth. It binds near the C-terminal domain and disrupt function of Hsp90. Cisplatin treatment of neuroblastoma cells leads to the degradation of the androgen and glucocorticoid steroid receptors, but does not affect other Hsp90-regulated proteins. The steroid-receptor-specific-proteolysis induced by cisplatin suggests that the compound specifically inhibits steroid receptor-Hsp90 complexes. Acquired resistance can limit its therapeutically potential.⁷⁷

EPIGALLOCATECHIN-3-GALLATE

Epigallocatechin-3-gallate (EGCG, Fig. 21) is a naturally occurring polyphenol extract from the green tea. It binds to the C-terminal ATP-binding site of the Hsp90. EGCG does not appear to prevent Hsp90 from forming heteroprotein complexes. It is also a potential neuroprotective agent in Parkinson's and Alzheimer's diseases.⁷⁸

TAXOL

Taxol (Fig. 21) is a clinically used chemotherapeutic agent for the treatment of cancer and is responsible for the stabilization of microtubules and block of mitosis.⁷⁹ However, Taxol has also been shown to induce the activation of kinases and transcription factors and mimic the effects of bacterial lipopolysaccharide (LPS), which is unrelated to its binding of tubulin. Rosen and co-workers studies suggest that in contrast to typical Hsp90-binding drugs, Taxol exhibits a stimulatory response, mediating the activation of macrophages and exerting the LPS-mimetic effects.⁸⁰ Recently it was reported that 17-AAG behaves synergistically with Taxol-induced apoptosis.

DERRUBONE

Derrubone, a prenylated isoflavones (Fig. 21), was originally isolated and characterized from the Indian tree *Derris robusta* in 1969. High-throughput screening of a library of diverse molecules identified it as a low micromolar inhibitor of Hsp90. Its analogues exhibit modest improvement in inhibitory

activity. Preliminary structure–activity trends demonstrate the importance of an electron-deficient core in the form of an isoflavones and of the 6-prenyl and 3-aryl sidechains for manifesting improved anti-proliferative activity.⁸¹

It can possibly act by stabilizing Hsp90-client interactions and preventing the progression of Hsp90/co-chaperone complex containing bound client through its reaction cycle. It inhibits Hsp90-dependent refolding of luciferase and antagonizes the ability of the Hsp90-specific inhibitor geldanamycin to disrupt complexes formed between Hsp90, Cdc37, and their client kinase, HRI. Furthermore, it exhibits potent antiproliferative effect and Her2 degradation in human breast cancer cell lines. The identification of Derrubone as an Hsp90 inhibitor provides a new natural product scaffold upon which the development of improved Hsp90 inhibitors can be pursued.⁸²

CURCUMIN

Curcumin (Fig. 21), is a natural polyphenol derivated from the plant *Curcuma longa*, which is commonly used as a yellow coloring and flavoring agent in foods. This natural compound can both prevent and treat cancer. The chemopreventive efficacy of curcumin has been ascribed to the modulation of signal-transduction pathways associated with malignant transformation and tumor promotion, through interaction with a variety of proteins implicated in cell proliferation, invasion, and angiogenesis. In addition, it has been described to exhibit effects on signaling pathways, leading to induction of apoptosis. Curcumin inhibits Hsp90 activity, causing depletion of many client proteins implicated in survival pathways (EGFR, Raf-1, Akt, and survivin).⁸³

As compared with 17-AAG, the potency of curcumin was substantially lower and the binding with Hsp90 is weaker. A lack of up-regulation of Hsp70 suggests a mechanism of interaction different from that of geldanamycin. However, in preliminary limited proteolysis experiments, the proteolysis pattern observed on HSP90 α indicated a protection of the N-terminal domain from the enzymatic hydrolysis.

Based on this observation, Giommarelli and co-workers studied the cellular effects of curcumin in combination with the pan-HDAC (histone deacetylase) inhibitors, which induce hyperacetylation of Hsp90, resulting in inhibition of its

chaperone function. The results have showed that, at subtoxic concentrations, curcumin markedly sensitizes tumor cells to HDAC inhibitors and induces growth inhibition and apoptosis. The sensitization is associated with persistent depletion of Hsp90 client proteins.⁸⁴

Recently a series of curcumin analogues including new 4-arylidene curcumin analogues were synthesized. Cell growth inhibition assays reveal that most 4-arylidene curcumin analogues can effectively decrease the growth of a panel of lung cancer cells at submicromolar and low micromolar concentrations.⁸⁵

2. Aim of the Thesis

Hsp90 has emerged as a promising drug target for the development of anti-cancer drugs, based upon its unique activity to function as a mediator of client protein conformation. “Client” proteins are involved in signal transduction, cell cycle regulation and hormone responsiveness. Several of these include a number of known over-expressed or mutant oncogenic proteins, associated with the six cancer hallmarks, as cell proliferation and tumor progression. Consequently, Hsp90 has evolved into promising anticancer target: multiple oncogenic proteins can be simultaneously degraded as consequence of Hsp90 inhibition.

Our group has been involved, for several years, on the design and synthesis of molecules related to flavonoids. These naturally occurring compounds exert a wide range of biological activities, including antiproliferative and antimitotic effects, but currently they have not yet been tested as potential Hsp90 inhibitors. We have selected chalcones as primary scaffolds, and functionalized their structures aiming to obtain radicicol-related derivatives.

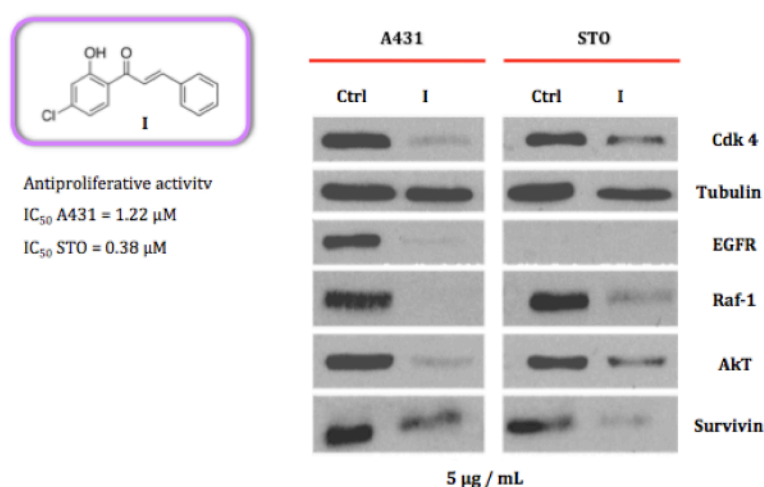


Fig. 22. Effect of chalcone I on antiproliferative assay and on Hsp90 protein levels in A431 (epidermoid carcinoma) and STO (mouse embryonic fibroblast) cell lines

In particular, the compound I showed an interesting antiproliferative activity and the ability to modulate Hsp90 client proteins expression (Fig. 22).

With the aim of continuing this work and to establish structure-activity relationships for this promising new class of Hsp90 inhibitors, alkyl- and aryl- amines were introduced at the para- and meta- positions of B ring, based on the results reported for well known derivatives (Fig. 23).

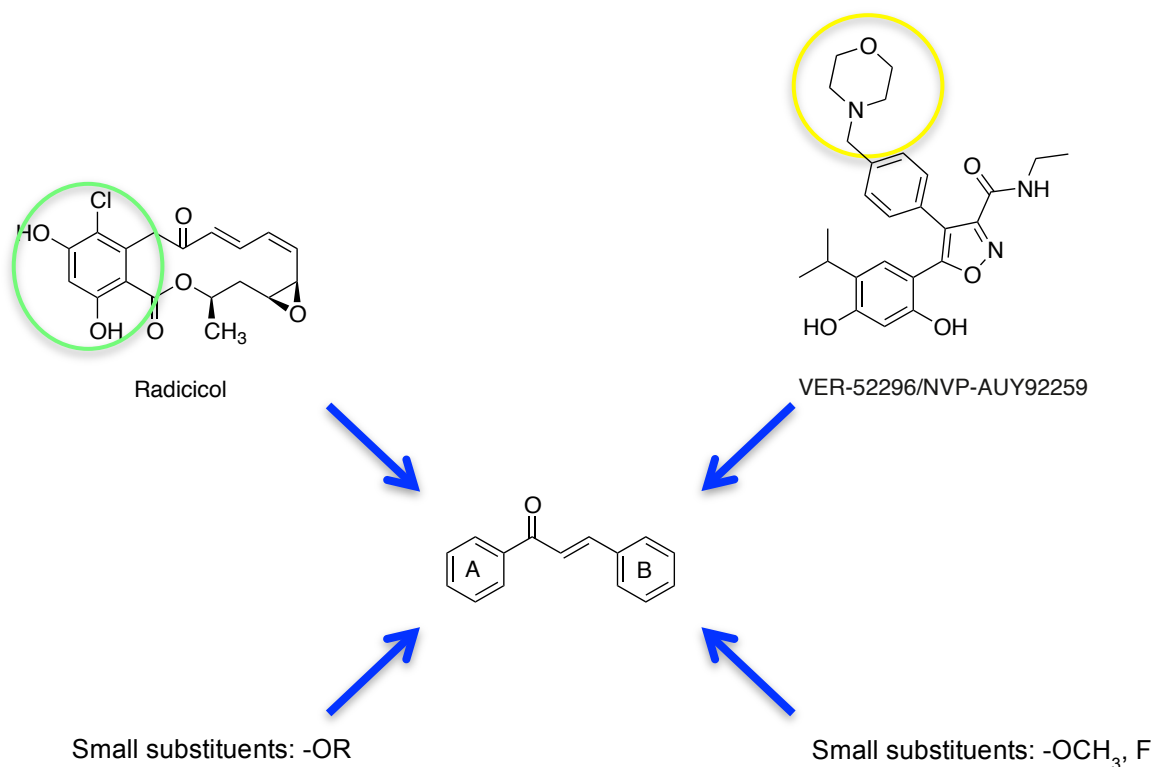
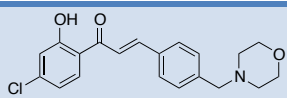
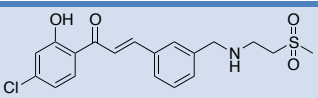
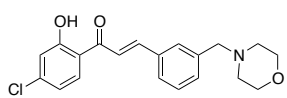
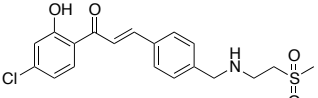
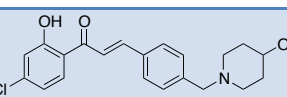
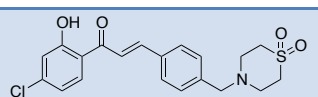
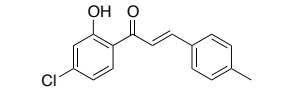
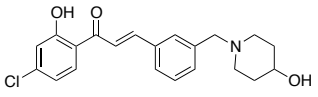
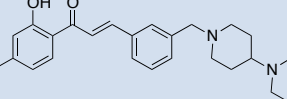
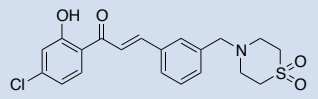
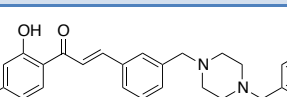
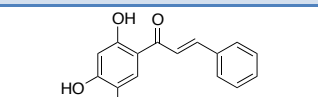
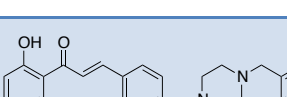
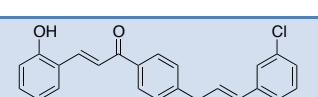
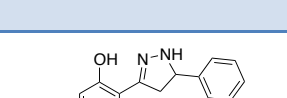
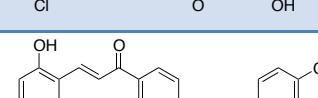

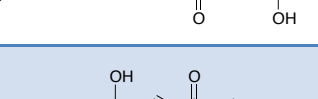


Fig. 23. Rationale representation

Afterwards, we introduced a cyclisation to reduce overall flexibility, 8, and another hydroxyl group on A ring to restore the radicicol core. Moreover, double molecules 16, 17 were also synthesized (Tab. 2).

Compound	Structure	Compound	Structure
1		10	
2		11	
3		12	
4		13	
5		14	
6		15	
7		16	
8		17	
9		18	

Tab. 2. Summary of synthesized compounds

Besides, with the aim of studying the chemical space, we introduced small substituents as methoxy, fluoro and ether chains at different positions (Tab. 3).

Compound	Structure	Compound	Structure
19		29	
20		30	
21		31	
22		32	
23		33	
24		34	
25		35	
26		36	
27		37	
28		38	

Tab. 3. Summary of synthesized compounds

3. Results Discussion and Conclusion

3.1. Drugs and Treatment Conditions

All the compounds tested were freshly prepared dissolving powder in dimethylsulfoxide (DMSO) (BDH Prolabo, Milan, Italy) and following dilution in culture medium. Cells were incubated with drugs for 24 or 72 h (depending on the assay), at 37 °C in culture medium supplemented with 10% (v/v) heat-inactivated fetal bovine serum; drug concentrations used for each assay are reported in Figures.

The human epidermoid carcinoma A431 and the peritoneal mesothelioma STO cell lines were used in this study. A431 and STO cells were routinely grown in RPMI 1640 or in 50/50 DMEM/Ham's F12 medium (Lonza, Switzerland), respectively, supplemented with 10% (v/v) heat-inactivated fetal bovine serum (Gibco®, Invitrogen, Segrate, Italy) at 37°C in a 5%/95% CO₂/air atmosphere.

3.1.1. Antiproliferative Assay

Cell sensitivity to drug treatment was determined by growth inhibition assay. Briefly, cells were seeded in 12-well plates (40,000 cells/well), 24 h before experiments. Cells were exposed to the drugs for 72 h and then adherent cells were trypsinized and counted by a cell counter (Beckam Coulter, Fullerton, CA, USA). IC₅₀ values, derived from dose-response curves, were defined as drug concentrations required for 50% inhibition of cell growth.

3.1.2. Western Blot Analysis

Twenty-four hour after seeding (100,000 cells/mL) on Petri dishes, cells were treated with drugs for 24 h and then processed to obtain whole-cell extracts. Cells were rinsed twice with ice-cold PBS supplemented with 0.1 mM sodium orthovanadate and then lysed in hot sample buffer. After determination of the protein concentration by BCA Protein Assay (Thermo Scientific, Rockford, IL, USA), cellular extracts (40 mg) were separated by sodium dodecylsulfate–polyacrylamide gel electrophoresis (SDS–PAGE) and transferred onto nitrocellulose membranes. Immunoreactive bands were revealed by enhanced chemiluminescence detection (Amersham Biosciences, Rockford, IL, USA) using anti-Raf-1 and anti-Cdk4 (Santa Cruz Biotechnology Inc., CA, USA), anti-EGFR (Upstate Biotechnology, Millipore Corporate, Billerica, MA, USA), anti-Survivin (Abcam, Cambridge, UK), anti-Akt (Transduction Laboratories, Lexington, USA), anti-Actin and anti-Tubulin antibodies (Sigma Chemical Co., St. Louis, MO, USA).

3.2. Results and Conclusion

3.2.1. Antiproliferative Assay

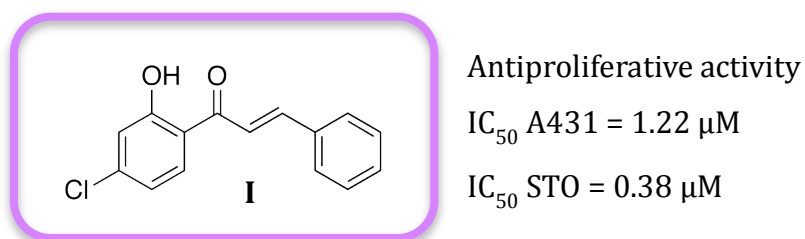
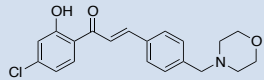
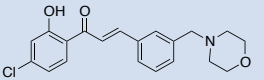
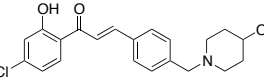
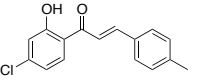
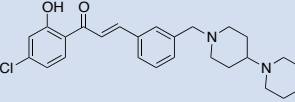
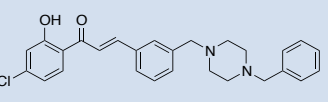
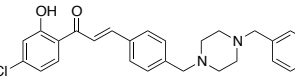
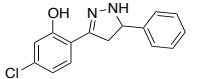
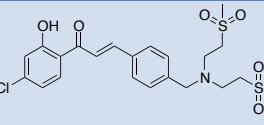
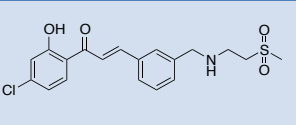
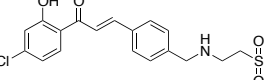
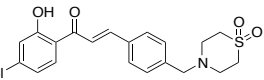
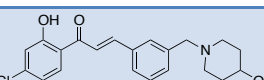
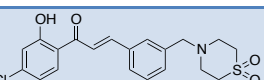
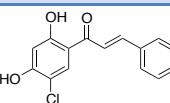
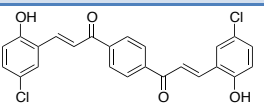
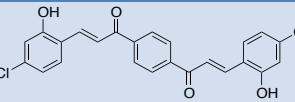
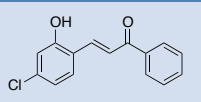


Fig. 24. Antiproliferative activity of I

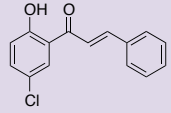
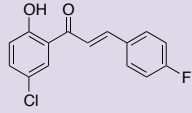
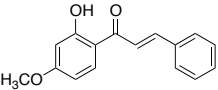
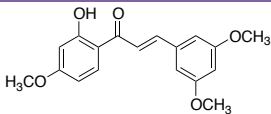
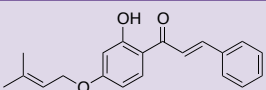
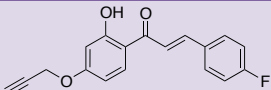
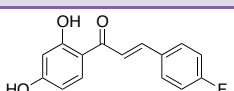
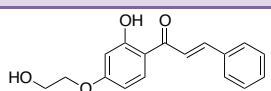
The introduction of alkyl or cyclic amine in para or meta position of B ring and the cyclisation in dihydropyrazole did not afford any enhancement of the antiproliferative activity compared to the lead compound I (Tab. 4).

Accordingly, and bearing in mind the experience gained from data, we focused on modification of A ring: we introduced another hydroxyl, mimicking the radicicol, we have doubled the scaffold and synthesized a retro chalcone.

N.	Compound	IC ₅₀ (μM)	N.	Compound	IC ₅₀ (μM)
1		A431: 10.0 STO: 8.0	2		A431: 12.0 STO: 8.0
3		A431: 5.0 STO: 5.0	4		A431: 15.0 STO: 12.0
5		A431: 10.0 STO: 8.0	6		A431: 15.0 STO: 10.0
7		A431: 6.7 STO: 6.7	8		A431: 14.7 STO: 7.4
9		A431: 20.0 STO: 20.0	10		A431: 25.4 STO: 15.3
11		A431: 25.4 STO: 25.4	12		A431: 6.2 STO: 6.2
13			14		
15			16		
17			18		

Tab. 4. Antiproliferative effects of synthesized compounds

With the aim of studying the chemical space, we have introduced small substituent in different positions (Tab. 5).

N.	Compound	IC ₅₀ (μM)	N.	Compound	IC ₅₀ (μM)
19		A431: 5.9 STO: 4.6	20		A431: 5.8 STO: 6.11
21		A431: - STO: -	22		A431: 1.26 STO: 0.9
23		A431: > 5 STO: > 5	24		A431: 20.0 STO: 12.0
25		A431: 11.0 STO: 5.0	26		A431: 2.0 STO: 0.8

Tab. 5. Antiproliferative effects of synthesized compounds

Regarding antiproliferative activity, with these modifications any significant improvement could be observed with respect to the lead compound, only 22 and 26 showed an antiproliferative activity comparable to I.

In the further series of molecules, the hydroxyethoxy chain was set in para-position on the A ring of the chalcone and small substituents, such as methoxy and fluorine, have been introduced in different positions on the B ring (Tab. 6).

In detail, the introduction of two meta-methoxy groups on B ring, 27, maintained the antiproliferative activity. The substitution with a fluorine atom in different positions gave compounds with an interesting cytotoxic effect, in particular in meta-position, 33, except for the difluoro-derivative, 35, which is the less active.

N.	Compound	IC ₅₀ (μM)	N.	Compound	IC ₅₀ (μM)
27		A431: 2.0 STO: 0.1	28		A431: 10.0 STO: 10.0
29		A431: 5.0 STO: 5.0	30		A431: - STO: -
31		A431: 10.0 STO: 10.0	32		A431: 2.0 STO: 2.0
33		A431: 1.0 STO: 0.2	34		A431: 2.0 STO: 2.0
35		A431: 3.0 STO: 3.0	36		A431: - STO: -
37		A431: - STO: -	38		A431: - STO: -

Tab. 6. Antiproliferative effects of synthesized compounds

3.2.2. Western Blot Analysis

The aptitude of molecules to inhibit Hsp90 has been related to its ability to interfere with the expression of specific client proteins.

In order to investigate the ability to directly inhibit Hsp90 function, the most interesting compounds 27, 33 and 34 were examined by western blot analysis (Fig. 25).

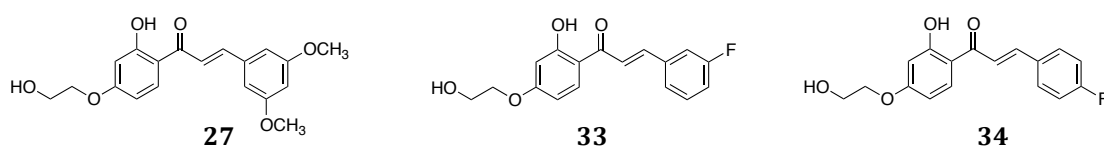


Fig. 25. Selected molecules for western blot

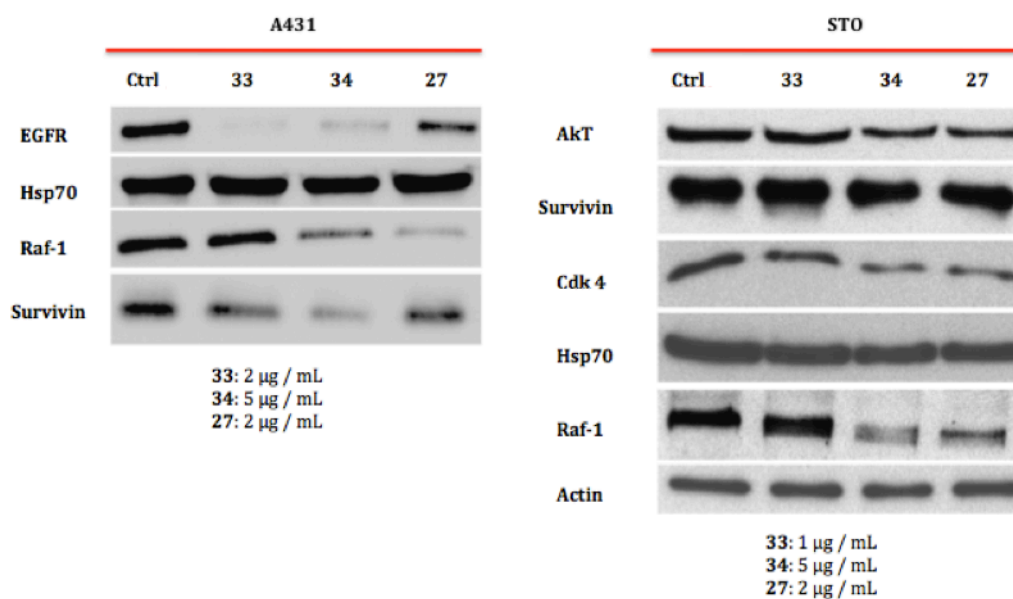


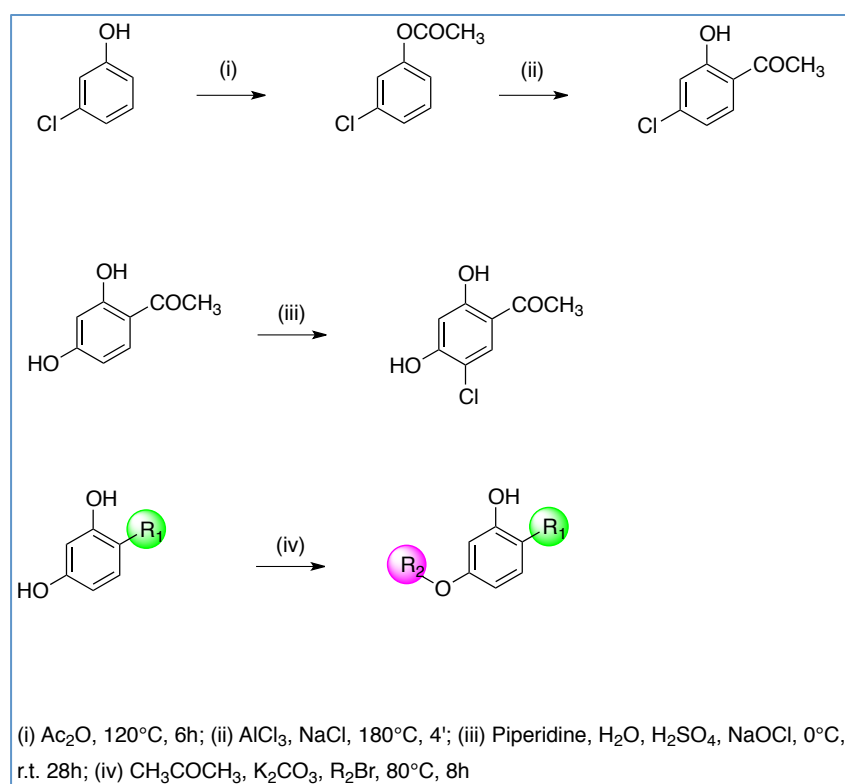
Fig. 26. Effect of 27, 33, 34 on cellular levels of Hsp90 client proteins

27, 33 and 34 were able to directly inhibit Hsp90 function, thereby promoting the chaperone dissociation and the degradation of several Hsp90 client proteins. As shown in Fig. 26, EGFR and Survivin protein expression were strongly downregulated by treatment in A431 cell line. In particular, 27 and 34 were able to decrease also the Raf-1 expression. These client proteins are involved in cell proliferation, invasion and antiapoptotic signals.

In conclusion selected compounds have been shown to modulate Hsp90 signaling pathways. The mechanism of Hsp90 interaction remains to be defined. On the basis of these promising preclinical results, the most active compounds were selected for optical biosensor analysis, with the aim of clarifying whether these molecules bind to Hsp90 and, eventually, the involved binding domain.

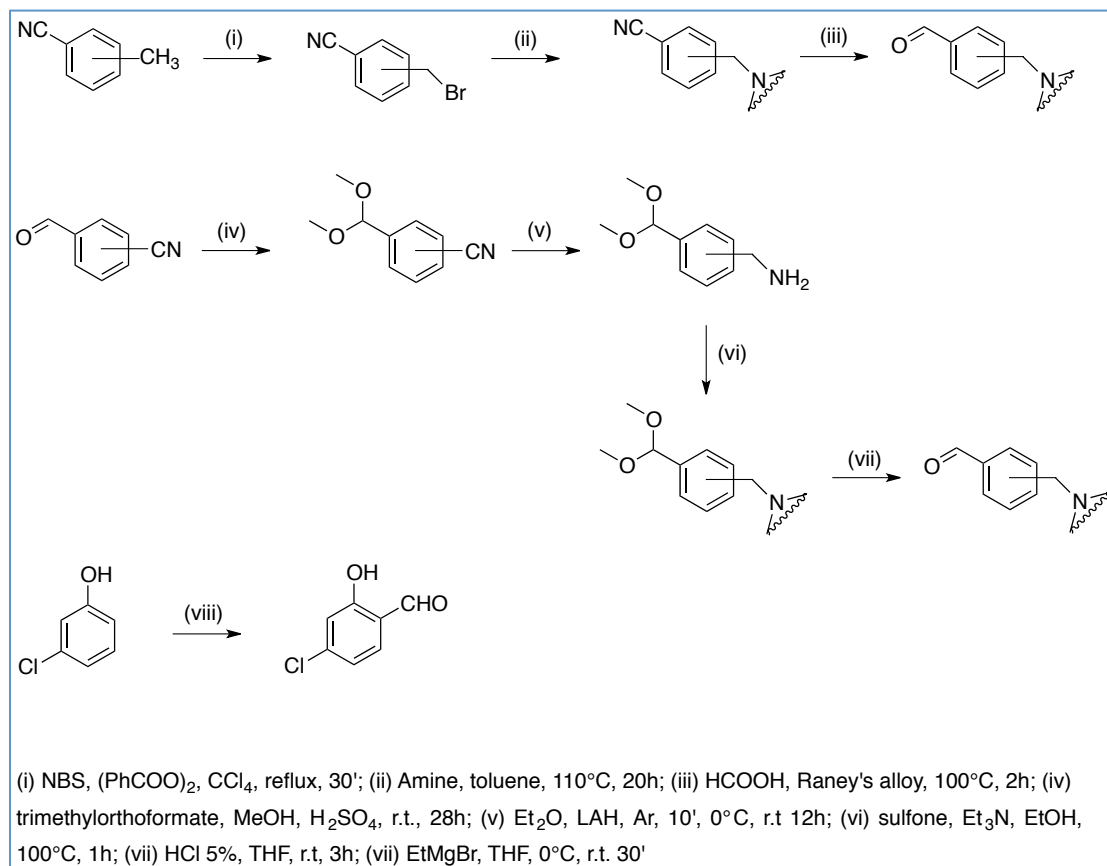
4. Experimental Section

4.1. Acetophenones Synthesis



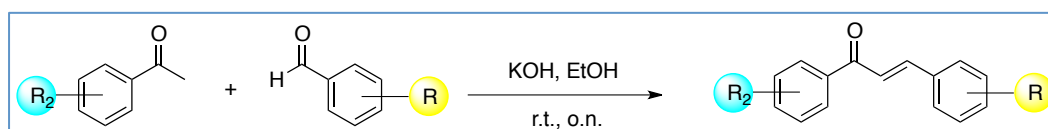
Scheme 1. Acetophenones synthesis

4.2. Aldehydes Synthesis



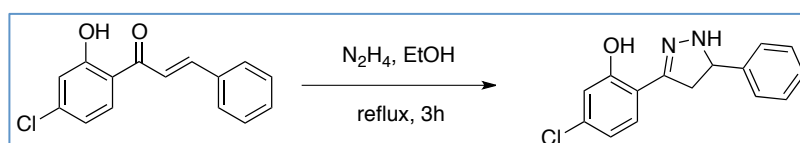
Scheme 2. Aldehydes synthesis

4.3. Aldol Condensation



Scheme 3. Aldol Condensation

4.4. Chalcone Cyclisation



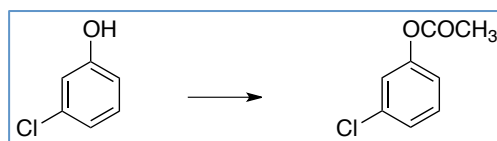
Scheme 4. Chalcone cyclisation

4.5. Experimental Section

General: All solvents were HPLC grade. Reactions were magnetically stirred and monitored by thin-layer chromatography (TLC) with E. Merck silica gel 60-F254 plates. Flash column chromatography was performed with Merck silica gel (0.04 – 0.63 μm , 240 – 400 mesh) under high pressure. NMR spectra were recorded with a 400 MHz spectrometer. Unless otherwise stated, all NMR spectra were measured in CDCl_3 solutions and referenced to the CHCl_3 signal. All ^1H and ^{13}C shifts are given in ppm (s = singlet; d = doublet; t = triplet; dd = quadruplet; dt = doublet of triplets, m = multiplet; br. = broad signal). Coupling constants J are given in Hz.

The commercially available reagents were used as received without further purification.

4.5.1. Acetylation

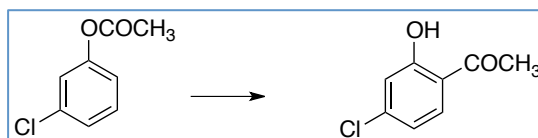


3-Chlorophenyl acetate

3-Chlorophenol (1 eq.) was dissolved in acetic anhydride (4.5 eq.). The temperature raised to 120°C . After 6 hours, the mixture was cooled and poured into an ice water and extracted with dichloromethane. The organic layer was washed with a saturated sodium hydrogenocarbonate solution, and brine and then dried over sodium sulfate and evaporated under reduced pressure. The oil obtained didn't need any further purification b.p. $116.\text{deg.}-118.\text{deg. C.}$ (2 mmHg), quantitative yield.

^1H NMR (400 MHz CDCl_3) δ 2.13 (s, 3 H) 6.97 – 6.99 (m, 1 H) 7.13 (t, 1 H) 7.17 – 7.21 (m, 1H) 7.25 – 7.29 (m, 1H).

4.5.2. Fries Rearrangement

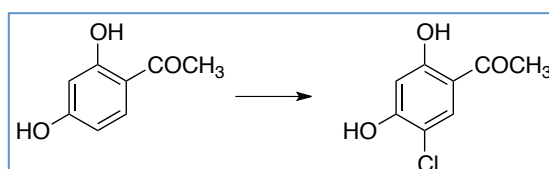


1-(4-chloro-2-hydroxyphenyl)ethanone

3-Chlorophenyl acetate (1 eq.) was heated together with aluminum chloride (3 eq.) and NaCl (1 eq.) at 180°C for 4' (caution: vigorous evolution of gas). The mixture was poured on ice-water and extracted with dichloromethane. The combined organic extracts were washed with a saturated sodium hydrogenocarbonate solution and then with brine, and dried over sodium sulfate. The removal of the solvent gave yellow oil, quantitative yield.

¹H NMR (400 MHz CDCl₃) δ 2.67 (s, 3 H) 6.87 (dd, *J*=8.4, 4.2 Hz, 1 H) 6.99 (s, 1 H) 7.65 (d, *J*=8.4 Hz, 1 H).

4.5.3. Chlorination

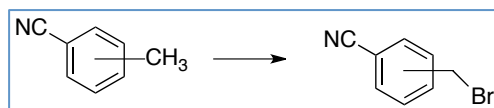


1-(5-Chloro-2,4-dihydroxyphenyl)ethanone

2,4-Dihydroxyacetophenone (1 eq.) was dissolved at room temperature in a solution of sulfuric acid (1.5 mL per mmol of acetophenone) and water (1.5 mL per mmol of acetophenone) and then cooled to 0°C. Piperidine (1.6 eq.) was added dropwise to a solution of aqueous sodium hypochlorite (1.14 eq.) at 0°C and then added dropwise to the aqueous sulfuric acid mixture and stirred for 48 h at room temperature. The chlorinated product was collected by filtration and washed with water. The product was a 1:2 mixture of 3- and 5-chloro isomers and was purified by flash chromatography (cyclohexanes: ethyl acetate= 3:1) to give a white solid (yield = 29%).

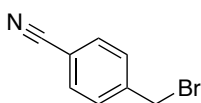
^1H NMR (400 MHz CDCl_3) δ 2.56 (s, 3 H) 6.04 (s, 1 H) 6.59 (s, 1 H) 7.26 (s, 1 H) 7.70 (s, 1 H).

4.5.4. Radical Bromination



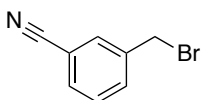
A mixture of para or meta-tolunitrile (1 eq.), N-bromosuccinimide (1 eq.) and benzoyl peroxide (0.01 eq.) was refluxed in tetrachloromethane for 30'. The completion of reaction was detected by TLC. The warm mixture was filtered on celite and the solvent was evaporated under reduced. After evaporation of solvent, the product was used for the next step without any further purification.

4-(bromomethyl)benzonitrile



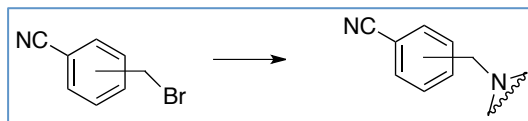
White solid. Yield = 94%. ^1H NMR (400 MHz CDCl_3) δ 4.46 (s, 2 H) 7.48 (d, J =8.8 Hz, 2 H) 7.62 (d, J =8.4 Hz, 2 H). ^{13}C NMR (100 MHz, CDCl_3) δ 31.6 - 112.1 - 118.4 - 129.7 - 132.6 - 142.8.

3-(bromomethyl)benzonitrile



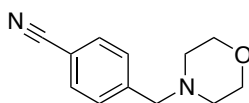
White solid. Yield = 75%. ^1H NMR (400 MHz CDCl_3) δ 4.42 (s, 2 H) 7.47 (t, 1 H) 7.58 – 7.64 (m, 2 H) 7.69 (s, 1 H).

4.5.5. Amination



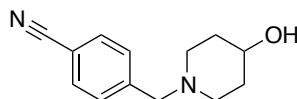
The amine (2 eq.) was added into a solution of meta or para-cyanobenzyl bromide (1 eq.) in toluene and the resulting mixture was stirred at 110°C for 20 hours. The reaction mixture was firstly cooled and then HCl (37%) was added to mixture. The aqueous mixture was extracted with ethyl ether. Potassium carbonate was added to the aqueous layer and they were extracted with dichloromethane. The organic extracts were dried (NaSO₄) and concentrated under vacuum to give an oil that was used without any further purification.

4-(morpholinomethyl)benzonitrile



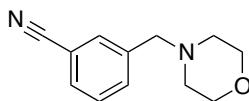
Pale oil. Quantitative yield. ¹H NMR (400 MHz CDCl₃) δ 2.43 (t, 4 H) 3.54 (s, 2 H) 3.71 (t, 4 H) 7.46 (d, *J*=8.4 Hz, 2 H) 7.61 (d, *J*=8.0 Hz, 2 H).

4-[(4-hydroxypiperidin-1-yl)methyl]benzonitrile



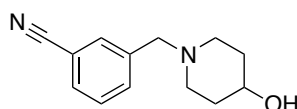
Pale oil. Yield = 90%. ¹H NMR (400 MHz CDCl₃) δ 1.56 – 1.62 (m, 2 H) 1.82 – 1.88 (m, 2 H) 2.16 (t, 2 H) 2.69 – 2.71 (m, 2 H) 3.53 (s, 2 H) 3.70 (m, 1 H) 7.43 (d, *J*=8.4 Hz, 2 H) 7.58 (d, *J*=8.0 Hz, 2 H).

3-(morpholinomethyl)benzonitrile



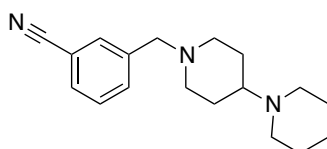
Pale oil. Yield = 97%. ^1H NMR (400 MHz CDCl_3) δ 2.40 (t, 4 H) 3.54 (s, 2 H) 3.71 (t, 4 H) 7.39 (t, 1 H) 7.50 – 7.58 (m, 2 H) 7.61 (s, 1 H)

3-[(4-hydroxypiperidin-1-yl)methyl]benzonitrile



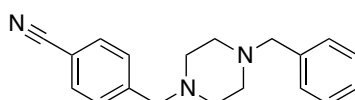
Pale oil. Yield = 97%. ^1H NMR (400 MHz CDCl_3) δ 1.56 – 1.62 (m, 2 H) 1.82 – 1.88 (m, 2 H) 2.16 (t, 2 H) 2.69 – 2.71 (m, 2 H) 3.48 (s, 2 H) 3.68 (m, 1 H) 7.39 (t, 1 H) 7.49 – 7.57 (m, 2 H) 7.60 (s, 1 H).

3-[[1,4'-bipiperidin]-1'-ylmethyl]benzonitrile



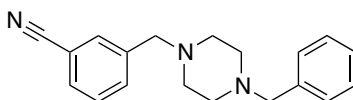
Pale oil. Yield = 96%. ^1H NMR (400 MHz CDCl_3) δ 1.42 – 1.63 (m, 10 H) 1.93 – 2.01 (m, 2 H) 2.24 – 2.30 (m, 1 H) 2.50 – 2.54 (m, 4 H) 2.85 – 2.88 (m, 2 H) 3.47 (s, 2 H) 7.38 (t, $J=7.6$ Hz, 1 H) 7.50 – 7.54 (m, 2 H) 7.61 (s, 1 H).

4-[(4-benzylpiperazin-1-yl)methyl]benzonitrile



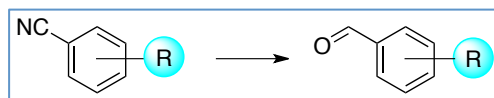
Pale oil. Yield = 58%. ^1H NMR (400 MHz C_6D_6) δ 2.14 (s, 4 H) 2.28 (s, 4 H) 2.97 (s, 2 H) 3.29 (s, 2 H) 6.85 (dd, $J=8.0, 0.4$ Hz, 2 H) 6.99 (dd, $J=6.4, 1.6$ Hz, 2 H) 7.07 – 7.17 (m, 3 H) 7.29 (dd, $J=8.8, 0.8$ Hz, 2 H).

3-((4-benzylpiperazin-1-yl)methyl)benzonitrile



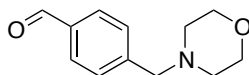
Pale oil. Yield = 97%. ^1H NMR (400 MHz C_6D_6) δ 2.15 (s, 4 H) 2.29 (s, 4 H) 2.99 (s, 2 H) 3.28 (s, 2 H) 6.76 (t, $J=8.0$ Hz, 1 H) 6.97 – 6.99 (m, 1 H) 7.05 – 7.17 (m, 4 H) 7.24 – 7.28 (m, 3H).

4.5.6. Reduction of Nitrile to Aldehyde



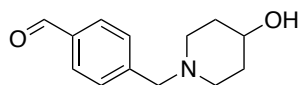
Benzonitrile (1 eq.) was dissolved in formic acid (75percent) and Raney's alloy (1 g per 1g of starting material) is added. After 2 hours at 100 $^{\circ}\text{C}$ the reaction mixture was filtered and neutralized with potassium carbonate. The aqueous mixture was extracted with dichloromethane and the organic layers were dried over sodium sulfate. The solvent was removed under pressure and the crude was purified by flash chromatography (ethyl acetate: petroleum ether= 4:1). A pale oil was obtained.

4-(morpholinomethyl)benzaldehyde



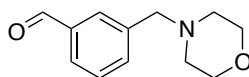
Pale oil. Yield = 90%. ^1H NMR (400 MHz CDCl_3) δ 2.44 (t, 4 H) 3.55 (s, 2 H) 3.70 (t, 4 H) 7.50 (d, $J=8.0$ Hz, 2 H) 7.82 (d, $J=8.0$ Hz, 2 H) 9.98 (s, 1 H).

4-((4-hydroxypiperidin-1-yl)methyl)benzaldehyde



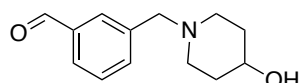
Pale oil. Yield = 37%. ^1H NMR (400 MHz CDCl_3) δ 1.70 – 1.79 (m, 2 H) 1.90 – 1.95 (m, 2 H) 2.30 (t, 2 H) 2.66 – 2.69 (m, 2 H) 3.57 (s, 2 H) 4.92 – 4.96 (m, 1 H) 7.49 (d, $J=8.0$ Hz, 2 H) 7.82 (d, $J=8.0$ Hz, 2 H) 9.98 (s, 1 H).

3-(morpholinomethyl)benzaldehyde



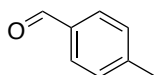
Pale oil. Yield = 86%. ^1H NMR (400 MHz CDCl_3) δ 2.40 (s, 4 H) 3.54 (s, 2 H) 3.69 (s, 4 H) 7.45 (t, 1 H) 7.58 (d, $J=4.0$ Hz, 1 H) 7.73 (d, $J=4.0$ Hz, 1 H) 7.81 (s, 1 H) 9.98 (s, 1 H).

3-((4-hydroxypiperidin-1-yl)methyl)benzaldehyde



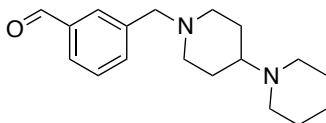
Pale oil. Yield = 85%. ^1H NMR (400 MHz CDCl_3) δ 1.70 – 1.79 (m, 2 H) 1.88 – 1.95 (m, 2 H) 2.29 (t, 2 H) 2.62 – 2.70 (m, 2 H) 3.58 (s, 2 H) 4.88 – 4.97 (m, 1 H) 7.46 (t, 1 H) 7.59 (d, $J=4.0$ Hz, 1 H) 7.75 (d, $J=4.0$ Hz, 1 H) 7.81 (s, 1 H) 9.98 (s, 1 H).

p-toluilbenzaldehyde



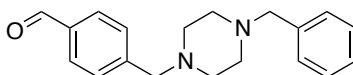
Pale oil. Quantitative yield. ^1H NMR (400 MHz CDCl_3) δ 2.41 (s, 3 H) 7.30 (d, $J=8.0$ Hz, 2 H) 7.75 (d, $J=8.4$ Hz, 2 H) 9.94 (s, 1 H).

3-[[1,4'-bipiperidin]-1'-ylmethyl]benzaldehyde



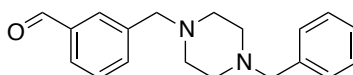
Pale oil. Yield = 88%. ^1H NMR (400 MHz CDCl_3) δ 1.42 – 1.63 (m, 10 H) 1.93 – 2.01 (m, 2 H) 2.24 – 2.30 (m, 1 H) 2.50 – 2.54 (m, 4 H) 2.85 – 2.88 (m, 2 H) 3.47 (s, 2 H) 7.46 (t, 1 H) 7.59 (d, $J=4.0$ Hz, 1 H) 7.75 (d, $J=4.0$ Hz, 1 H) 7.81 (s, 1 H) 9.98 (s, 1 H).

4-[(4-benzylpiperazin-1-yl)methyl]benzaldehyde



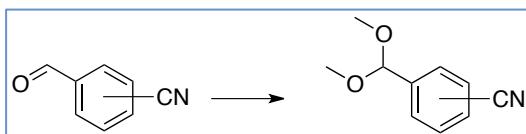
Pale oil. Yield = 85%. ^1H NMR (400 MHz CDCl_3) δ 2.50 (s, 8 H) 3.49 (s, 4 H) 7.18 – 7.42 (m, 5 H) 7.49 (d, $J=8.0$ Hz, 2 H) 7.82 (d, $J=8.0$ Hz, 2 H) 9.98 (s, 1 H).

3-[(4-benzylpiperazin-1-yl)methyl]benzaldehyde



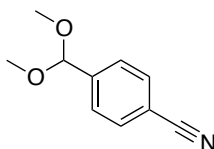
Pale oil. Yield = 38%. ^1H NMR (400 MHz C_6D_6) δ 2.15 – 2.45 (s, 8 H) 3.15 (s, 2 H) 3.28 (s, 2 H) 6.98 (t, $J=7.6$ Hz, 1 H) 7.06 – 7.17 (m, 4 H) 7.28 (dd, $J=7.2, 1.2$ Hz, 2 H) 7.45 (d, $J=7.2$ Hz, 1 H) 7.67 (s, 1H) 9.68 (s, 1 H).

4.5.7. Aldehyde Protection



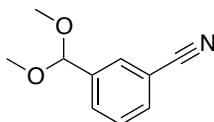
3 or 4-Cyanobenzaldehyde (1 eq.), trimethylorthoformate (1.63 eq.), anhydrous methanol and sulfuric acid (2 drops) were stirred at room temperature for 28 h., treated with saturated aqueous NaHCO₃, extracted three times with diethyl ether, dried (NaSO₄), the solvent was evaporated and distilled in vacuo.

4-(dimethoxymethyl)benzonitrile



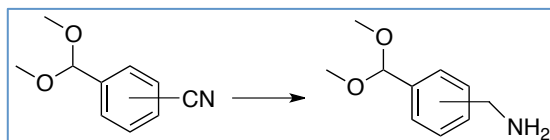
Colorless oil, b.p. 128 – 130°C/ 18 mbar. Yield = 79%. ¹H NMR (400 MHz CDCl₃) δ 3.31 (s, 6 H) 5.41 (s, 1 H) 7.56 (d, *J*=8.2 Hz, 2 H) 7.65 (d, *J*=8.4 Hz, 2 H). ¹³C NMR (100 MHz, CDCl₃) δ 52.9 - 101.9 - 112.5 - 118.8 - 127.8 - 132.2 - 143.4.

3-(dimethoxymethyl)benzonitrile

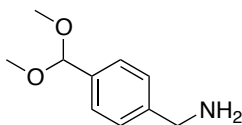


Colorless oil, b.p. 154 – 155°C/ 23 mbar. Yield = 94%. ¹H NMR (400 MHz CDCl₃) δ 3.31 (s, 6 H) 5.39 (s, 1 H) 7.46 (t, *J*=7.6 Hz, 1 H) 7.58 - 7.61 (m, 1 H) 7.67 (dd, *J*=7.6, 1.2 Hz, 1 H) 7.75 (s, 1 H).

4.5.8. Reduction of Nitrile to Amine



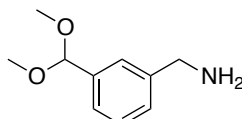
(4-(dimethoxymethyl)phenyl)methanamine



4-Dimethoxymethyl)benzonitrile (1 eq.) in anhydrous diethyl ether was added dropwise to a suspension of lithium aluminum hydride (2.0 eq.) in anhydrous diethyl ether at 0°C under argon atmosphere within 10', allowed to come to room temperature, stirred for 12 h, cooled with ice, treated dropwise with cooling 20% aqueous NaOH and extracted three times with diethyl ether. The combined organic phases were dried (NaSO₄), filtrated and evaporated in vacuo to give a pale oil (yield = 89%).

¹H NMR (400 MHz, CDCl₃): δ 1.51 (s, 2 H), 3.26 (s, 6 H), 3.78 (s, 2 H), 5.32 (s, 1 H), 7.25 (d, *J*=8.1 Hz, 2 H), 7.36 (d, *J*=8.0 Hz, 2 H). ¹³C NMR (100 MHz, CDCl₃): δ 46.4 - 52.8 - 103.2 - 127.1 - 136.8 - 143.7.

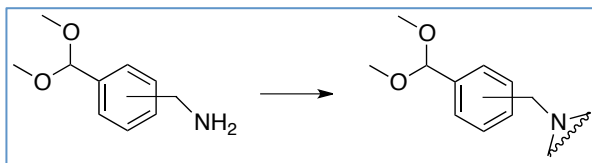
(3-(dimethoxymethyl)phenyl)methanamine



3-Dimethoxymethyl)benzonitrile (1 eq.) in anhydrous tetrahydrofuran was added dropwise to a suspension of lithium aluminium hydride (2.0 eq.) in anhydrous diethyl ether at 0°C under argon atmosphere within 10 min, allowed to come to room temperature, stirred for 12 h, cooled with ice, treated dropwise with cooling 20% aqueous NaOH and extracted three times with diethyl ether. The combined organic phases were dried (NaSO₄), filtrated and evaporated in vacuo to give a pale oil (yield = 84%).

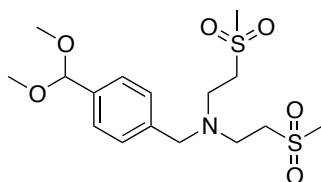
¹H NMR (400 MHz, CDCl₃): δ 1.62 (s, 2 H), 3.30 (s, 6 H), 3.84 (s, 2 H), 5.34 (s, 1 H), 7.24 – 7.26 (m, 1 H), 7.25 – 7.30 (m, 2 H) 7.37 (s, 1 H).

4.5.9. Coupling with Sulfone



***N*-(4-(dimethoxymethyl)benzyl)-2-(methylsulfonyl)-*N*-(2-(methylsulfonyl)ethyl)ethanamine**

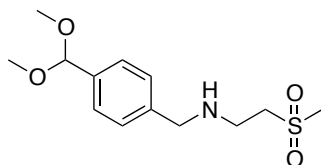
METHOD A: Triethylamine (17.6 eq.) was added to a solution of amine (1 eq.) in EtOH. Divinyl sulfone (31.4 eq.) was added and the mixture was then heated at 100 °C for 1 h. The EtOH was removed in vacuo and dichloromethane was added. The organic layers were washed twice with water and dried over sodium sulfate, filtered and the filtrate solvents removed in vacuo to afford the crude product. The residue was purified by flash chromatography (ethyl acetate: hexanes = 2:1) to afford an oil, quantitative yield.



^1H NMR (400 MHz CDCl_3) δ 2.87 (s, 6 H) 3.00 (t, $J=7.2$ Hz, 4 H) 3.14 (t, $J=6.8$ Hz, 4 H) 3.29 (s, 6 H) 3.64 (s, 2 H) 5.34 (s, 1 H) 7.26 (d, $J=8.4$ Hz, 2 H) 7.39 (d, $J=8.4$ Hz, 2 H).

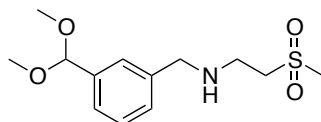
METHOD B: Triethylamine (3 - 15 eq.) was added to a solution of amine (1 eq.) in EtOH. Sulphone (1 eq.) was added and the mixture was then heated at 100 °C for 1 h. The EtOH was removed in vacuo and dichloromethane was added. The organic layers were washed twice with water and dried over sodium sulfate, filtered and the filtrate solvents removed in vacuo to afford the crude product. The residue was purified by flash chromatography (ethyl acetate: petroleum ether = 5:1) to afford the desired compound.

***N*-(4-(dimethoxymethyl)benzyl)-2-(methylsulfonyl)ethanamine**



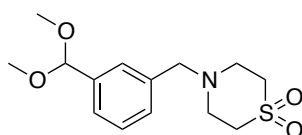
Colorless oil. Quantitative yield. ^1H NMR (400 MHz CDCl_3) δ 2.91 (s, 3 H) 3.07 (m, 4 H) 3.26 (s, 6 H) 3.68 (s, 2 H) 5.30 (s, 1 H) 7.26 (d, $J=8.4$ Hz, 2 H) 7.39 (d, $J=8.4$ Hz, 2 H).

***N*-(3-(dimethoxymethyl)benzyl)-2-(methylsulfonyl)ethanamine**



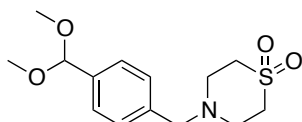
Colorless oil. Quantitative yield. ^1H NMR (400 MHz CDCl_3) δ 2.97 (s, 3 H) 3.12 (s, 4 H) 3.31 (s, 6 H) 3.80 (s, 2 H) 5.35 (s, 1 H) 7.24 – 7.30 (m, 1 H) 7.32 – 7.36 (m, 2 H) 7.39 (s, 1 H).

4-(3-(dimethoxymethyl)benzyl)thiomorpholine 1,1-dioxide



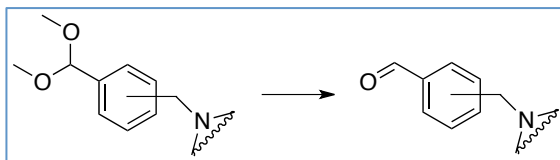
Yellow oil. Yield = 82%. ^1H NMR (400 MHz CDCl_3) δ 2.91 – 3.01 (m, 8 H) 3.29 (s, 6 H) 3.61 (s, 2 H) 5.32 (s, 1 H) 7.22 – 7.34 (m, 4 H).

4-(4-(dimethoxymethyl)benzyl)thiomorpholine 1,1-dioxide



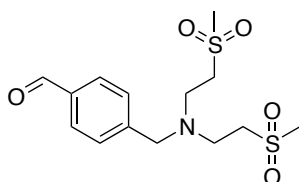
Yellow oil. Yield = 57%. ^1H NMR (400 MHz CDCl_3) δ 2.94 – 3.02 (m, 8 H) 3.31 (s, 6 H) 3.62 (s, 2 H) 5.33 (s, 1 H) 7.28 (d, $J=8.0$ Hz, 2 H) 7.39 (d, $J=8.4$ Hz, 2 H).

4.5.10. Aldehyde Deprotection



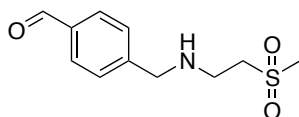
A solution of acetal (1 eq.) in tetrahydrofuran was stirred vigorously and aqueous HCl 5% was added dropwise. The mixture was stirred for 3 hours at room temperature and then solid K_2CO_3 was added slowly until CO evolution ceased. The mixture was transferred to a separatory funnel with diethyl ether and the organic phase was washed with water and a saturated NaCl solution. The organic extract was dried over NaSO_4 and the solvent was removed on a rotary evaporator. The oil crude was used without further purification.

4-((bis(2-(methylsulfonyl)ethyl)amino)methyl)benzaldehyde



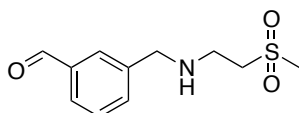
Pale oil. Yield = 49%. ^1H NMR (400 MHz CDCl_3) δ 2.92 (s, 6 H) 3.05 (t, $J=7.2$ Hz, 4 H) 3.17 (t, $J=6.8$ Hz, 4 H) 3.64 (s, 2 H) 7.50 (d, $J=8.4$ Hz, 2 H) 7.84 (d, $J=8.4$ Hz, 2 H) 9.98 (s, 1 H).

4-(((2-(methylsulfonyl)ethyl)amino)methyl)benzaldehyde



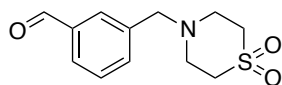
Pale oil. Quantitative yield. ^1H NMR (400 MHz, CDCl_3) δ 1.90 - 2.07 (m, 1 H) 2.91 - 3.01 (m, 3 H) 3.04 - 3.23 (m, 4 H) 3.85 (s, 2 H) 7.44 (d, $J=8.25$ Hz, 2 H) 7.72 - 7.85 (m, 2 H) 9.93 (s, 1 H).

3-(((2-(methylsulfonyl)ethyl)amino)methyl)benzaldehyde



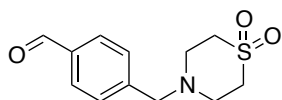
Pale oil. Yield = 50%. ^1H NMR (400 MHz CDCl_3) δ 2.97 (s, 3 H) 3.14 - 3.19 (m, 4 H) 3.88 (s, 2 H) 7.48 (t, $J=7.6$ Hz, 1 H) 7.58 (d, $J=7.6$ Hz, 1 H) 7.76 (d, $J=7.6$ Hz, 1 H) 7.82 (s, 1 H) 9.97 (s, 1 H).

3-((1,1-dioxidothiomorpholino)methyl)benzaldehyde



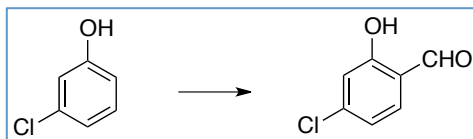
Pale oil. Yield = 98%. ^1H NMR (400 MHz CDCl_3) δ 2.96 - 3.06 (m, 8 H) 3.71 (s, 2 H) 7.50 (t, $J=7.6$ Hz, 1 H) 7.58 (d, $J=6.4$ Hz, 1 H) 7.76 - 7.78 (m, 1 H) 7.82 (s, 1 H) 9.99 (s, 1 H).

4-((1,1-dioxidothiomorpholino)methyl)benzaldehyde



Pale oil. Quantitative yield. ^1H NMR (400 MHz CDCl_3) δ 2.96 - 3.06 (m, 8 H) 3.71 (s, 2 H) 7.48 (d, $J=8.4$ Hz, 2 H) 7.83 (d, $J=8.4$ Hz, 2 H) 9.97 (s, 1 H).

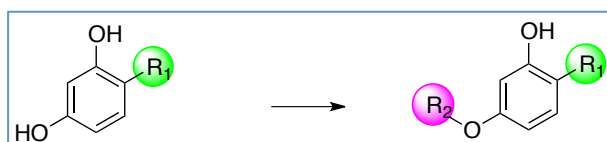
4.5.11. 4-Chloro-2-Hydroxybenzaldehyde Synthesis



A stirred solution of ethyl magnesium bromide (0.95 eq.) in THF was cooled in an ice-bath and 3-chlorophenol (1 eq.) was added batchwise. Upon completion of addition, the reaction mixture was allowed to warm to room temperature where it stirred for 30'. After this time, paraformaldehyde, HMPA and toluene were added and the reaction mixture was heated to 80°C for 22 h. The solvent was removed under reduced pressure. The residue was taken up in dichloromethane and washed with HCl 0.1 N. The organic layer was dried and concentrated. The crude was purified by flash chromatography (cyclohexanes: diethyl ether= 8:1) and afforded a yellow solid (yield = 40%).

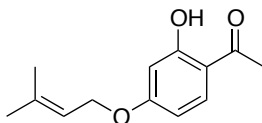
^1H NMR (400 MHz CDCl_3) δ 6.97 – 7.00 (m, 2 H) 7.47 (d, $J=8.8$ Hz, 1 H) 9.84 (s, 1 H) 11.15 (s, 1 H).

4.5.12. Williamson Reaction



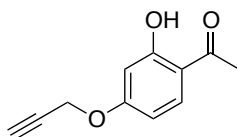
To a solution of 2,4-dihydroxyacetophenone (1 eq.) in acetone at room temperature was added K_2CO_3 (0.4 eq.), followed by alkyl bromide (1 eq.). The reaction mixture was refluxed for 8 h at 80 °C. The reaction progress was monitored by TLC. Upon reaction completion, the mixture was filtered, and the solvent evaporated under reduced pressure. The resulting crude product was purified by column chromatography over a silica gel column (hexane: ethyl acetate = 9:1) to give the desired product.

1-(2-hydroxy-4-((3-methylbut-2-en-1-yl)oxy)phenyl)ethanone



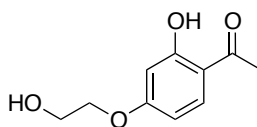
Mp: 40-42 °C. Yield = 95%. ^1H NMR (300 MHz, CDCl_3) δ 6.40 (d, $J=2.0$ Hz, 1 H) 6.44 (dd, $J=8.0, 2.0$ Hz, 1 H) 7.60 (d, $J=8.0$ Hz, 1 H) 12.74 (s, 1 H). ^{13}C NMR (75 MHz, CDCl_3) δ 202.3 - 165.2 - 164.9 - 138.7 - 132.0 - 118.5 - 113.5 - 107.8 - 101.2 - 64.9 - 25.8 - 25.5 - 17.9.

1-(2-hydroxy-4-(prop-2-yn-1-yloxy)phenyl)ethanone



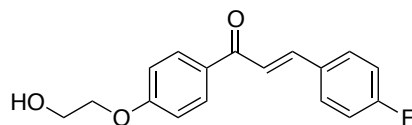
Mp: 64-66 °C. Yield = 93%. ^1H -NMR (400 MHz, CDCl_3) δ 2.58 - 2.55 (m, 4 H) 4.72 (d, 2 H) 6.52 (m, 2 H) 7.66 (d, 1 H) 12.70 (s, 1 H).

1-(2-hydroxy-4-(2-hydroxyethoxy)phenyl)ethanone



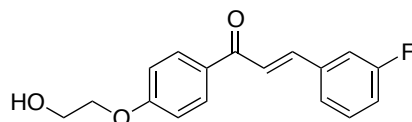
Mp: 64-66. Yield = 65%. ^1H NMR (200 MHz CDCl_3) δ 2.56 (s, 3 H) 3.95 - 4.01 (m, 2 H) 4.10 - 4.14 (m, 2 H) 6.42 - 6.50 (m, 2 H) 7.64 (d, $J=8.6$ Hz, 1 H).

(E)-3-(4-fluorophenyl)-1-(4-(2-hydroxyethoxy)phenyl)prop-2-en-1-one
(36)



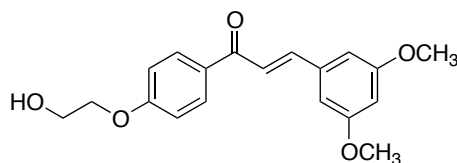
Yellow solid. Yield = 75%. ^1H NMR (400 MHz CDCl_3) δ 3.81 - 3.88 (m, 2 H) 4.14 - 4.16 (m, 2 H) 7.04 - 7.07 (m, 2 H) 7.17 - 7.22 (m, 2 H) 7.72 (d, $J=15.6$ Hz, 1 H) 7.77 (d, $J=15.6$ Hz, 1 H) 7.85 - 7.89 (m, 2 H) 8.10 - 8.14 (m, 2 H).

(E)-3-(3-fluorophenyl)-1-(4-(2-hydroxyethoxy)phenyl)prop-2-en-1-one
(37)



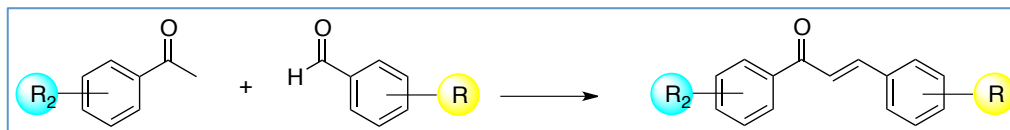
Yellow solid. Yield = 68%. ^1H NMR (400 MHz CDCl_3) δ 3.81 - 3.88 (m, 2 H) 4.14 - 4.16 (m, 2 H) 7.04 - 7.06 (m, 2 H) 7.14 - 7.18 (m, 1 H) 7.43 - 7.49 (m, 1 H) 7.58 - 7.72 (m, 3 H) 7.91 (d, $J=15.6$ Hz, 1 H) 8.12 - 8.15 (m, 2 H).

(E)-3-(3,5-dimethoxyphenyl)-1-(4-(2-hydroxyethoxy)phenyl)prop-2-en-1-one
(38)



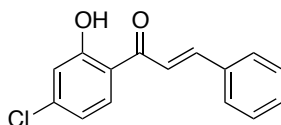
Yellow solid. Yield = 81%. ^1H NMR (400 MHz CDCl_3) δ 3.81 (s, 6 H) 3.88 (t, 2 H) 4.15 (t, 2 H) 6.53 (m, 1 H) 6.96 (m, 2 H) 7.02 - 7.05 (m, 2 H) 7.65 (d, $J=15.6$ Hz, 1 H) 7.83 (d, $J=15.6$ Hz, 1 H) 8.09 - 8.12 (m, 2 H).

4.5.13. Aldol Condensation



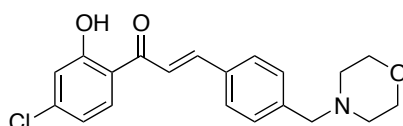
Acetophenone (1 eq.) was dissolved ethanol, then 1 eq. of benzaldehyde was added to solution, followed by an aqueous solution of KOH (50%, 6 eq.) dropwise. The mixture was stirred at room temperature over night. The solvent was removed under reduced pressure. A solution of aqueous HCl (2 N) was added to the crude and then the aqueous mixture was extracted with dichloromethane. The organic layers were dried over sodium sulfate and the solvent was removed under pressure. The crude was purified by flash chromatography (cyclohexanes: ethyl acetate).

(E)-1-(4-chloro-2-hydroxyphenyl)-3-phenylprop-2-en-1-one LEAD I



Yellow solid. Yield = 53%. ¹H NMR (400 MHz, CDCl₃) δ 7.00 (d, *J*=8.8 Hz, 1H) 7.44 – 7.47 (m, 4 H) 7.58 (d, *J*=15.6 Hz, 1 H) 7.68 – 7.71 (m, 2 H) 7.88 (d, *J*=2.4 Hz, 1 H) 7.96 (d, *J*=15.2 Hz, 1 H).

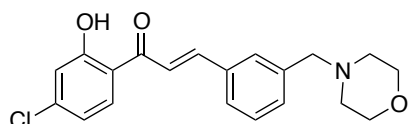
(E)-1-(4-chloro-2-hydroxyphenyl)-3-(4-(morpholinomethyl)phenyl)prop-2-en-1-one (1)



Yellow solid. Yield = 25%. ¹H NMR (400 MHz CDCl₃) δ 2.02 - 2.21 (m, 4 H) 3.14 (s, 2 H) 3.47 - 3.61 (m, 4 H) 4.23 (s, 1 H) 6.57 (dd, *J*=8.61, 2.02 Hz, 1 H) 7.01 - 7.15

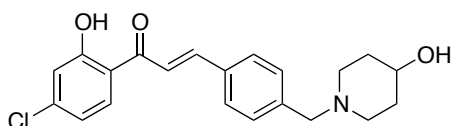
(m, 7 H) 7.89 (d, $J=15.40$ Hz, 1 H). ^{13}C NMR (100 MHz, C_6D_6) δ 192.95 – 165.14 – 145.61 – 142.12 – 133.80 – 130.87 – 129.64 – 128.97 – 127.56 – 119.70 – 119.21 – 119.02 – 118.89 – 67.01 – 63.16 – 53.99.

(*E*)-1-(4-chloro-2-hydroxyphenyl)-3-(3-(morpholinomethyl)phenyl)prop-2-en-1-one (2)



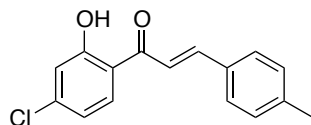
Yellow solid. Yield = 11%. ^1H NMR (400 MHz, C_6D_6) δ 2.04 - 2.22 (m, 4 H) 3.14 (s, 2 H) 3.41 - 3.60 (m, 4 H) 6.54 (dd, $J=8.61$, 2.02 Hz, 1 H) 7.00 - 7.11 (m, 5 H) 7.19 (d, $J=7.33$ Hz, 1 H) 7.37 (s, 1 H) 7.89 (d, $J=15.40$ Hz, 1 H). ^{13}C NMR (100 MHz, CDCl_3) δ 192.97 – 165.12 – 145.81 – 142.12 – 139.63 – 134.99 – 131.81 – 130.90 – 129.62 – 129.00 – 128.63 – 120.15 – 119.25 – 118.98 – 118.84 – 66.96 – 63.21 – 53.98.

(*E*)-1-(4-chloro-2-hydroxyphenyl)-3-(4-((4-hydroxypiperidin-1-yl)methyl)phenyl)prop-2-en-1-one (3)



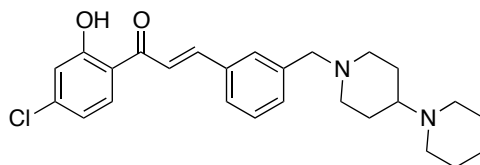
Yellow solid. Yield = 9%. ^1H NMR (400 MHz, C_6D_6) δ 1.39 - 1.50 (m, 2 H) 1.55 - 1.65 (m, 2 H) 1.88 (t, $J=9.44$ Hz, 2 H) 2.46 - 2.56 (m, 2 H) 3.21 (s, 2 H) 3.34 (dt, $J=8.39$, 4.33 Hz, 1 H) 4.17 - 4.31 (m, 1 H) 6.57 (dd, $J=8.52$, 2.11 Hz, 1 H) 7.00 - 7.05 (m, 2 H) 7.07 (s, 1 H) 7.13 (s, 1 H) 7.15 - 7.20 (m, 2 H) 7.20 - 7.25 (m, 2 H) 7.88 (d, $J=15.40$ Hz, 1 H). ^{13}C NMR (100 MHz, C_6D_6) δ 192.88 – 165.03 – 145.64 – 143.08 – 141.96 – 133.53 – 130.78 – 129.33 – 128.91 – 128.52 – 127.65 – 127.43 – 127.25 – 119.02 – 118.90 – 118.80 – 67.43 – 62.70 – 51.15 – 34.75.

(E)-1-(4-chloro-2-hydroxyphenyl)-3-(p-tolyl)prop-2-en-1-one (4)



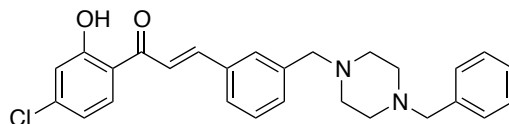
Yellow solid. Yield = 17%. ^1H NMR (400 MHz CDCl_3) δ 2.41 (s, 3 H) 6.92 (d, $J=8.0$ Hz, 1 H) 7.02 (s, 1 H) 7.25 (d, $J=8.0$ Hz, 2 H) 7.75 (s + d, $J=8.4$ Hz, 3 H) 7.86 (d, $J=8.0$ Hz, 1 H) 7.92 (d, $J=15.6$ Hz, 1 H). ^{13}C NMR (100 MHz, CDCl_3) δ 193.00 – 164.28 – 146.19 – 142.00 – 141.89 – 131.71 – 130.56 – 129.85 – 128.81 – 119.45 – 118.67 – 118.64 – 21.61.

(E)-3-(3-([1,4'-bipiperidin]-1'-ylmethyl)phenyl)-1-(4-chloro-2-hydroxyphenyl)prop-2-en-1-one (5)



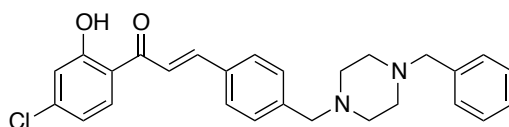
Yellow solid. Yield = 9%. ^1H NMR (400 MHz, CDCl_3) δ 1.33 - 1.51 (m, 2 H) 1.51 - 1.70 (m, 6 H) 1.78 (d, $J=12.10$ Hz, 2 H) 1.89 - 2.07 (m, 2 H) 2.28 (ddd, $J=11.41$, 8.02, 3.48 Hz, 1 H) 2.40 - 2.63 (m, 4 H) 2.94 (d, $J=11.55$ Hz, 2 H) 3.46 - 3.58 (m, 2 H) 6.93 (dd, $J=8.61$, 2.02 Hz, 1 H) 6.99 - 7.10 (m, 1 H) 7.31 - 7.44 (m, 2 H) 7.48 - 7.66 (m, 3 H) 7.80 - 7.99 (m, 2 H). ^{13}C NMR (100 MHz, CDCl_3) δ 192.94 – 164.25 – 146.19 – 142.07 – 139.85 – 134.35 – 131.92 – 130.63 – 129.14 – 128.91 – 127.52 – 119.62 – 119.47 – 118.57 – 62.76 – 62.67 – 53.53 – 50.20 – 27.81 – 26.34 – 24.75.

(E)-3-(3-((4-benzylpiperazin-1-yl)methyl)phenyl)-1-(4-chloro-2-hydroxyphenyl)prop-2-en-1-one (6)



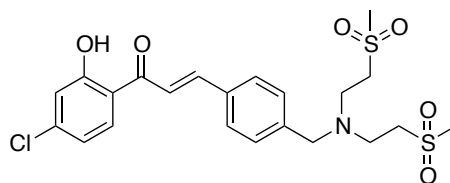
Yellow solid. Yield = 5%. ^1H NMR (400 MHz, $\text{DMSO}-d_6$) δ 2.45 - 2.52 (m, 12 H) 7.04 (dd, $J=8.61$, 2.20 Hz, 1 H) 7.13 (d, $J=2.02$ Hz, 1 H) 7.35 - 7.47 (m, 3 H) 7.48 - 7.69 (m, 4 H) 7.78 (d, $J=15.58$ Hz, 1 H) 7.86 - 7.94 (m, 1 H) 7.98 (d, $J=15.58$ Hz, 1 H) 8.18 (d, $J=8.61$ Hz, 2 H).

(E)-3-(4-((4-benzylpiperazin-1-yl)methyl)phenyl)-1-(4-chloro-2-hydroxyphenyl)prop-2-en-1-one (7)



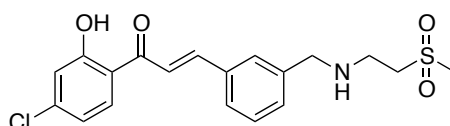
Yellow solid. Yield = 8%. ^1H NMR (400 MHz, C_6D_6) δ 2.45 - 2.52 (br, 8 H) 3.50 (s, 2 H) 3.53 (s, 2 H) 6.89 (dd, $J=8.8$, 2.0 Hz, 1 H) 7.02 (d, $J=1.6$ Hz, 1 H) 7.22 - 7.29 (m, 5 H) 7.38 (d, $J=6.4$ Hz, 2 H) 7.52 - 7.60 (m, 2 H) 7.80 - 7.84 (m, 2 H) 7.90 (d, $J=15.6$ Hz, 1 H). ^{13}C NMR (100 MHz, C_6D_6) δ 192.95 - 165.14 - 145.74 - 142.06 - 133.65 - 130.89 - 129.57 - 129.23 - 128.99 - 128.52 - 127.30 - 127.06 - 119.56 - 119.18 - 118.99 - 63.26 - 63.84 - 53.63 - 53.49.

(E)-3-(4-((bis(2-(methylsulfonyl)ethyl)amino)methyl)phenyl)-1-(4-chloro-2-hydroxyphenyl)prop-2-en-1-one (9)



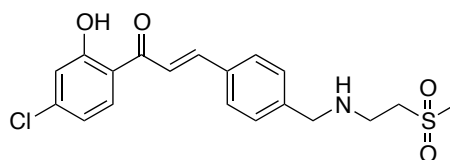
Yellow solid. Yield = 25%. ^1H NMR (400 MHz, CDCl_3) δ 2.93 - 2.97 (m, 6 H) 3.06 - 3.13 (m, 4 H) 3.16 - 3.25 (m, 4 H) 3.69 - 3.77 (m, 2 H) 6.90 - 6.96 (m, 1 H) 7.05 (d, $J=2.20$ Hz, 1 H) 7.40 (d, $J=8.06$ Hz, 2 H) 7.57 (d, $J=15.40$ Hz, 1 H) 7.65 (d, $J=8.25$ Hz, 2 H) 7.85 (d, $J=8.61$ Hz, 1 H) 7.91 (d, $J=15.58$ Hz, 1 H). ^{13}C NMR (100 MHz, CDCl_3) δ 192.84 - 164.29 - 145.21 - 142.25 - 140.26 - 134.15 - 130.58 - 130.43 - 129.57 - 129.07 - 126.25 - 120.07 - 119.56 - 118.73 - 118.55 - 64.18 - 58.65 - 52.17 - 47.13 - 42.16

(*E*)-1-(4-chloro-2-hydroxyphenyl)-3-(3-(((2-(methylsulfonyl)ethyl)amino)methyl)phenyl)prop-2-en-1-one (10)



Yellow solid. Yield = 53%. ^1H NMR (400 MHz, CDCl_3) δ 1.75 - 2.03 (m, 1 H) 3.00 (s, 3 H) 3.12 - 3.26 (m, 4 H) 3.86 (s, 2 H) 6.86 - 6.96 (m, 1 H) 7.01 (d, $J=2.02$ Hz, 1 H) 7.33 - 7.44 (m, 2 H) 7.53 (dt, $J=6.37, 2.04$ Hz, 1 H) 7.60 (d, $J=15.40$ Hz, 1 H) 7.64 (s, 1 H) 7.83 - 7.95 (m, 2 H). ^{13}C NMR (100 MHz, CDCl_3) δ 192.85 - 164.15 - 145.73 - 142.05 - 140.38 - 134.62 - 130.75 - 130.70 - 129.20 - 127.90 - 127.80 - 119.90 - 119.46 - 118.52 - 118.49 - 54.71 - 53.14 - 42.49 - 42.04.

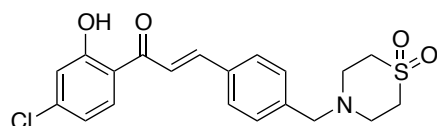
(*E*)-1-(4-chloro-2-hydroxyphenyl)-3-(4-(((2-(methylsulfonyl)ethyl)amino)methyl)phenyl)prop-2-en-1-one (11)



Yellow solid. Yield = 34%. ^1H NMR (400 MHz, CDCl_3) δ 1.66 (br. s., 1 H) 3.00 (s, 3 H) 3.12 - 3.27 (m, 4 H) 3.87 (s, 2 H) 6.93 (dd, $J=8.61, 2.02$ Hz, 1 H) 7.05 (d, $J=2.02$ Hz, 1 H) 7.39 (d, $J=8.25$ Hz, 2 H) 7.57 (d, $J=15.40$ Hz, 1 H) 7.64 (d, $J=8.06$ Hz, 2 H) 7.85 (d, $J=8.80$ Hz, 1 H) 7.92 (d, $J=15.40$ Hz, 1 H). ^{13}C NMR (100 MHz, CDCl_3) δ

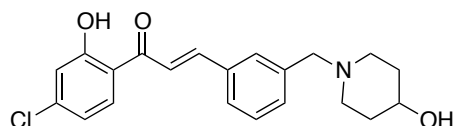
192.89 – 164.27 – 145.62 – 142.14 – 133.49 – 130.56 – 128.99 – 128.69 – 119.53
– 119.51 – 118.70 – 118.58 – 54.85 – 53.31 – 42.62 – 42.10.

(E)-1-(4-chloro-2-hydroxyphenyl)-3-(4-((1,1-dioxidothiomorpholino)methyl)phenyl)prop-2-en-1-one (12)



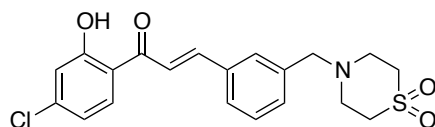
Yellow solid. Yield = 22%. ¹H NMR (400 MHz, CDCl₃) δ 2.96 - 3.15 (m, 8 H) 3.71 (s, 2 H) 6.92 (dd, *J*=8.4, 2.0 Hz, 1 H) 7.03 (d, *J*=2.0 Hz, 1 H) 7.39 (d, *J*=8.0 Hz, 2 H) 7.56 (d, *J*=15.6 Hz, 1 H) 7.61 (d, *J*=8.0 Hz, 2 H) 7.83 (d, *J*=8.0 Hz, 1 H) 7.91 (d, *J*=15.6 Hz, 1 H). ¹³C NMR (100 MHz, CDCl₃) δ 192.80 – 164.25 – 145.36 – 142.18 – 140.74 – 133.92 – 130.53 – 129.33 – 128.97 – 119.77 – 119.50 – 118.69 – 118.52 – 61.15 – 51.49 – 50.70.

(E)-1-(4-chloro-2-hydroxyphenyl)-3-(3-((4-hydroxypiperidin-1-yl)methyl)phenyl)prop-2-en-1-one (13)



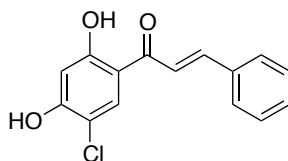
Yellow solid. Yield = 9%. ¹H NMR (400 MHz, C₆D₆) δ 1.42 - 1.70 (m, 4 H) 1.88 (m, 2 H) 2.46 - 2.56 (m, 2 H) 3.26 (s, 2 H) 3.40 (m, 1 H) 6.63 (dd, *J*=8.4, 2.02 Hz, 1 H) 6.82 (s, 1 H) 6.96 (d, *J*=7.6 Hz, 1 H) 7.08 – 7.12 (m, 3 H) 7.20 (d, *J*=7.6 Hz, 1 H) 7.28 (s, 1 H) 7.79 (d, *J*=8.40 Hz, 1 H).

(E)-1-(4-chloro-2-hydroxyphenyl)-3-(3-((1,1-dioxidothiomorpholino)methyl)phenyl)prop-2-en-1-one (14)



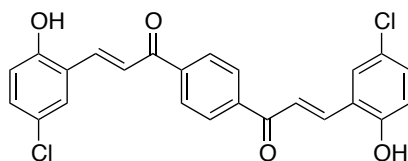
Yellow solid. Yield = 16%. ^1H NMR (400 MHz, CDCl_3) δ 2.97 - 3.13 (m, 8 H) 3.70 (s, 2 H) 6.94 (dd, $J=8.61, 2.20$ Hz, 1 H) 7.06 (d, $J=2.02$ Hz, 1 H) 7.38 - 7.47 (m, 2 H) 7.54 - 7.64 (m, 3 H) 7.85 (d, $J=8.61$ Hz, 1 H) 7.92 (d, $J=15.58$ Hz, 1 H). ^{13}C NMR (100 MHz, CDCl_3) δ 192.81 - 164.31 - 145.58 - 142.30 - 138.44 - 134.86 - 131.43 - 130.57 - 129.41 - 129.09 - 127.97 - 120.15 - 119.56 - 118.77 - 118.52 - 61.23 - 51.47 - 50.72.

(E)-1-(5-chloro-2,4-dihydroxyphenyl)-3-phenylprop-2-en-1-one (15)



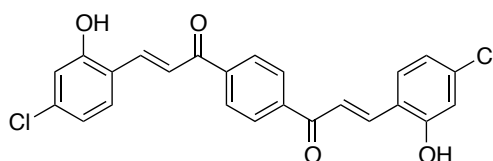
Yellow solid. Yield = 42%. ^1H NMR (400 MHz, CDCl_3) δ 6.56 - 6.72 (m, 1 H) 7.36 - 7.55 (m, 4 H) 7.60 - 7.74 (m, 2 H) 7.84 - 7.98 (m, 2 H). ^{13}C NMR (100 MHz, CDCl_3) δ 191.36 - 165.00 - 157.75 - 145.63 - 134.45 - 131.03 - 130.01 - 129.05 - 128.91 - 128.88 - 128.70 - 119.57 - 115.03 - 104.82.

(2E,2'E)-1,1'-(1,4-phenylene)bis(3-(5-chloro-2-hydroxyphenyl)prop-2-en-1-one) (16)



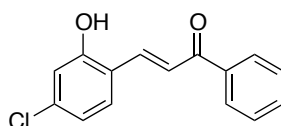
Yellow solid. Yield = 62%. ^1H NMR (400 MHz, $\text{DMSO-}d_6$) δ 6.94 (d, $J=8.80$ Hz, 2 H) 7.30 (dd, $J=8.80, 2.57$ Hz, 2 H) 7.93 - 8.06 (m, 6 H) 8.27 (s, 4 H). ^{13}C NMR (100 MHz, $\text{DMSO-}d_6$) δ 189.73 - 157.05 - 141.48 - 139.19 - 132.37 - 129.49 - 128.35 - 123.80 - 123.64 - 122.66 - 118.70.

(2*E*,2'*E*)-1,1'-(1,4-phenylene)bis(3-(4-chloro-2-hydroxyphenyl)prop-2-en-1-one) (17)



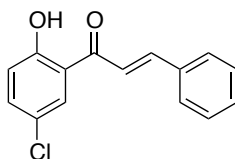
Yellow solid. Yield = 13%. ^1H NMR (400 MHz, $\text{DMSO-}d_6$) δ 6.87 - 7.00 (m, 4 H) 7.86 - 8.04 (m, 6 H) 8.23 (s, 4 H). ^{13}C NMR (100 MHz, $\text{DMSO-}d_6$) δ 189.08 - 158.05 - 140.80 - 138.80 - 135.94 - 130.27 - 128.70 - 121.50 - 120.50 - 119.54 - 115.86.

(*E*)-3-(4-chloro-2-hydroxyphenyl)-1-phenylprop-2-en-1-one (18)



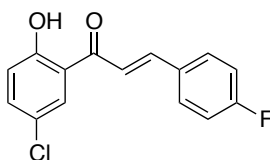
Yellow solid. Yield = 89% (EtOH). ^1H NMR (400 MHz, CD_3OD) δ 6.86 - 6.90 (m, 2 H) 7.51 (t, $J=7.6$ Hz, 2 H) 7.59 (d, $J=7.2$ Hz, 2 H) 7.63 (d, $J=8.4$ Hz, 2 H) 7.77 (d, $J=15.6$ Hz, 1 H) 8.00 - 8.04 (m, 3 H). ^{13}C NMR (100 MHz, CD_3OD) δ 192.91 - 159.46 - 141.14 - 139.54 - 138.06 - 134.03 - 131.54 - 129.85 - 129.77 - 129.59 - 129.56 - 123.09 - 122.16 - 121.07 - 117.02.

(E)-1-(5-chloro-2-hydroxyphenyl)-3-phenylprop-2-en-1-one (19)



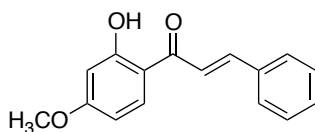
Mp: 80-81°C (EtOH). Yield = 53%. ¹H NMR (400 MHz, DMSO-*d*₆) δ 6.91-7.02 (m, 2 H) 7.49-7.66 (m, 7 H) 7.90 (d, *J*=16.0 Hz, 1 H) 12.76 (s, 1 H).

(E)-1-(5-chloro-2-hydroxyphenyl)-3-(4-fluorophenyl)prop-2-en-1-one (20)



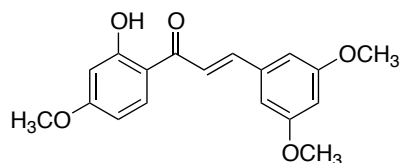
Mp: 60-83°C (EtOH). Yield = 51%. ¹H NMR (400 MHz, CDCl₃) δ 7.01 (s, 1 H) 7.17 (d, *J*=8.8 Hz, 1 H) 7.45 (dd, *J*=8.8, 2.6 Hz, 1 H) 7.48 (d, *J*=15.4 Hz, 1 H) 7.69 (dd, *J*=8.8, 5.4 Hz, 2 H) 7.86 (d, *J*=2.4 Hz, 1 H) 7.91 (d, *J*=15.4 Hz, 1 H) 7.99 (d, *J*=9.2 Hz, 1 H).

(E)-1-(2-hydroxy-4-methoxyphenyl)-3-phenylprop-2-en-1-one (21)



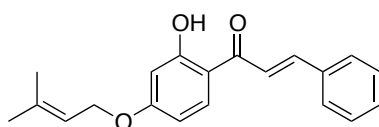
Mp: 92-95°C (EtOH). Yield = 74%. ¹H NMR (400 MHz, CDCl₃) δ 3.84 (s, 3 H), 6.46(d, *J*=2.6 Hz, 1 H) 6.48 (dd, *J*=8.7, 2.6 Hz, 1 H) 7.40 - 7.42 (m, 3 H) 7.56 (d, *J*=15.5 Hz, 1 H) 7.62 - 7.65 (m, 2 H) 7.81 (d, *J*=8.7 Hz, 1 H) 7.87 (d, *J*=15.5 Hz, 1 H), 13.44 (s, 1 H). ¹³C NMR (100 MHz, CDCl₃) 191.84 - 166.73 - 166.25 - 144.39 - 134.81 - 131.27 - 130.67 - 129.00 - 128.55 - 120.32 - 114.12 - 107.74 - 101.12 - 55.59.

(E)-3-(3,5-dimethoxyphenyl)-1-(2-hydroxy-4-methoxyphenyl)prop-2-en-1-one (22)



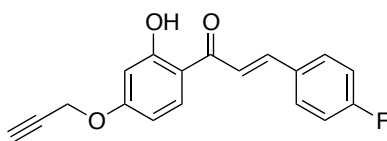
Mp: 163-165°C (EtOH). Yield = 66%. ¹H NMR (400 MHz, CDCl₃) δ 3.86 (s, 9 H) 6.47 – 6.49 (m, 2 H) 6.54 (t, *J*=2.2 Hz, 1 H) 6.78 (d, *J*=2.2 Hz, 2 H) 7.52 (d, *J*=15.3 Hz, 1 H) 7.79 (d, *J*=15.3 Hz, 1 H) 7.81 (d, *J*=8.5 Hz, 1 H).

(E)-1-(2-hydroxy-4-((3-methylbut-2-en-1-yl)oxy)phenyl)-3-phenylprop-2-en-1-one (23)



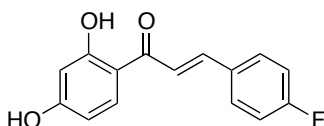
Mp: 87-89°C (EtOH). Yield = 65%. ¹H NMR (300 MHz, CDCl₃) δ 1.76 (s, 3 H) 1.81 (s, 3) 4.56 (d, *J*=6.0 Hz, 2 H) 5.47 (t, *J*=6.0 Hz, 1 H) 6.49 (m, 2 H) 7.43 (m, 3 H) 7.60 (d, *J*=15.3 Hz, 1 H) 7.63 (m, 2 H) 7.82 (d, *J*=9.0 Hz, 1 H) 7.89 (d, *J*=15.3 Hz, 1 H) 13.45 (s, 1 H). ¹³C NMR (75 MHz, CDCl₃) d 191.2 - 166.1 - 165.0 - 143.7 - 138.6 - 134.2 - 130.7 - 130.1 - 128.4 - 128.4 - 128.0 - 119.8 - 118.1 - 113.4 - 107.7 - 101.2 - 64.6 - 25.3 - 17.7.

(E)-3-(4-fluorophenyl)-1-(2-hydroxy-4-(prop-2-yn-1-yloxy)phenyl)prop-2-en-1-one (24)



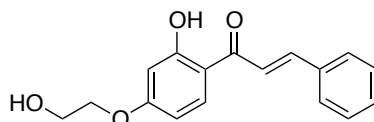
Mp: 95-98°C (EtOH). Yield = 68%. ¹H NMR (200 MHz CDCl₃) δ 2.32 (t, 1 H) 4.50 (m, 2 H) 6.28 – 6.32 (m, 2 H) 6.82 – 7.00 (m, 2 H) 7.20 – 7.42 (m, 3 H) 7.56 – 7.64 (m, 2 H).

(E)-1-(2,4-dihydroxyphenyl)-3-(4-fluorophenyl)prop-2-en-1-one (25)



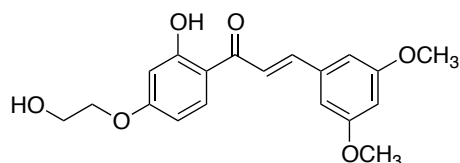
Mp: 125-127°C (EtOH). Yield = 35%. ¹H NMR (500 MHz, DMSO-*d*₆) δ 6.35 (d, *J*=2.4 Hz, 1 H) 6.46 (dd, *J*=8.9, 2.4 Hz, 1 H) 7.47 (m, 3 H) 7.82 (d, *J*=15.2 Hz, 1 H) 7.90 (m, 2 H) 8.00 (d, *J*=15.2 Hz, 1 H) 8.22 (d, *J*=8.9 Hz, 1 H) 10.75 (s, 1 H) 13.41 (s, 1 H). ¹³C NMR (125 MHz, DMSO-*d*₆) δ 191.4 - 165.8 - 165.2 - 143.6 - 134.6 - 133.1 - 130.6 - 129.0 - 128.8 - 121.3 - 113.0 - 108.3 - 102.6.

(E)-1-(2-hydroxy-4-(2-hydroxyethoxy)phenyl)-3-phenylprop-2-en-1-one (26)



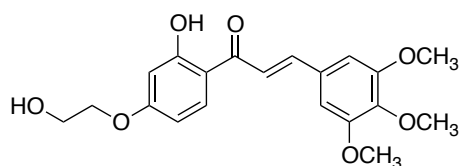
Mp: 77-80°C (EtOH). Yield = 48%. ¹H NMR (300 MHz CDCl₃) δ 1.95 (t, *J*=6.0 Hz, 1 H) 4.00 - 4.04 (m, 2 H) 4.13 – 4.18 (m, 2 H) 6.47 (d, *J*=2.4 Hz, 1 H) 6.55 (dd, *J*=8.8, 2.4 Hz, 1 H) 7.11 – 7.16 (m, 2 H) 7.40 - 7.43 (m, 3 H) 7.46 (d, *J*=15.6 Hz, 1 H) 7.85 (d, *J*=15.2 Hz, 1 H) 7.87 (d, *J*=2.4 Hz, 1 H).

(E)-3-(3,5-dimethoxyphenyl)-1-(2-hydroxy-4-(2-hydroxyethoxy)phenyl)prop-2-en-1-one (27)



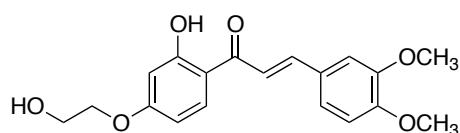
Mp: 161-163°C (EtOH). Yield = 78%. ^1H NMR (400 MHz CDCl_3) δ 3.85 (s, 6 H) 4.01 (t, 2 H) 4.15 (t, 2 H) 6.49 – 6.55 (m, 3 H) 6.79 (d, $J=15.2$ Hz, 2 H) 7.53 (d, $J=8.61$ Hz, 1 H) 7.79 (s, 1 H) 7.84 (d, $J=9.2$ Hz, 1 H). ^{13}C NMR (100 MHz, CDCl_3) δ 198.01 - 166.59 - 161.10 - 150.97 - 144.57 - 131.37 - 120.77 - 107.88 - 106.48 - 102.84 - 101.78 - 82.75 - 69.52 - 61.11 - 56.90 - 55.50.

(E)-1-(2-hydroxy-4-(2-hydroxyethoxy)phenyl)-3-(3,4,5-trimethoxyphenyl)prop-2-en-1-one (28)



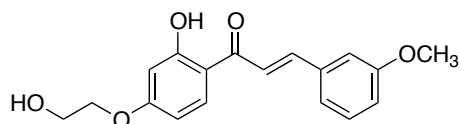
Mp: 186-188°C (EtOH). Yield = 71%. ^1H NMR (200 MHz CDCl_3) δ 3.91 (s, 3 H) 3.94 (s, 6 H) 4.02 (m, 2 H) 4.13 – 4.17 (m, 2 H) 6.48 – 6.55 (m, 2 H) 6.87 (s, 2 H) 7.45 (d, $J=15.4$ Hz, 1 H) 7.78 (s, 1 H) 7.83 – 7.87 (m, 1 H).

(E)-3-(3,4-dimethoxyphenyl)-1-(2-hydroxy-4-(2-hydroxyethoxy)phenyl)prop-2-en-1-one (29)



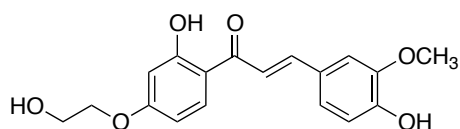
Mp: 161-163°C (EtOH). Yield = 78%. ¹H NMR (200 MHz CDCl₃) δ 3.95 – 4.01 (m, 8 H) 4.13 – 4.17 (m, 2 H) 6.48 – 6.54 (m, 2 H) 6.91 (d, *J*=8.4 Hz, 2 H) 7.16 – 7.27 (m, 3 H) 7.44 (d, *J*=15.4 Hz, 1 H) 7.82 – 7.99 (m, 2 H).

(*E*)-1-(2-hydroxy-4-(2-hydroxyethoxy)phenyl)-3-(3-methoxyphenyl)prop-2-en-1-one (30)



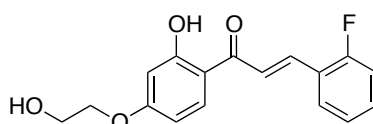
Mp: 106-108°C (EtOH). Yield = 59%. ¹H NMR (300 MHz CDCl₃) δ 3.95 (s, 3 H), 3.98 (t, *J*=5.6 Hz, 2 H) 4.13 (t, *J*=5.6 Hz, 2 H) 6.48 (d, *J*=2.4 Hz, 1 H) 6.50 (dd, *J*=8.8, 2.4 Hz, 1 H) 6.95 (dd, *J*=8.8, 1.8 Hz, 1 H) 7.12 (d, *J*=1.8 Hz, 1 H) 7.23 - 7.35 (m, 2 H) 7.43 (d, *J*=16.0 Hz, 1 H) 7.81 (d, *J*=8.4 Hz, 1 H) 7.84 (d, *J*=15.2 Hz, 1 H).

(*E*)-3-(4-hydroxy-3-methoxyphenyl)-1-(2-hydroxy-4-(2-hydroxyethoxy)phenyl)prop-2-en-1-one (31)



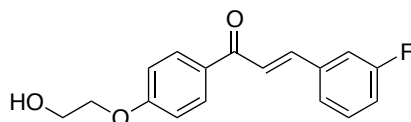
Mp: 124-127°C (EtOH). Yield = 41%. ¹H NMR (200 MHz CDCl₃) δ 1.53 (br, 1 H) 3.97 – 4.01 (m, 5 H) 4.13 – 4.16 (m, 2 H) 5.92 (br, 1 H) 6.47 – 6.54 (m, 2 H) 6.94 – 6.98 (m, 1 H) 7.13 (m, 1 H) 7.23 – 7.26 (m, 2 H) 7.38 – 7.45 (m, 1 H) 7.82 – 7.87 (m, 2 H).

(*E*)-3-(2-fluorophenyl)-1-(2-hydroxy-4-(2-hydroxyethoxy)phenyl)prop-2-en-1-one (32)



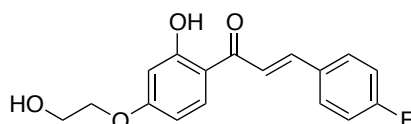
Mp: 128-130°C (EtOH). Yield = 63%. ¹H NMR (200 MHz CDCl₃) δ 1.53 (br, 1 H) 3.97 – 4.02 (m, 2 H) 4.12 – 4.17 (m, 2 H) 6.48 – 6.55 (m, 2 H) 7.14 – 7.26 (m, 2 H) 7.37 – 7.42 (m, 2 H) 7.73 (s, 1 H) 7.83 (dd, *J*=8.8 Hz, 1 H) 7.96 (d, *J*=15.8 Hz, 1 H).

(*E*)-3-(3-fluorophenyl)-1-(4-(2-hydroxyethoxy)phenyl)prop-2-en-1-one
(33)



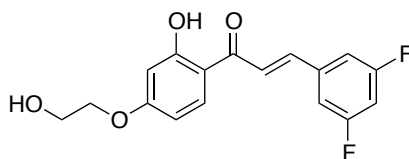
Mp: 130-132°C (EtOH). Yield = 65%. ¹H NMR (400 MHz CDCl₃) δ 1.95 (t, *J*=6.0 Hz, 1 H) 4.00 - 4.03 (m, 2 H) 4.12 – 4.17 (m, 2 H) 6.49 (d, *J*=2.4 Hz, 1 H) 6.52 (dd, *J*=8.8, 2.4 Hz, 1 H) 7.11 – 7.16 (m, 1 H) 7.35 (d, *J*=8.8 Hz, 1 H) 7.40 -7.43 (m, 3 H) 7.56 (d, *J*=15.6 Hz, 1 H) 7.84 (d, *J*=8.0 Hz, 1 H) 7.85 (d, *J*=15.2 Hz, 1 H).

(*E*)-3-(4-fluorophenyl)-1-(2-hydroxy-4-(2-hydroxyethoxy)phenyl)prop-2-en-1-one
(34)



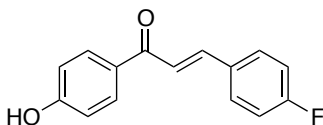
Mp: 136-139°C (EtOH). Yield = 66%. ¹H NMR (400 MHz CDCl₃) δ 1.95 (t, *J*=6.0 Hz, 1 H) 4.00 (t, *J*=5.6 Hz, 2 H) 4.13 (t, *J*=5.6 Hz, 2 H) 6.44 (d, *J*=2.4 Hz, 1 H) 6.49 (dd, *J*=8.8, Hz, 1 H) 7.13 (t, *J*=8.8 Hz, 2 H) 7.58 (d, *J*=16.0 Hz, 1 H) 7.68 (d, *J*=8.8 Hz, 2H) 7.79 (d, *J*=8.0 Hz, 1 H) 7.85 (d, *J*=15.2 Hz, 1 H).

(E)-3-(3,5-difluorophenyl)-1-(2-hydroxy-4-(2-hydroxyethoxy)phenyl)prop-2-en-1-one (35)



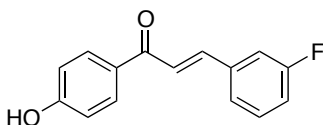
Mp: 131-133°C (EtOH). Yield = 42%. ¹H NMR (200 MHz CDCl₃) δ 4.03 (m, 2 H) 4.16 (m, 2 H) 6.44 – 6.56 (m, 2 H) 6.87 (m, 1 H) 7.14 – 7.17 (m, 2 H) 7.54 (d, *J*=15.4 Hz, 1 H) 7.73 (s, 1 H) 7.82 (d, *J*=15.4 Hz, 1 H).

(E)-3-(4-fluorophenyl)-1-(4-hydroxyphenyl)prop-2-en-1-one



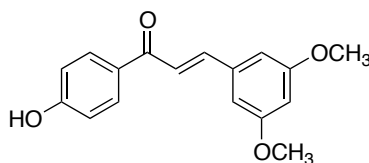
Pale oil. Yield = 39%. ¹H NMR (400 MHz CDCl₃) δ 6.92 – 6.95 (m, 2 H) 7.16 – 7.20 (m, 2 H) 7.69 (d, *J*=15.6 Hz, 1 H) 7.79 (d, *J*=15.6 Hz, 1 H) 7.83 – 7.87 (m, 2 H) 8.03 – 8.06 (m, 2 H).

(E)-3-(3-fluorophenyl)-1-(4-hydroxyphenyl)prop-2-en-1-one



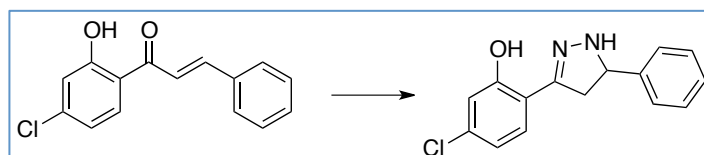
Pale oil. Yield = 35%. ¹H NMR (400 MHz CDCl₃) δ 6.93 – 6.95 (m, 2 H) 7.14 – 7.18 (m, 1 H) 7.43 – 7.49 (m, 1 H) 7.57 -7.70 (m, 3 H) 7.89 (d, *J*=15.6 Hz, 1 H) 8.06 – 8.08 (m, 2 H).

(E)-3-(3,5-dimethoxyphenyl)-1-(4-hydroxyphenyl)prop-2-en-1-one



Pale oil. Yield = 45%. ^1H NMR (400 MHz CDCl_3) δ 3.81 (s, 6 H) 6.53 (t, 1 H) 6.92 – 6.95 (m, 4 H) 7.62 (d, $J=15.6$ Hz, 1 H) 7.80 (d, $J=15.6$ Hz, 1 H) 8.03 – 8.05 (m, 2 H).

4.5.14. Cyclisation



5-chloro-2-(5-phenyl-4,5-dihydro-1H-pyrazol-3-yl)phenol (8**)**

To a solution of chalcones (1 eq.) in ethanol, an excess of hydrazine hydrate (98% aqueous solution, 0.4 mL per mg of chalcone) was added. The mixture was then refluxed for a period of 3 h and then was cooled. The solvent was removed under reduced pressure and dichloromethane was added. The mixture was washed twice with an aqueous solution of HCl (0.1 N). The organic layers were dried over sodium sulfate and the solvent was removed under reduced pressure. The crude was crystallized from hot methanol to give a yellow solid (yield = 62%).

^1H NMR (400 MHz CDCl_3) δ 3.11 (dd, $J=16.40, 8.71$ Hz, 1 H) 3.53 (dd, $J=16.8, 10.4$ Hz, 1 H) 4.89 (t, $J=10.8$ Hz, 1 H) 6.85 (dd, $J=8.43, 2.02$ Hz, 1 H) 7.02 (d, $J=2.02$ Hz, 1 H) 7.06 (d, $J=8.25$ Hz, 1 H) 7.32 – 7.37 (m, 5 H).

5. References

1. Rusak, G., Effects of Structurally Related Flavonoids on hsp Gene Expression in Human Promyeloid Leukaemia Cells. Gutzeit, H. O., Ed. 2002; Vol. 40, pp 267-273.
2. Li, Y.; Fang, H.; Xu, W., Recent advance in the research of flavonoids as anticancer agents. *Mini Rev Med Chem* **2007**, 7 (7), 663-78.
3. Pietta, P.-G., Flavonoids as Antioxidants. *Journal of Natural Products* **2000**, 63 (7), 1035-1042.
4. Pietta, P. G.; Mauri, P. L.; Simonetti, P.; Testolin, G., HPLC and MEKC determination of major flavonoids in selected food pools. *Fresenius Journal of Analytical Chemistry* **1995**, 352 (7-8), 788-792.
5. Franke, A. A.; Custer, L. J.; Cerna, C. M.; Narala, K. K., Quantitation of phytoestrogens in legumes by HPLC. *Journal of Agricultural and Food Chemistry* **1994**, 42 (9), 1905-1913.
6. Beecher, G. R., Overview of dietary flavonoids: nomenclature, occurrence and intake. *J Nutr* **2003**, 133 (10), 3248S-3254S.
7. Grotewold, E., *The Science of Flavonoids*. Springer: 2006.
8. Aherne, S. A.; O'Brien, N. M., Dietary flavonols: Chemistry, food content, and metabolism. *Nutrition* **2002**, 18 (1), 75-81.
9. Gilbert, E. R.; Liu, D., Flavonoids influence epigenetic-modifying enzyme activity: structure - function relationships and the therapeutic potential for cancer. *Curr Med Chem* **2010**, 17 (17), 1756-68.
10. Stobiecki, M.; Kachlicki, P., Isolation and Identification of Flavonoids. In *The Science of Flavonoids*, Grotewold, E., Ed. Springer: Columbus, 2006; pp 47-69.
11. Kühnau, J., The flavonoids. A class of semi-essential food components: their role in human nutrition. *World Rev Nutr Diet* **1976**, 24, 117-91.
12. Smith, G. J.; Thomsen, S. J.; Markham, K. R.; Andary, C.; Cardon, D., The photostabilities of naturally occurring 5-hydroxyflavones, flavonols, their glycosides and their aluminium complexes. *Journal of Photochemistry and Photobiology A: Chemistry* **2000**, 136 (1-2), 87-91.

13. Harborne, J. B.; Williams, C. A., Advances in flavonoid research since 1992. *Phytochemistry* **2000**, *55* (6), 481-504.
14. Clifford, M. N., A nomenclature for phenols with special reference to tea. *Crit. Rev. Food Sci. Nutr.* **2001**, *41*, 393-397.
15. Okuda, T.; Yoshida, T.; Hatano, T., Classification of oligomeric hydrolysable tannins and specificity of their occurrence in plants. *Phytochemistry* **1993**, *32* (3), 507-521.
16. Mazza, G.; Miniati, E., Anthocyanins in Fruits, Vegetables and Grains. CRC Press: Boca Raton, FL, 1993.
17. Pietta, P.; Simonetti, P., 19 - Dietary Flavonoids and Interaction with Physiologic Antioxidants. In *Antioxidant Food Supplements in Human Health*, Lester, P.; Midori Hiramatsu and Toshikazu YoshikawaA2 - Lester Packer, M. H.; Toshikazu, Y., Eds. Academic Press: San Diego, 1999; pp 283-308.
18. Harborne, J. B., *The flavonoids: Advances in Research Since 1986*. Chapman and Hall: London, 1994.
19. Brenda W, S., Flavonoid biosynthesis: 'new' functions for an 'old' pathway. *Trends in Plant Science* **1996**, *1* (11), 377-382.
20. Colic, M.; Pavelic, K., Molecular mechanisms of anticancer activity of natural dietetic products. *Journal of Molecular Medicine-Jmm* **2000**, *78* (6), 333-336.
21. Nijveldt, R. J.; van Nood, E.; van Hoorn, D. E. C.; Boelens, P. G.; van Norren, K.; van Leeuwen, P. A. M., Flavonoids: a review of probable mechanisms of action and potential applications. *American Journal of Clinical Nutrition* **2001**, *74* (4), 418-425.
22. Duthie, S. J.; Dobson, V. L., Dietary flavonoids protect human colonocyte DNA from oxidative attack in vitro. *European Journal of Nutrition* **1999**, *38* (1), 28-34.
23. Lin, J.-K.; Weng, M.-S., Flavonoids as Nutraceuticals. In *The Science of Flavonoids*, Grotewold, E., Ed. Springer: Columbus, 2006; pp 213-238.
24. Williamson, G.; Faulkner, K.; Plumb, G. W., Glucosinolates and phenolics as antioxidants from plant food. *European Journal of Cancer Prevention* **1998**, *7* (1), 17-21.

25. Cappelletti, V.; Fioravanti, L.; Miodini, P.; Di Fronzo, G., Genistein blocks breast cancer cells in the G2M phase of the cell cycle. *Journal of Cellular Biochemistry* **2000**, 79 (4), 594-600.
26. Blake, D.; Winyard, P. G., *Immunopharmacology of Free Radical Species*. Academic Press: San Diego, 1995.
27. Patil, C. B.; Mahajan, S. K.; Katti, S. A., Chalcone: A Versatile Molecule. *Journal of Pharmaceutical Sciences and Research* **2009**, 1 (3), 11-22.
28. Patel, J. M., A Review of Potential Health Benefits of Flavonoids. *Lethbridge Undergraduate Research Journal* **2008**, 3 (2).
29. Terao, J.; Kawai, Y.; Murota, K., Vegetable flavonoids and cardiovascular disease. *Asia Pac J Clin Nutr* **2008**, 17 Suppl 1, 291-3.
30. Szent-Györgyi, A.; Rusznyak, I., Vitamin nature of flavones. *Nature* **1936**, 138 (3497), 798.
31. Hertog, M. G. L.; Feskens, E. J. M.; Kromhout, D.; Hollman, P. C. H.; Katan, M. B., Dietary antioxidant flavonoids and risk of coronary heart disease: the Zutphen Elderly Study. *The Lancet* **1993**, 342 (8878), 1007-1011.
32. Narayana, K. R.; Reddy, S. M.; Chaluvadi, M. R.; Krishna, D. R., Bioflavonoids classification, pharmacological, biochemical effects and therapeutic potential. *Indian Journal of Pharmacology* **2001**, 33, 2-16.
33. Hosokawa, N.; Hirayoshi, K.; Nakai, A.; Hosokawa, Y.; Marui, N.; Yoshida, M.; Sakai, T.; Nishino, H.; Aoike, A.; Kawai, K., Flavonoids inhibit the expression of heat shock proteins. *Cell structure and function* **1990**, 15 (6), 393-401.
34. Go, M. L.; Wu, X.; Liu, X. L., Chalcones: An Update on Cytotoxic and Chemoprotective Properties. *Current Medicinal Chemistry* **2005**, 12, 483-499.
35. Bandgar, B. P.; Gawande, S. S.; Bodade, R. G.; Totre, J. V.; Khobragade, C. N., Synthesis and biological evaluation of simple methoxylated chalcones as anticancer, anti-inflammatory and antioxidant agents. *Bioorganic & Medicinal Chemistry* **2010**, 18 (3), 1364-1370.
36. Rojas, J.; Payá, M.; Dominguez, J. N.; Luisa Ferrándiz, M., The synthesis and effect of fluorinated chalcone derivatives on nitric oxide production. *Bioorganic & Medicinal Chemistry Letters* **2002**, 12 (15), 1951-1954.
37. Laskin, D. L.; Pendino, K. J., Macrophages and inflammatory mediators in tissue injury. *Annu Rev Pharmacol Toxicol* **1995**, 35, 655-77.

38. Kaur, H.; Halliwell, B., Evidence for nitric oxide-mediated oxidative damage in chronic inflammation Nitrotyrosine in serum and synovial fluid from rheumatoid patients. *FEBS Letters* **1994**, *350* (1), 9-12.
39. Satyanarayana, M.; Tiwari, P.; Tripathi, B. K.; Srivastava, A. K.; Pratap, R., Synthesis and antihyperglycemic activity of chalcone based aryloxypropanolamines. *Bioorganic & Medicinal Chemistry* **2004**, *12* (5), 883-889.
40. Reddy, M. V. B.; Su, C.-R.; Chiou, W.-F.; Liu, Y.-N.; Chen, R. Y.-H.; Bastow, K. F.; Lee, K.-H.; Wu, T.-S., Design, synthesis, and biological evaluation of Mannich bases of heterocyclic chalcone analogs as cytotoxic agents. *Bioorganic & Medicinal Chemistry* **2008**, *16* (15), 7358-7370.
41. Awasthi, S.; Mishra, N.; Kumar, B.; Sharma, M.; Bhattacharya, A.; Mishra, L.; Bhasin, V., Potent antimalarial activity of newly synthesized substituted chalcone analogs in vitro. *Medicinal Chemistry Research* **2009**, *18* (6), 407-420.
42. Liu, M.; Wilairat, P.; Croft, S. L.; Tan, A. L.-C.; Go, M.-L., Structure-activity relationships of antileishmanial and antimalarial chalcones. *Bioorganic & Medicinal Chemistry* **2003**, *11* (13), 2729-2738.
43. Aponte, J. C.; Verástegui, M.; Málaga, E.; Zimic, M.; Quiliano, M.; Vaisberg, A. J.; Gilman, R. H.; Hammond, G. B., Synthesis, Cytotoxicity, and Anti-Trypanosoma cruzi Activity of New Chalcones. *Journal of Medicinal Chemistry* **2008**, *51* (19), 6230-6234.
44. Daskiewicz, J. B.; Comte, G.; Barron, D.; Di Pietro, A.; Thomasson, F., Organolithium mediated synthesis of prenylchalcones as potential inhibitors of chemoresistance. *Tetrahedron Letters* **1999**, *40* (39), 7095-7098.
45. Sebti, S. d.; Solhy, A.; Tahir, R.; Boulaajaj, S. d.; Mayoral, J. A.; Fraile, J. M.; Kossir, A.; Oumimoun, H., Calcined sodium nitrate/natural phosphate: an extremely active catalyst for the easy synthesis of chalcones in heterogeneous media. *Tetrahedron Letters* **2001**, *42* (45), 7953-7955.
46. Eddarir, S.; Cotellet, N.; Bakkour, Y.; Rolando, C., An efficient synthesis of chalcones based on the Suzuki reaction. *Tetrahedron Letters* **2003**, *44* (28), 5359-5363.

47. Stoyanov, E. V.; Champavier, Y.; Simon, A.; Basly, J.-P., Efficient liquid-Phase synthesis of 2'-Hydroxychalcones. *Bioorganic & Medicinal Chemistry Letters* **2002**, 12 (19), 2685-2687.
48. Iwata, S.; Nishino, T.; Inoue, H.; Nagata, N.; Satomi, Y.; Nishino, H.; Shibata, S., Antitumorigenic activities of chalcones (II). Photo-isomerization of chalcones and the correlation with their biological activities. *Biol Pharm Bull* **1997**, 20 (12), 1266-70.
49. Rastelli, G.; Antolini, L.; Benvenuti, S.; Costantino, L., Structural bases for the inhibition of aldose reductase by phenolic compounds. *Bioorganic & Medicinal Chemistry* **2000**, 8 (5), 1151-1158.
50. Amolins, M. W.; Blagg, B. S., Natural product inhibitors of Hsp90: potential leads for drug discovery. *Mini Rev Med Chem* **2009**, 9 (2), 140-52.
51. Jolly, C.; Morimoto, R. I., Role of the heat shock response and molecular chaperones in oncogenesis and cell death. *J Natl Cancer Inst* **2000**, 92 (19), 1564-72.
52. Subbarao Sreedhar, A.; Kalmár, É.; Csermely, P.; Shen, Y.-F., Hsp90 isoforms: functions, expression and clinical importance. *FEBS Letters* **2004**, 562 (1-3), 11-15.
53. Xiao, L.; Lu, X.; Ruden, D. M., Effectiveness of Hsp90 Inhibitors as Anti-Cancer Drugs. *Mini Reviews in Medicinal Chemistry* **2006**, 6 (10), 1137-1143.
54. Blagg, B. S. J.; Kerr, T. D., Hsp90 inhibitors: Small molecules that transform the Hsp90 protein folding machinery into a catalyst for protein degradation. *Medicinal Research Reviews* **2006**, 26 (3), 310-338.
55. Donnelly, A.; Blagg, B., Novobiocin and Additional Inhibitors of the Hsp90 C-Terminal Nucleotide-binding Pocket. *Current Medicinal Chemistry* **2008**, 15 (26), 2702-2717.
56. Soti, C.; Vermes, A.; Haystead, T. A.; Csermely, P., Comparative analysis of the ATP-binding sites of Hsp90 by nucleotide affinity cleavage: a distinct nucleotide specificity of the C-terminal ATP-binding site. *Eur J Biochem* **2003**, 270 (11), 2421-8.
57. Wandinger, S. K.; Richter, K.; Buchner, J., The Hsp90 chaperone machinery. *J Biol Chem* **2008**, 283 (27), 18473-7.

58. Hanahan, D.; Weinberg, R. A., The hallmarks of cancer. *Cell* **2000**, *100* (1), 57-70.
59. Hanahan, D.; Weinberg, R. A., Hallmarks of cancer: the next generation. *Cell* **2011**, *144* (5), 646-74.
60. DeBoer, C.; Meulman, P. A.; Wnuk, R. J.; Peterson, D. H., Geldanamycin, a new antibiotic. *J Antibiot (Tokyo)* **1970**, *23* (9), 442-7.
61. Whitesell, L.; Mimnaugh, E. G.; Decosta, B.; Myers, C. E.; Neckers, L. M., Inhibition of Heat-Shock Protein Hsp90-PP60 (v-Src) heteroprotein complex-formation by benzoquinone ansamycins-essential role for stress proteins in oncogenic transformation. *Proceedings of the National Academy of Sciences of the United States of America* **1994**, *91* (18), 8324-8328.
62. Neckers, L.; Schulte, T. W.; Mimnaugh, E., Geldanamycin as a potential anti-cancer agent: Its molecular target and biochemical activity. *Investigational New Drugs* **1999**, *17* (4), 361-373.
63. Taldone, T.; Sun, W.; Chiosis, G., Discovery and development of heat shock protein 90 inhibitors. *Bioorganic & Medicinal Chemistry* **2009**, *17* (6), 2225-2235.
64. Soga, S.; Shiotsu, Y.; Akinaga, S.; Sharma, S. V., Development of radicicol analogues. *Current cancer drug targets* **2003**, *3* (5), 359-69.
65. Soga, S.; Neckers, L. M.; Schulte, T. W.; Shiotsu, Y.; Akasaka, K.; Narumi, H.; Agatsuma, T.; Ikuina, Y.; Murakata, C.; Tamaoki, T.; Akinaga, S., KF25706, a novel oxime derivative of radicicol, exhibits in vivo antitumor activity via selective depletion of Hsp90 binding signaling molecules. *Cancer Research* **1999**, *59* (12), 2931-2938.
66. Ikuina, Y.; Amishiro, N.; Miyata, M.; Narumi, H.; Ogawa, H.; Akiyama, T.; Shiotsu, Y.; Akinaga, S.; Murakata, C., Synthesis and antitumor activity of novel O-carbamoylmethyloxime derivatives of radicicol. *Journal of Medicinal Chemistry* **2003**, *46* (12), 2534-2541.
67. Agatsuma, T.; Ogawa, H.; Akasaka, K.; Asai, A.; Yamashita, Y.; Mizukami, T.; Akinaga, S.; Saitoh, Y., Halohydrin and oxime derivatives of radicicol: Synthesis and antitumor activities. *Bioorganic & Medicinal Chemistry* **2002**, *10* (11), 3445-3454.
68. Yamamoto, K.; Garbaccio, R. M.; Stachel, S. J.; Solit, D. B.; Chiosis, G.; Rosen, N.; Danishefsky, S. J., Total synthesis as a resource in the discovery of potentially

valuable antitumor agents: Cycloproparadicicol. *Angewandte Chemie-International Edition* **2003**, 42 (11), 1280-1284.

69. Moulin, E.; Zoete, V.; Barluenga, S.; Karplus, M.; Winssinger, N., Design, synthesis, and biological evaluation of HSP90 inhibitors based on conformational analysis of radicicol and its analogues. *Journal of the American Chemical Society* **2005**, 127 (19), 6999-7004.

70. Chiosis, G.; Vilenchik, M.; Kim, J.; Solit, D., Hsp90: the vulnerable chaperone. *Drug Discovery Today* **2004**, 9 (20), 881-888.

71. Chiosis, G.; Huezo, H.; Rosen, N.; Mimnaugh, E.; Whitesell, L.; Neckers, L., 17AAG: Low target binding affinity and potent cell activity - Finding an explanation. *Molecular Cancer Therapeutics* **2003**, 2 (2), 123-129.

72. Chiosis, G.; Lucas, B.; Shtil, A.; Huezo, H.; Rosen, N., Development of a purine-scaffold novel class of Hsp90 binders that inhibit the proliferation of cancer cells and induce the degradation of Her2 tyrosine kinase. *Bioorganic & Medicinal Chemistry* **2002**, 10 (11), 3555-3564.

73. Dymock, B.; Barril, X.; Beswick, M.; Collier, A.; Davies, N.; Drysdale, M.; Fink, A.; Fromont, C.; Hubbard, R. E.; Massey, A.; Surgenor, A.; Wright, L., Adenine derived inhibitors of the molecular chaperone HSP90 - SAR explained through multiple X-ray structures. *Bioorganic & Medicinal Chemistry Letters* **2004**, 14 (2), 325-328.

74. Rowlands, M. G.; Newbatt, Y. M.; Prodromou, C.; Pearl, L. H.; Workman, P.; Aherne, W., High-throughput screening assay for inhibitors of heat-shock protein 90 ATPase activity. *Analytical Biochemistry* **2004**, 327 (2), 176-183.

75. Brough, P. A.; Aherne, W.; Barril, X.; Borgognoni, J.; Boxall, K.; Cansfield, J. E.; Cheung, K.-M. J.; Collins, I.; Davies, N. G. M.; Drysdale, M. J.; Dymock, B.; Eccles, S. A.; Finch, H.; Fink, A.; Hayes, A.; Howes, R.; Hubbard, R. E.; James, K.; Jordan, A. M.; Lockie, A.; Martins, V.; Massey, A.; Matthews, T. P.; McDonald, E.; Northfield, C. J.; Pearl, L. H.; Prodromou, C.; Ray, S.; Raynaud, F. I.; Roughley, S. D.; Sharp, S. Y.; Surgenor, A.; Walmsley, D. L.; Webb, P.; Wood, M.; Workman, P.; Wright, L., 4,5-diarylisoazole HSP90 chaperone inhibitors: Potential therapeutic agents for the treatment of cancer. *Journal of Medicinal Chemistry* **2008**, 51 (2), 196-218.

76. Yu, X. M.; Shen, G.; Neckers, L.; Blake, H.; Holzbeierlein, J.; Cronk, B.; Blagg, B. S. J., Hsp90 inhibitors identified from a library of novobiocin analogues. *Journal of the American Chemical Society* **2005**, *127* (37), 12778-12779.
77. Rosenhagen, M. C.; Söti, C.; Schmidt, U.; Wochnik, G. M.; Hartl, F. U.; Holsboer, F.; Young, J. C.; Rein, T., The heat shock protein 90-targeting drug cisplatin selectively inhibits steroid receptor activation. *Mol Endocrinol* **2003**, *17* (10), 1991-2001.
78. Palermo, C. M.; Westlake, C. A.; Gasiewicz, T. A., Epigallocatechin gallate inhibits aryl hydrocarbon receptor gene transcription through an indirect mechanism involving binding to a 90 kDa heat shock protein. *Biochemistry* **2005**, *44* (13), 5041-5052.
79. Wani, M. C.; Taylor, H. L.; Wall, M. E.; Coggon, P.; McPhail, A. T., Plant antitumor agents. VI. The isolation and structure of taxol, a novel antileukemic and antitumor agent from *Taxus brevifolia*. *Journal of the American Chemical Society* **1971**, *93* (9), 2325-7.
80. Byrd, C. A.; Bornmann, W.; Erdjument-Bromage, H.; Tempst, P.; Pavletich, N.; Rosen, N.; Nathan, C. F.; Ding, A., Heat shock protein 90 mediates macrophage activation by Taxol and bacterial lipopolysaccharide. *Proceedings of the National Academy of Sciences of the United States of America* **1999**, *96* (10), 5645-5650.
81. Mays, J. R.; Hill, S. A.; Moyers, J. T.; Blagg, B. S. J., The synthesis and evaluation of flavone and isoflavone chimeras of novobiocin and derrubone. *Bioorganic & Medicinal Chemistry* **2010**, *18* (1), 249-266.
82. Hadden, M. K.; Galam, L.; Gestwicki, J. E.; Matts, R. L.; Blagg, B. S. J., Derrubone, an inhibitor of the Hsp90 protein folding machinery. *Journal of Natural Products* **2007**, *70* (12), 2014-2018.
83. Wu, L. X.; Xu, J. H.; Huang, X. W.; Zhang, K. Z.; Wen, C. X.; Chen, Y. Z., Down-regulation of p210(bcr/abl) by curcumin involves disrupting molecular chaperone functions of Hsp90. *Acta Pharmacologica Sinica* **2006**, *27* (6), 694-699.
84. Giommarelli, C.; Zuco, V.; Favini, E.; Pisano, C.; Dal Piaz, F.; De Tommasi, N.; Zunino, F., The enhancement of antiproliferative and proapoptotic activity of HDAC inhibitors by curcumin is mediated by Hsp90 inhibition. *Cellular and Molecular Life Sciences* **2010**, *67* (6), 995-1004.

85. Qiu, X.; Du, Y.; Lou, B.; Zuo, Y.; Shao, W.; Huo, Y.; Huang, J.; Yu, Y.; Zhou, B.; Du, J.; Fu, H.; Bu, X., Synthesis and Identification of New 4-Arylidene Curcumin Analogues as Potential Anticancer Agents Targeting Nuclear Factor-kappa B Signaling Pathway. *Journal of Medicinal Chemistry* **2010**, *53* (23), 8260-8273.

*SECTION B: SYNTHESIS OF A
NEW CLASS OF POTENTIAL
NON- STEROIDAL
ANTIANDROGENS*

1. Introduction

1.1. The Androgen Receptor (AR)

Androgen receptor (AR), a member of the steroid receptor super-family, is a ligand-dependent transcription factor that mediates androgen action in cells. AR belongs to the largest class of DNA binding transcription factors, called nuclear receptors, comprised of 48 members. The members of this family are divided into three classes:

- Class I: containing receptors for estrogen, progesterone, mineralocorticoids, glucocorticoids and androgens;
- Class II: containing receptors for vitamin D, retinoids and thyroids;
- Class III: containing receptors for which ligands have not yet been identified, classified as “orphans”.

The AR is widely distributed among cardiac muscle, skeletal and smooth muscle, gastrointestinal vesicular thyroid follicular cells, adrenal cortex, liver, pineal, and numerous brain cortical and sub-cortical regions, including spinal motor neurons.

1.1.1. Structure and Function of AR

The AR DNA sequence is present in the X chromosome, which has 8 exons spanning 90 kb sequences encoding a 919 A.A. protein.¹ Like the PR and ER, AR exists as 2 isoforms, AR and AR-A, which lacks the first 187 amino acids of AR. However, this isoform is not as well characterized and its functions remain unknown.

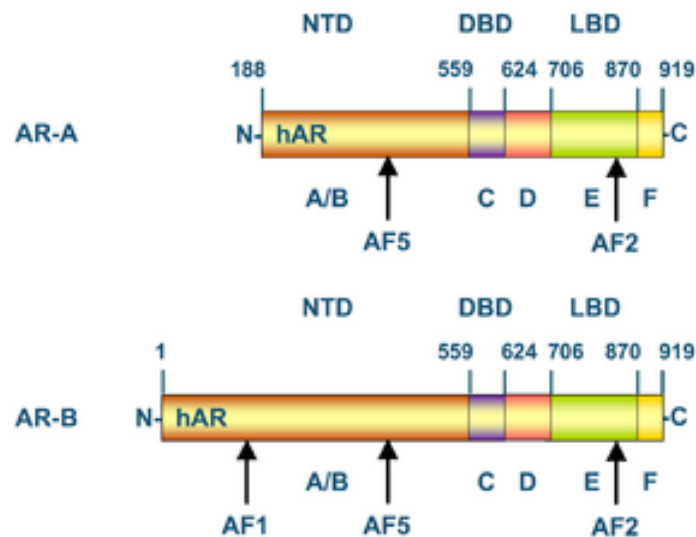


Fig. I. Structural domains of the two isoforms (AR-A and AR-B) of the human androgen receptor. Number above the bars refer to the amino acid residues that separate the domains starting from the N-terminus (left) to C-terminus (right). NTD = N-terminal domain, DBD = DNA binding domain. LBD = ligand binding domain. AF = activation function.
http://en.wikipedia.org/wiki/Androgen_receptor

AR is composed of the following major domains, labeled **A** through **F** (Fig. I):

- NH₂-terminal domain (NTD, **A/B** Fig. I), which contains the activation function AF-1, required for full ligand activated transcriptional activity and the activation function AF-5, responsible for the constitutive activity (activity without bound ligand). The NTD is the major coactivator interaction surface for AR and mediates the growth factor- and cell signaling-dependent transactivation;
- DNA-binding domain, (DBD, **C** Fig. I), which is the most highly conserved domain and, as the name indicates, is responsible for the binding of AR to the promiscuous androgen responsive element (ARE), 5'-AGAACANNNTGTTCT-3', on the promoter of androgen responsive genes². The DBD has 2 classical cysteine zinc finger motifs, responsible for DNA recognition and dimerization;
- “Hinge” region (**D** Fig. I) that lies between the DBD and the ligand binding domain (LBD). It is a lysine-rich region, important for the nuclear localization signal (NLS) of the receptor.^{3,4} Deletion of this domain eliminates nuclear localization of AR in the presence of ligand and, hence, loss of transcriptional activity;

- COOH-terminal ligand-binding domain (LBD, **E/F** Fig. I), responsible for ligand binding and is comprised of 11 helices. The LBD contains a second activation function (AF-2) that is important for the ligand-dependent activation of the receptor.

1.1.2. Mechanism of AR Action

In the absence of ligand, AR is maintained in an inactive conformation by heat shock proteins HSP 70 and HSP 90 in the cytoplasm (Fig. II). After binding to androgens, the C-terminal helix 12 in the LBD shifts position to close the ligand binding pocket. HSPs dissociate from the receptor, leading to homo-dimerization. This facilitates a series of conformational changes, following the dissociation of corepressor complexes. AR translocates to the nucleus and binds to Androgen Response Elements (AREs) in the promoter of androgen-responsive genes.

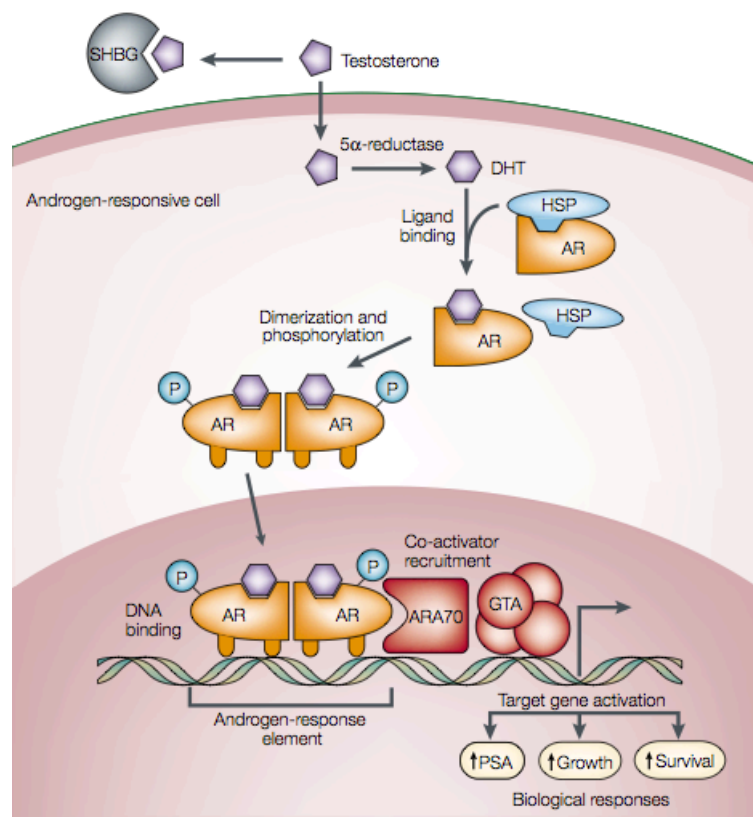


Fig. II. Androgen action⁵

Activated AR has been shown to recruit coregulators and general transcription factors, subsequently leading to the enhancement or repression of transcription of target genes.⁶ It regulates expression of AR target reproductive and non-reproductive tissues, including the prostate and seminal vesicles, male and female external genitalia, skin, testis, ovary, cartilage, sebaceous glands, hair follicles, sweat glands, genes.^{7,8}

1.2. Androgens: Testosterone Biosynthesis

The predominant circulating androgen, testosterone, T, is primarily (95%) secreted by the Leydig cells of the testes (males) and adrenal cortex (females and castrated males) under the control of the hypothalamic-pituitary-gonadal (HPG) axis (Fig. III). Testosterone is synthesized in response to luteinizing hormone (LH), which is secreted by the anterior pituitary gland. High levels of testosterone or exogenous androgens bind to androgen receptor (AR) in the CNS and exert feedback inhibition of testosterone synthesis.

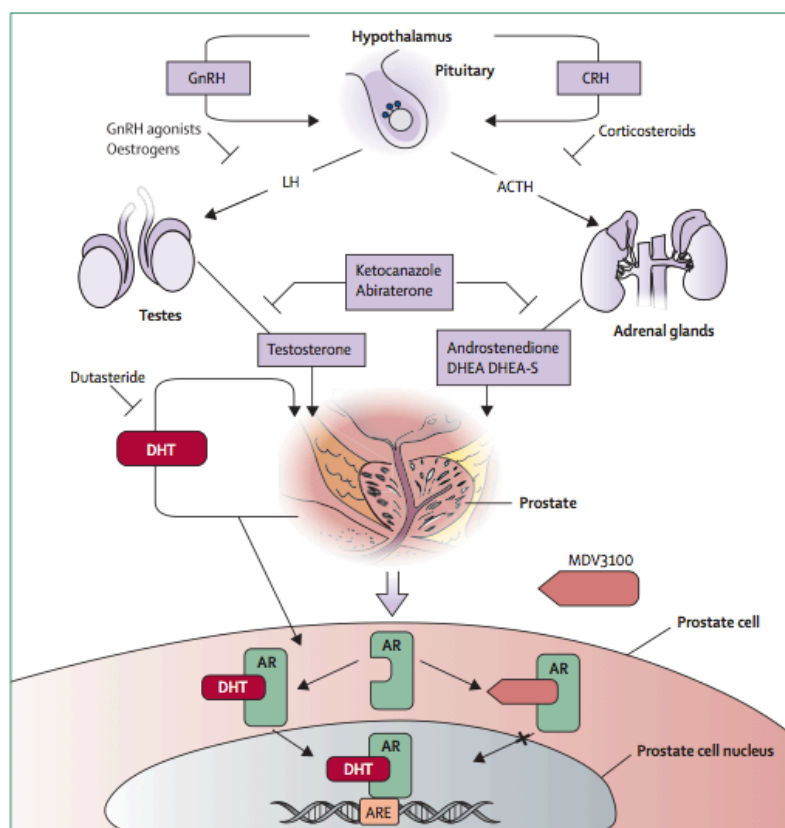


Fig. III. The androgen-signaling axis and its inhibitors⁹

Testosterone circulates in the blood, where it is bound to albumin and sex-hormone-binding globulin (SHBG), with a small fraction dissolved freely in the serum. When free testosterone enters prostate cells, 90% is converted to dihydrotestosterone (DHT) by the enzyme 5 α -reductase (SRD5A2). DHT is the more active hormone, having fivefold higher affinity for the androgen receptor (AR) than does testosterone.⁵

Endogenous androgens play crucial physiological roles in establishing and maintaining the male phenotype. Their actions are essential for the differentiation and growth of male reproductive organs, initiation and regulation of spermatogenesis, and control of male sexual behavior. In addition, androgens are important for the development of male characteristics in certain extragenital structures such as muscle, bone, hair, larynx, skin, lipid tissue, and kidney. In females, the precise physiological roles of androgens are not completely understood, but the age-related decline in circulating androgen levels has been linked to symptoms such as decreased libido and sexuality, lack of vigor, diminished well being, and loss of bone mineral density in postmenopausal women.¹⁰

Testosterone and dihydrotestosterone, endogenous AR agonists, and metribolone, a synthetic agonist with a steroidal skeleton (Fig. IV) have two polar moieties, a carbonyl group and a hydroxyl group, at the ends of the hydrophobic steroid skeleton. It is reasonable to assume that the two hydrophilic functional groups, as well as the hydrophobic core structure between them, play important roles for effective interaction with the AR ligand binding domain.¹¹

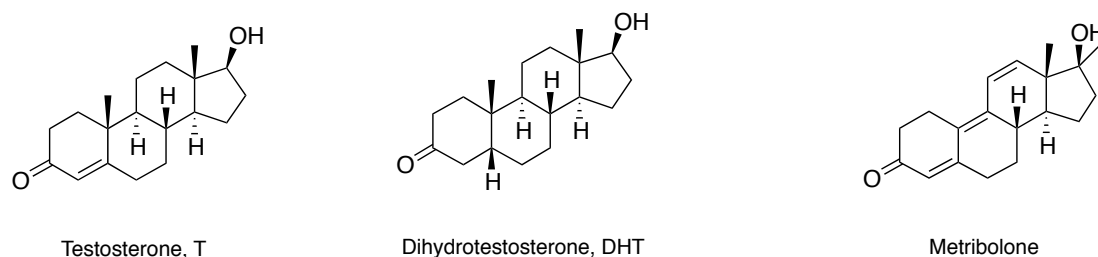


Fig. IV. The structure of steroidal ligands

1.3. Prostate Cancer

Prostate cancer is the most commonly diagnosed visceral cancer and second most common cause of cancer-related death in American men.

Prostate cancer may cause problems in urinating (nocturia, difficulty starting and maintaining a steady stream of urine, haematuria and dysuria), sexual dysfunctions (difficulty achieving erection or painful ejaculation). The most common additional symptom is bone pain, often in the vertebrae, pelvis or ribs. The cancer in the spine can also compress the spinal cord, causing leg weakness and urinary and faecal incontinence.^{12,13}

Heterogeneity in the biological behavior of prostate tumors may be a result of genetic variability or a result of exposure to different environmental factors, which influence genetic instability and types of mutation present. Prostate cancer tends to develop in men over fifty years old and the average age of diagnosis is seventy.

Genetic background may contribute to prostate cancer risk, as suggested by associations with race, family and specific gen. Men who have first-degree family members with prostate cancer appear to have double the risk of getting the disease compared to men without prostate cancer in the family. This risk appears to be greater for men with an affected brother than for men with an affected father. Numerous epidemiological studies indicate that prostate cancer incidence is 10–20 times higher in United States, in particular among black men, than in Asian countries.

Epidemiological studies suggest environmental factors such as **diet** may be critical factors in prostate cancer risk, in fact Japanese immigrants in United States prostate cancer with an increasing frequency. In addition similar trends have been observed in Japan since World War II, after the westernization of the Asian diet and life style.^{14,15}

High consumption of fat, especially animal fats, refined sugars, red meat, alcohol and dairy products in parallel with a lower intake of fruits and vegetables, fewer complex carbohydrates, vitamin D and fiber may increase the risks of contracting the disease.¹⁶

Mounting evidence suggests that obesity is linked to an array of illnesses

including diabetes, cardiovascular disease and various types of cancer.

The relationship of obesity and prostate cancer risk has been examined in several studies. Study conducted in men from the Cancer Prevention Study I and II (CPS I and CPS II) cohorts demonstrated that obese man had higher relative risk of prostate cancer death than the non-obese ones.

Sexually transmitted infections and elevated levels of testosterone in blood seem to increase the risk for prostate cancer.

1.3.1. Pathophysiology

The prostate is a part of the male reproductive system that helps make and store seminal fluid. It is located in the pelvis, under urinary bladder and in front of the rectum. Because of its location prostate disease often affect urination, ejaculation and rarely defecation.

The prostate contains many small glands, which make about twenty percent of the fluid constituting semen. In prostate cancer, the cells of these prostate glands mutate into cancer cells that require male hormone to work properly.

The process of prostate carcinogenesis from a normal glandular epithelium to cancer is not clearly understood. One of the proposed mechanisms explaining the effects of inflammation on prostate tissue suggests that presence of reactive oxygen species, nitric oxide and other reactive molecules released from activated macrophages results in massive tissue damage. In the attempt to regenerate lost/injured tissue epithelial cells proliferate at a higher rate. This gives rise to a lesion called proliferative inflammatory atrophy (PIA).^{17,18,19} PIA is characterized by increased proliferation in an attempt to regenerate injured tissue and infiltration of inflammatory cells. Moreover, this lesion demonstrates reduced expression of p27, a cyclin-dependent kinase inhibitor, and increased expression of Bcl-2, an anti-apoptotic protein. These gene expression patterns resemble those observed in prostatic intraepithelial neoplasia (PIN).²⁰ PIN is characterized by increased proliferation of the intraductal and intra-acinal epithelial cells associated with presence of multiple layers of cells and nuclear atypia (hyperchromasia, variability in nuclear shape and size)²¹. Glands containing PIN are sometimes larger than normal with disrupted layer of basal cells, that usually

difficult to observe. Although there is no proof that PIN is a cancer precursor, it is closely associated with cancer.

Other steps essential for progression toward prostate cancer include developing independence from growth factors that provide survival signals inhibiting apoptosis, gaining limitless proliferative potential and resistance to anti-growth signaling.²² Gaining ability to induce formation of new blood vessels (angiogenesis) is one of the essential steps in carcinogenesis. New blood vessels provide the tumor with adequate supply of nutrients and remove metabolites, and also facilitate local tissue invasion and facilitate distal metastasis. Prostate cancer most commonly metastasizes to the bones, lymphnodes, and may invade rectum, bladder and lower ureters after local progression. The route of metastasis to bone is thought to be venous as the prostatic venous plexus draining the prostate connects with the vertebral veins.²³

Growth of normal prostate epithelium is dependent on and regulated by androgens.

In order for the prostate tumor to gain independence of the androgen, androgen receptor signaling is subject to various mutations, which increase its sensitivity, allow for non-specific ligand binding, or amplify the number of receptors in the cellular membrane. Androgen independence is achieved through activation of ligand- independent signaling pathways in some cases.

Each one of the stages in prostate cancer development described above typically occurs over years and the entire process requires decades.

1.3.2. The Development of Androgen-Independent Prostate Cancer (AIPC)

The normal prostate and early-stage prostate cancer depend on androgens for growth and survival and androgen ablation causes regression of androgen-dependent tumors. However, many men fail this therapy and die of recurrent androgen-independent prostate cancer (AIPC). AIPC is a lethal form of prostate cancer that progresses and metastasizes. At the present, there is no effective therapy for it. There are five potential mechanisms by which AIPC can develop. Some of these also apply to other form of steroid-hormone-independent cancer,

such as breast cancer.⁵

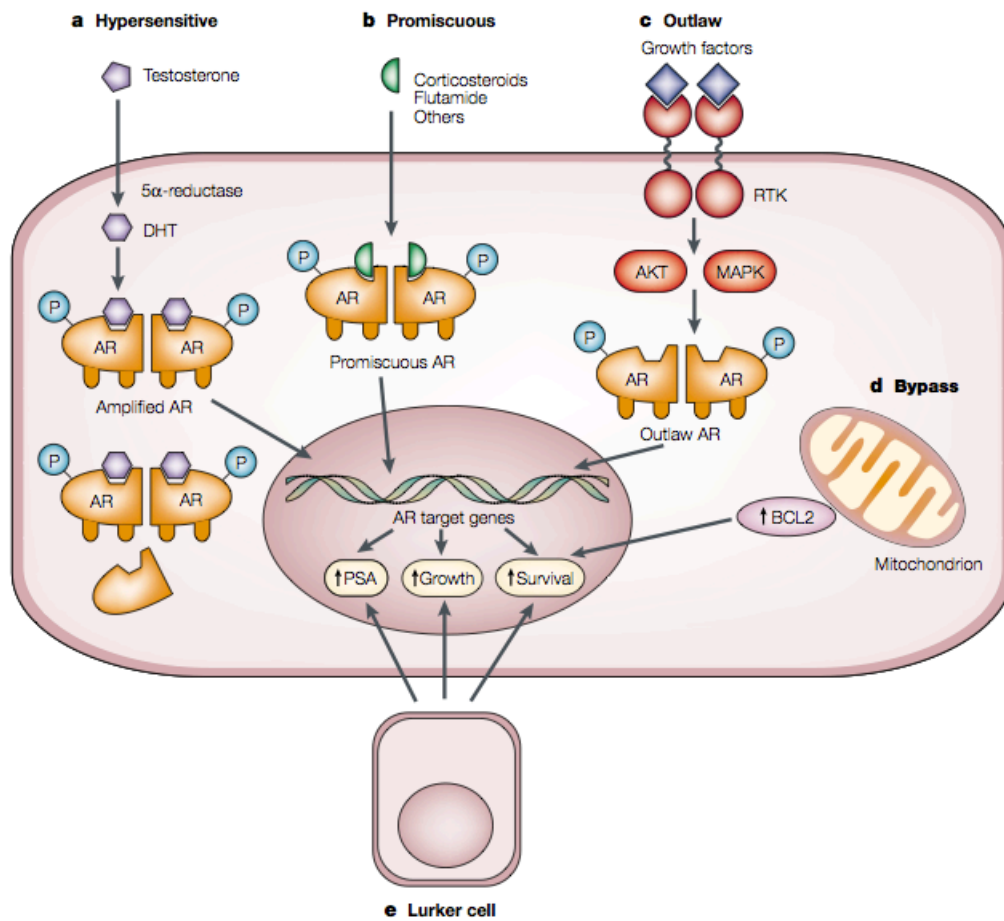


Fig. V. Five possible pathways to AIPC⁵

1.3.2.1. Hypersensitive Pathway (a, Fig. V)

The AR receptor increases its sensitivity to very low levels of androgens. There are several mechanisms that are responsible of this hypersensitivity.

More AR is produced; approximately 30% of tumors that become androgen-independent after the ablation have amplified the AR gene. AR-amplified tumors maintain dependency on residual androgens in serum.

Sometimes AR has enhanced sensibility to compensate for low levels of androgen. This pathway results in high-level expression of the AR, increased stability, and enhanced nuclear localization of AR in recurrent tumor cells.

In addition more testosterone is converted to the more potent DHT, by increasing 5 α -reductase activity.⁵

1.3.2.2. Promiscuous Pathway (b, Fig. V)

The specificity of the AR is broadened so that other non-androgenic molecules normally present in the circulation can activate it.

The most common mechanism of specificity lost, is the acquisition of genetic changes that lead to aberrant activation of AR.²⁴

The first AR mutation of this type was discovered in LNCaP cells.²⁵ LNCaP cells express high levels of AR, and androgens stimulate them to grow and express Prostate-Specific Antigen (PSA), a widely used and clinically important marker for prostate cancer cells. However, owing to a mutation in the AR, other steroid hormones, as well as the androgen antagonist flutamide, activate the AR and stimulate proliferation. Sequencing of the AR gene from LNCaP cells revealed a missense mutation in amino acid 877, which is located in the ligand-binding domain. This mutation results in the substitution of alanine for threonine at position 877 (T877A).^{5,26}

Hara et al. found exactly two different mutations in codon 741: W741C, where tryptophan is substituted by a cysteine and W741L (leucine; W741L). Probably, this AR mutation is responsible for the switch of bicalutamide from antagonist to agonist.²⁷

1.3.2.3. Outlaw Pathway (c, Fig. V)

In the outlaw pathway, receptor tyrosine kinases (RTKs) are activated, and the AR is phosphorylated by either the AKT (protein kinase B) or the mitogen-activated protein kinase (MAPK) pathway, producing a ligand-independent AR.

1.3.2.4. Bypass Pathway (d, Fig. V)

In the bypass pathway, parallel survival pathways, such as that involving the anti-apoptotic protein BCL2 (B-cell lymphoma 2), obviate the need for AR or its ligand.

1.3.2.5. Lurker Cell Pathway (e, Fig. V)

Finally, in the lurker cell pathway, androgen-independent cancer cells that are present all the time in the prostate — possibly epithelial stem cells — might be selected for by therapy.

1.3.3. Treatment of prostate cancer

AR hypersensitivity, as a result of AR gene mutation and/or amplification, over-expression of co-activators, often occurs and plays crucial roles in prostate cancer development, progression, and androgen-independent growth.^{8,28,29} Therefore, in most cases advanced prostate cancer, it has been directly linked to the androgen receptor (AR). Most prostatic tumors are stimulated to grow by androgens, and consequently androgen withdrawal is a well-established therapy for prostate cancer treatment. Androgen deprivation therapies consist of surgical castration, through orchiectomy or medical castration by administration of a luteinizing hormone-releasing hormone analogue (LHRH-A), such as goserelin (Fig. VI).³⁰

Goserelin acetate (Zoladex, AstraZeneca) is an injectable Gonadotropin releasing hormone superagonist (GnRH agonist), also known as a luteinizing hormone releasing hormone (LHRH) agonist. Structurally, it is a decapeptide. Goserelin stimulates the production of the sex hormones testosterone and estrogen in a non-physiological manner. This causes the disruption of the endogenous hormonal feedback systems, resulting in the down-regulation of testosterone and estrogen production.

Zoladex approved by the U.S. Food and Drug Administration in 1989 for treatment of prostate cancer.

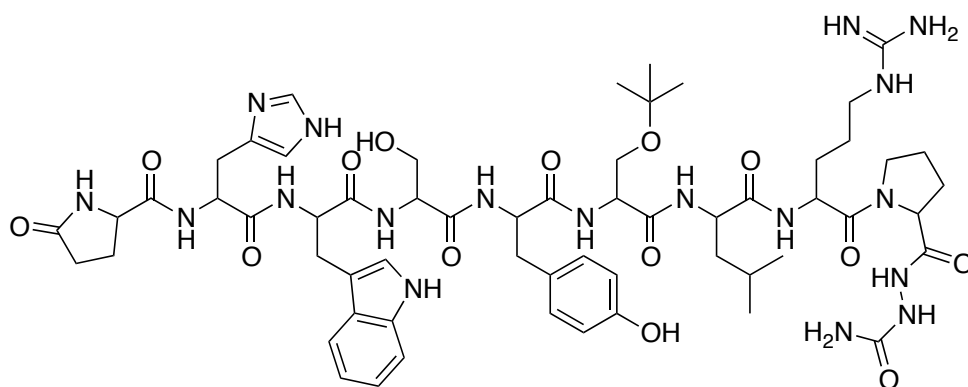


Fig. VI. Goserelin

However, although castration removes androgen release from the testes, androgen biosynthesis in the adrenals ($8 \pm 10\%$ of total circulating androgens) is not affected. In addition orchiectomy is unpopular with the patients and can result in psychological problems, and it exposes the elderly patients to trauma of surgery. Because of this, a widely used management strategy for advanced prostate cancer is a combination of surgical or chemical castration and administration of antiandrogens.³¹

Frequently, many patients stop responding to hormonal therapies and manifest a Hormone-Refractory metastatic Prostate Cancer (HRPC). Sawyers and co-workers demonstrated that HRPC was still dependent on AR ligand binding domain for growth.²⁸ Therapeutic options for HPCR patients are limited, with lack of evidence for long-term survival. In this case, Docetaxel is recommended as a possible treatment. It is an anti-mitotic chemotherapy medication, which interferes with cell division (Fig. VII).³²

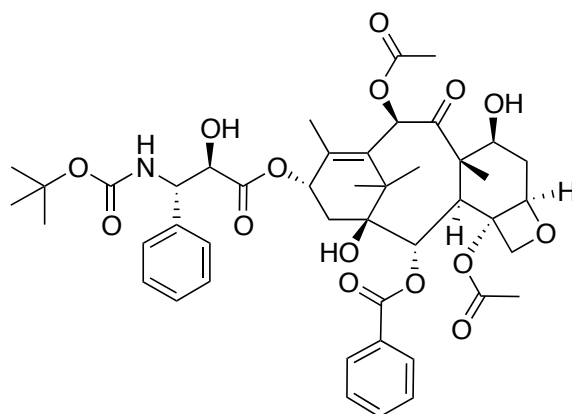


Fig. VII. Docetaxel

1.4. Antiandrogens

Antiandrogens bind to the AR and inhibit all androgens at the target cell level. In particular, antiandrogens compete with endogenous androgens for binding sites of the androgen receptors in the prostate cell nucleus, thereby promoting apoptosis and inhibiting prostate cancer growth. By contrast with androgens, however, the receptor-antiandrogen complex is unstable so that gene transcription and protein synthesis are not stimulated.³³

Ideally, an antiandrogen should possess high specificity and affinity for the androgen receptor, being devoid of other hormonal or anti-hormonal activity. Antiandrogens act by two primary mechanisms: inhibition of ligand (androgen) binding to the AR, and inhibition of androgen-independent activation of the receptor. It is more accurate to refer to these compounds as androgen-receptor antagonists, since they inhibit activation, whether this is androgen-mediated or not. These and other agents have been the subject of extensive clinical investigations for use either alone as single-agent therapy or in combination with a LHRH agonist.

There are two structurally distinct types of antiandrogen:

- Steroidal
- Nonsteroidal

The steroidal antiandrogen, cyproterone acetate (Fig. VIII), is currently available commercially. In addition, it is also a potent progestin and inhibits gonadotropin secretion. It is effective in the treatment of prostate cancer but among its side effects may be listed loss of libido, gynecomastia, fluid retention, thrombosis and an apparent hepatotoxicity associated with long-term use.

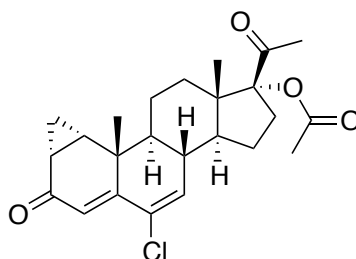


Fig. VIII. Cyproterone acetate

1.4.1. Nonsteroidal Antiandrogens

Nonsteroidal antiandrogens, such as bicalutamide (Casodex™), flutamide (Eulexin™) and nilutamide (Nilandron™) seem to be better tolerated than steroidal analogues, and are currently the only established means to avoid castration in the prostate cancer endocrine treatment (Fig. IX). These compounds are often referred to as “pure antiandrogens”, because they exert their effects through competitive inhibition of the binding of testosterone, and its metabolite 5 α -dihydrotestosterone (5 α -DHT), to the nuclear androgen receptor. As testosterone levels are not blocked by nonsteroidal antiandrogens, these drugs offer the possibility of maintaining sexual interest and potency. Within the class of nonsteroidal antiandrogens, there is variation in the degree to which ligand-independent activation is inhibited.

Flutamide is a pure antiandrogen; that is, it does not exhibit other hormonal activities. It is effective in the treatment of prostate cancer and the main side effect reported being gynecomastia. One consequence of its pure antiandrogenic profile is that it prevents androgens from exerting their negative feedback mechanism on the hypothalamus, which results in an increased pituitary secretion of, inter alia, luteinizing hormone (LH), which stimulates androgen production by the testes. The antagonist, therefore, brings about the increased production of natural agonist, which is effectively diminishes its efficacy at the target organ.³⁴

Nilutamide is a derivate of flutamide, which was approved in 1996 in combination with orchiectomy.⁹

Preclinical data suggest that non-steroidal antiandrogen bicalutamide may be a more effective drug in the treatment of prostate cancer with respect to flutamide and nilutamide.³⁴ It is best-tolerated, shows agonistic properties when the AR is over-expressed, such as in HRPC, and a superior pharmacokinetic profile along minor side effects.³⁵ It has a two-time increased affinity for the androgen receptor compared with flutamide and nilutamide, and a longer half-life of one week. Bicalutamide was derived from flutamide by addition of bulky 4-fluorophenylsulfonyl moiety.

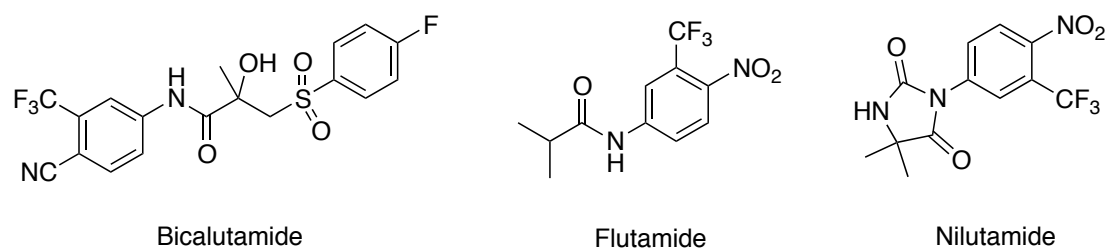


Fig. IX. Nonsteroidal antiandrogens

The endocrine therapy using nonsteroidal antiandrogens and LHRH analogues is initially very effective but is time-limited. Nearly half of all patients with these tumors develop resistance to this therapy after several years, suggesting the development of androgen-independent prostate cancer cells or the ability of adrenal androgens to support tumor growth. This leads to serious clinical inconveniences.

Surprisingly, clinical benefit has been observed following the withdrawal of anti-androgens (*Anti-Androgen Withdrawal Response, AAWR*) in a subset of prostate cancer patients with therapy-resistant disease.³⁶ It has been proposed that anti-androgen withdrawal syndrome is likely associated with AR mutations such as Thr877 → Ala, Trp741 → Leu and Trp741 → Cys which cause the antagonists flutamide and bicalutamide to act as agonists.²⁶

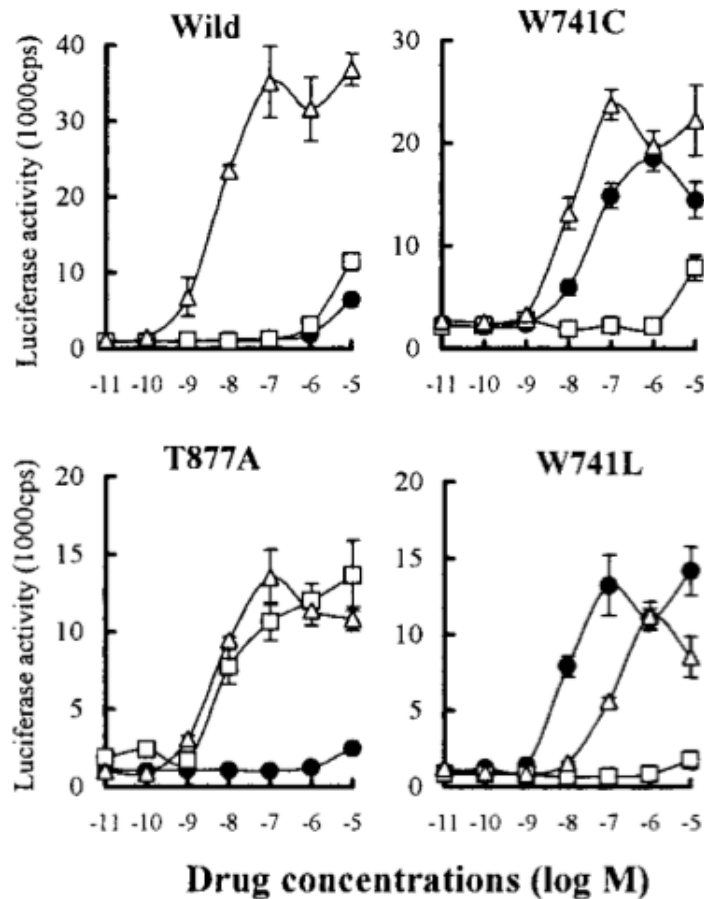


Fig. X. Transactivation assays. The W741C and W741L mutant ARs are activated by bicalutamide. Luciferase activity was assayed 24h after treatment: bicalutamide, ●, hydroxyflutamide, □, DHT, Δ.

To clarify the role of the AR mutation in codon 741 on conversion of bicalutamide to an agonist, Hara et al. assessed the transcriptional responses to bicalutamide and hydroxyflutamide (active metabolite of flutamide) of the wild-type; the single mutants W741C, W741L, and T877A ARs in transactivation assays. Interestingly, the mutants W741C and W741L ARs had a substantial transactivation response to bicalutamide (Fig. X). This observation is consistent with the findings that hydroxyflutamide worked as an agonist and bicalutamide worked as an antagonist for the T877A mutant AR in transactivation assays. The mutant W741C and W741L ARs responded only slightly to hydroxyflutamide (Fig. X), indeed bicalutamide switches to an agonist.²⁷

1.4.2. Mechanism of AR Antagonism by Bicalutamide

The ligand-binding domain (LBD) is the heart of the receptor and has been the focus of AR-based drug discovery. Crystal structures of the AR LBD containing numerous bound ligands and coactivator peptides have been determined.^{37,38,39,40,41} When the hormone binds to the hormone binding site (HBS), an uncharacterized reorganization of the receptor occurs, primarily thought to be the registration of helix 12 (H12) to bind the coactivator. This reorganization results in the formation of an effective coactivator-binding site (AF-2 site), a surface-exposed cleft involving helices H3, H4, and H12 (Fig. XI).⁴²

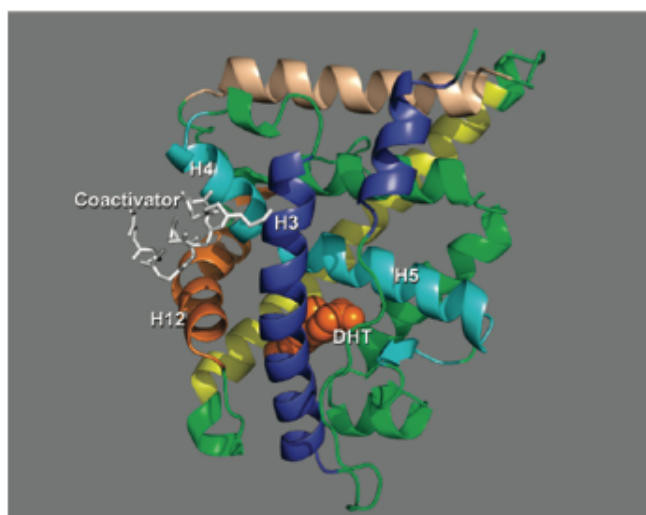


Fig. XI. AR LBD with DHT (orange space-filling diagram) and coactivator peptide (white sticks) shown. Binding of DHT at the HBS organizes H12 that, along with H3 and H4, forms the AF-2 site allowing coactivator bind (Estebanez-Perpina et al. Protein Data Bank entry 1T63)

The precise mechanism by which AR antagonists block the transcription of target genes remains elusive. The preponderance of evidence from X-ray structures of several nuclear receptor antagonist complexes suggests that the general mechanism involves perturbing helix 12, displacing it from its hormone-bound configuration, and distorting the AF-2 site. This in turn interferes with coactivator binding, a requisite for transcription.⁴²

When bicalutamide is complexed with wild-type AR, antagonism occurs due to steric clash of bulky phenyl ring with helix 12, preventing its repositioning over the ligand pocket and leading to partial unfolding of the receptor LBD.⁴³

Recently, the structure of bicalutamide with the bicalutamide-resistant mutant AR (W741L) was solved in the receptor's agonist conformation (Fig. XII).⁴⁴ In the bicalutamide/AR (W741L), the B-ring occupies the cavity created by the absence of the Trp indole in the mutated complex, while the A-ring is virtually in the same environment as the A-ring of DHT. So, the 4-fluorophenyl sulfone group is situated between residues of H12 and the side chain of Leu741, suggesting that in wild-type receptor the larger Trp741 side chain would require bicalutamide to push against H12.⁴³

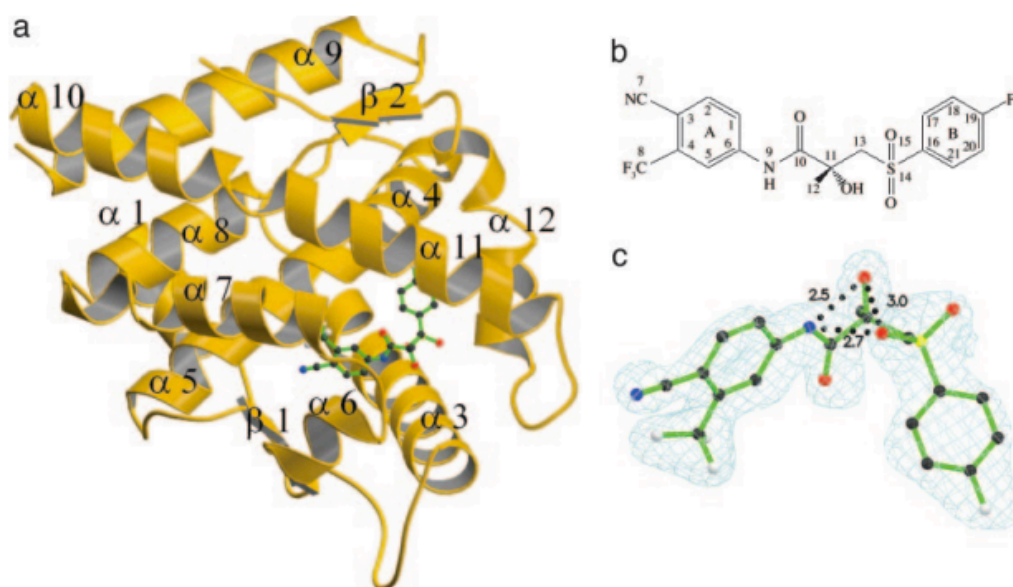


Fig. XII. Structure and binding conformation of R-bicalutamide. (a) W741L AR LBD-R-bicalutamide complex. (b) Structure and numbering scheme of R-bicalutamide (c) R-bicalutamide within the Fo-Fc simulated annealing omit map with R-bicalutamide omitted. Intramolecular hydrogen bonds are denoted by distances in Å. Nitrogen, blue; oxygen, red; carbon, black; sulfur, yellow; fluorine, white⁴⁴

1.4.3. A New Generation of Antiandrogens: Diarylthiohydantoins

Sawyer and co-workers showed that a 3- to 5-fold up-regulation of the AR was the likely cause of the resistance to antiandrogens.²⁸ They further demonstrated that castration resistant prostate cancer was still dependent on the ligand-binding domain of AR for growth. They specifically engineered a class of diarylthiohydantoins, to search for overcoming deficiencies of available androgen receptor antagonists, including low binding affinity and partial

agonism, which partly explain the clinical responses that are detected on discontinuation of these agents (Fig. XIII).⁴⁵

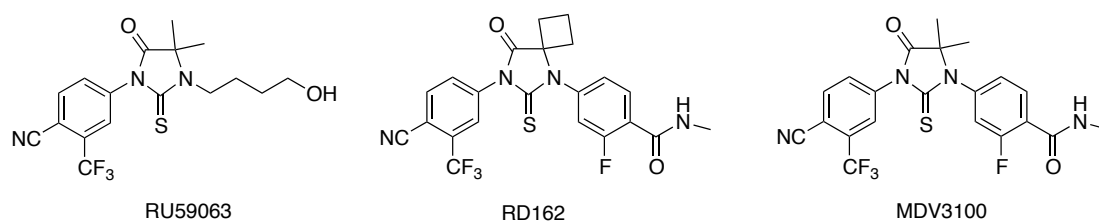


Fig. XIII. Diarylthiohydantoins

RU59063 has been chosen as a starting chemical scaffold on the basis of its relatively high affinity for AR and selectivity for AR over other nuclear hormone receptors. The RU59063 structure has been varied systematically in each of the functional groups and the binding affinity has been measured.⁴⁶ The structure-activity relationship (SAR) study led to choice of RD162 and MDV3100, as the lead compounds for further biological studies (Fig. XIII).⁴⁵

MDV3100 is a novel small molecule AR pure antagonist that blocks nuclear translocation of AR, DNA binding, coactivator recruitment and has no agonist activity when AR is overexpressed. It has higher affinity for the receptor than does bicalutamide.⁹ MDV3100 might be a true androgen-receptor antagonist, without partial agonist properties.

In a competition assay with 16 β -[¹⁸F] fluoro-5 α -DHT (18-FDHT) to measure relative AR binding affinity, both RD162 and MDV3100 bound AR in castration-resistant LNCaP/AR human prostate cancer cells with five- to eight-fold greater affinity than bicalutamide and only two- to three-fold reduced affinity relative to the derivative of the native ligand FDHT (Fig. XIV A).

Expression of the AR target genes PSA and transmembrane serine protease 2 (TMPRSS2) was induced by bicalutamide but not by RD162 or MDV3100 (Fig. XIV B), indicating that RD162 and MDV3100 do not have agonist activity in a castration-resistant setting. Both RD162 and MDV3100 antagonized induction of PSA and TMPRSS2 by the synthetic androgen R1881 in parental LNCaP cells.

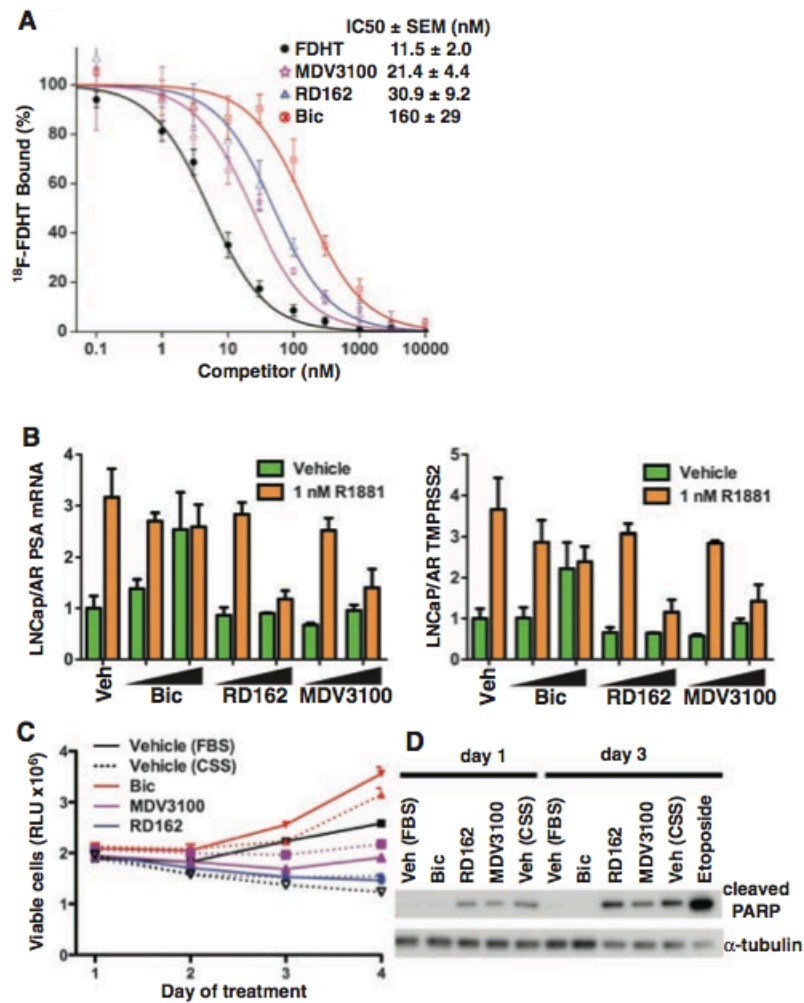


Fig. XIV. Effect of RD162 and MDV3100 in human prostate cancer cells in vitro⁴⁵

In the human prostate cancer cell line VCaP, which has endogenous AR gene amplification, RD162 and MDV3100 suppressed growth and induced apoptosis, whereas bicalutamide did not (Fig. XIV, C and D). This growth suppression was reversed by cotreatment with the synthetic androgen R1881, which competes for AR binding and was not observed in the AR- negative DU145 human prostate cancer cells. In addition, RD162 and MDV3100 inhibited the transcriptional activity of a mutant AR protein (W741C) isolated from a patient with acquired resistance to bicalutamide.

On the basis of these promising preclinical results, MDV3100 was selected for clinical development in the Prostate Cancer Clinical Trials Consortium. Actually, it has completed phase 1-2 clinical trials and has now entered a phase 3 randomized trials for drug registration.^{45,47}

1.5. SARMs: Selective Androgen Receptor Modulators

Interest in the development and therapeutic potential of nonsteroidal tissue-selective androgen receptor modulators (SARMs) has increased dramatically within the past decade. They are a novel class of androgen receptor ligand, intended to have the same kind of effects as androgenic drugs like anabolic steroids but be much more selective in their action.⁴⁸

Androgens are important in male physiology because of their essential role in male sexual differentiation, male puberty changes, and maintenance of muscle and bone mass, prostate growth and spermatogenesis in adults.³⁵ Synthesized steroidal androgens, due to their ability to mimic the actions of their endogenous counterparts, have been used clinically as valuable therapeutic agents to target a variety of male and female disorders resulting from androgen deficiency. The principle clinical indication for androgens is hypogonadism in men. Other documented clinical uses of androgens include hormone-replacement therapy in postmenopausal women, delayed puberty in boys, anemias, primary osteoporosis, hereditary angioneurotic edema, endometriosis, estrogen receptor-positive breast cancer, and muscle wasting and diseases, male contraception, benign prostatic hyperplasia (BPH) and prostate cancer. Also, androgens have been investigated as hormone replacement therapy for aging men and for regulation of male fertility.¹⁰

Currently used androgens to treat both primary (testicular) and secondary (lack of gonadotropins) hypogonadism are typically injectable or skin delivery formulations of testosterone or testosterone esters (e.g. methyltestosterone and fluoxymesterone). Although treatment with testosterone is effective generally, the efficacy of treatment and its serum levels need to be monitored carefully because of the inconsistent pharmacokinetic profile of most preparations. Orally available synthetic steroidal androgens (e.g. nandrolone and oxandrolone) are also used, but they often cause unacceptable hepatotoxicity and have poor tissue selectivity hence, they are not recommended for long-term androgen therapy. Another common concern about steroidal androgens is the undesirable effects resulting from the cross-reactivity of the androgens or their *in vivo* metabolites with steroid receptors other than the androgen receptor (AR).³⁵

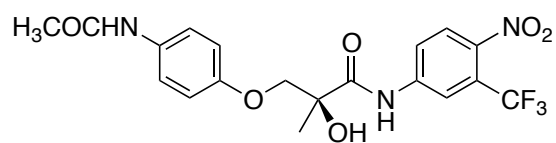
An ideal SARM should have:

1. High specificity for the AR;
2. Improved oral bioavailability;
3. Tissue-selective pharmacological activities.

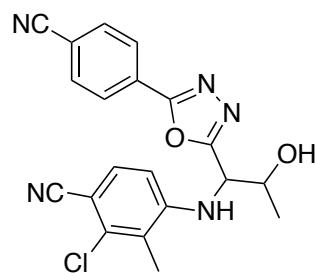
Non-steroidal AR agonists are still in the early stages of drug discovery, Ostarine (MK-2866, Fig. XV) is an investigational selective androgen receptor modulator (SARM) from GTx, Inc, for treatment of cancer cachexia, muscle wasting, osteoporosis, colorectal cancer, non-Hodgkin lymphoma, chronic lymphocytic leukemia and breast cancer. The most common side effects reported among all subjects in the trial were fatigue, anemia, nausea and diarrhea.³⁵

Recently, Miller et al. have discovered RAD140 (Fig. XV), which has all the hallmarks of a SARM. It is potency selective, since it stimulates muscle weight increases at a lower dose than that required stimulating prostate weight increases. Moreover, it is also efficacy selective, because it is fully anabolic on muscle but demonstrates less than complete efficacy on the prostate and seminal vesicles and, in fact, can partially antagonize the stimulation of the seminal vesicles induced by testosterone. RAD140 has excellent pharmacokinetics and is a potent anabolic in nonhuman primates as well. This compound has completed preclinical toxicology in both rats and monkeys and it has been currently prepared for phase I clinical studies in patients suffering from severe weight loss due to cancer cachexia.⁴⁹

The tissue selectivity of these agents offers an exciting opportunity to differentially regulate the androgen effects in various target tissues, thus minimizing the interference to normal physiological processes while targeting desirable therapeutic goals. For example, SARMs with potent anabolic activity but minimal androgenic activity would be ideal for the treatment of patients who bear muscular diseases (such as sarcopenia or trauma- induced muscle wasting) but are contraindicated for androgenic stimuli (such as for aging population or prostate cancer patients).



Ostarine



RAD140

Fig. XV. SARMs

In perspective, not only could SARMs be used as superior alternatives to current steroidal androgens in therapy of male hypogonadism but also they could expand the scope of androgen therapy to include wasting syndromes, aging-related disorders due to declined androgen levels, male fertility regulation, and other androgen deficiency-related diseases.

2. Aim of the Thesis

Commercially available antiandrogens show a common scaffold: two aromatic rings linked by a linear or cyclic spacer (Fig. XVI).

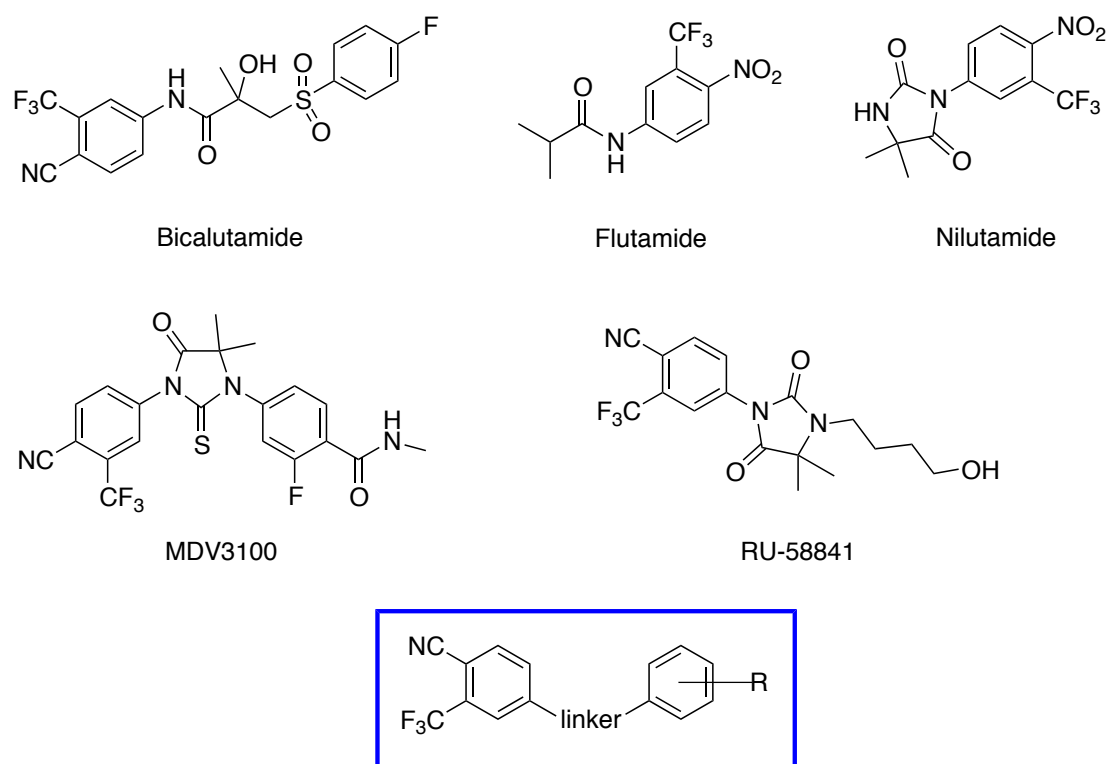


Fig. XVI. Commercially available antiandrogens

Based on literature, we have introduced, as linker between two aromatic rings, a triazole moiety (Tab. I). As evidenced, 1,2,3-triazole pharmacophores display a broad spectrum of biological activities associated with antibacterial, antifungal and herbicidal, antiallergic, and anti-HIV. This five-membered ring is found in potent agonist or antagonist receptor ligands. Furthermore, triazole derivatives have been used as mimics of the amide bond, with the aim of increasing molecule bioavailability and of favouring hydrogen bonding and dipolar interactions.

Furthermore, the encouraging advances in the click chemistry field, particular reference to the copper (I)-catalyzed 1,3-dipolar cycloaddition of organic azides with alkynes, which allows efficient construction of the triazole framework under mild conditions (Fig. XVII), prompted us to choose triazoles as suitable linkers.

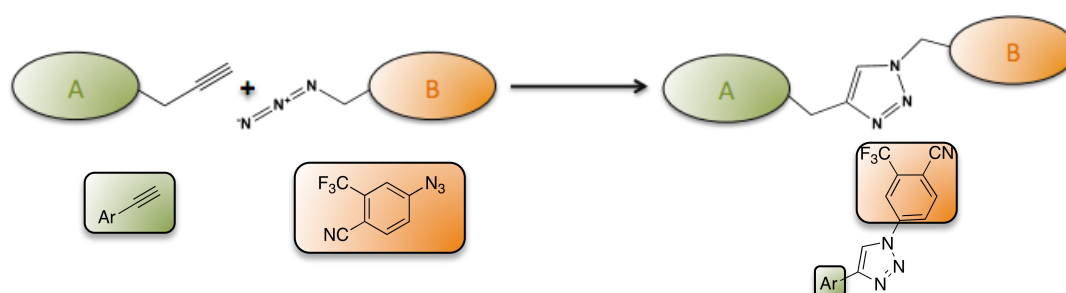


Fig. XVII. Click chemistry

Compound	Structure	Compound	Structure
1		6	
2		7	
3		8	
4		9	
5		10	

Tab. I. Summary of the synthesized compounds

Compound	Structure	Compound	Structure
11		19	
12		20	
13		21	
14		22	
15		23	
16		24	
17		25	
18		26	

Tab. I. Summary of the synthesized compounds

3. Results Discussion and Conclusion

In this section, available biological data are shown and discussed.

3.1. Quantitative Real-time Reverse Transcription-Polymerase Chain Reaction

The inhibitory activity of the newly synthesized compounds was studied in a PSA expression experiment, using Quantitative Real-time Reverse Transcription-Polymerase Chain Reaction.

Prostate-specific antigen is a glycoprotein that is secreted by epithelial cells of the prostate gland. PSA levels between 4 and 10 ng/mL (nanograms per milliliter) are considered to be suspicious for prostate cancer.

LNCaP cells, an epithelial cell line derived from a human prostate carcinoma, were incubated with our compounds for 20 h at 37°C. RNA was then isolated from cells using the RNeasy mini kit (Qiagen). cDNA was generated using equal concentrations of RNA and the Taqman High Capacity Reverse Transcription kit in the GeneAmp PCR System 9700 machine (Applied Biosystems). Diluted cDNA was combined with the forward primer, reverse primer, SYBR green and RNase-free water in 96-well plate and analysis of mRNA expression was carried out using the ABI 7500 Real Time PCR machine (Applied Biosystems). All samples were normalized to the level of 18S ribosomal RNA (rRNA). The number of PCR cycles to reach the fluorescence threshold value is the cycle threshold (Ct). Ct values for each transcript were determined, and relative RNA levels were calculated by the comparative Ct method as described by the manufacturer.

The primer sequences for real-time PCR were as follows:

PSA

forward 5'GCAGCATTGAACCAGAGGAGTT-3'

reverse 5' CACGTCATTGGAAATAACATGGA-3'

18S rRNA

forward 5'-AGTCCCTGCCCTTTGTACACA-3'

reverse 5'-CGATCCGAGGGCCTCACTA-3'

N.	Structure	N.	Structure	N.	Structure
1		2		3	
4		5		6	
7		8		9	
10		11		12	
13		14		15	
16		17		18	
19		20		21	
22		23		24	
25		26			

Tab. II. Summary of the synthesized compounds

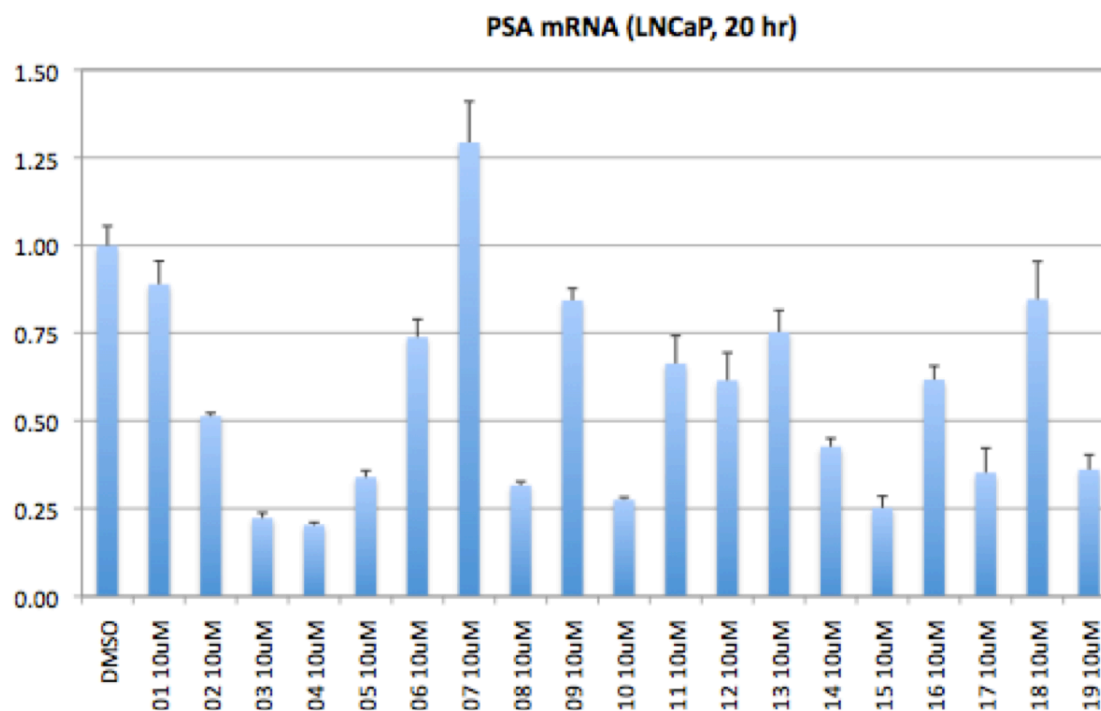


Fig. XVIII. Quantitative Real-time Reverse Transcription-Polymerase Chain Reaction

The PSA expression of the new molecules proved to be generally decreased (Fig. XVIII). In detail, 03, 04 and 15 showed the best inhibitory activity of the series, reducing the protein expression to below 25%. The 02, 05, 08, 10, 14, 17 and 19 compounds also reduced PSA levels. Only 01 and 18 compounds seemed to make no appreciable changes in protein expression, while compound 07 enhanced PSA expression, making this last compound particularly interesting as potential agonist or a selective antiandrogen receptor modulator.

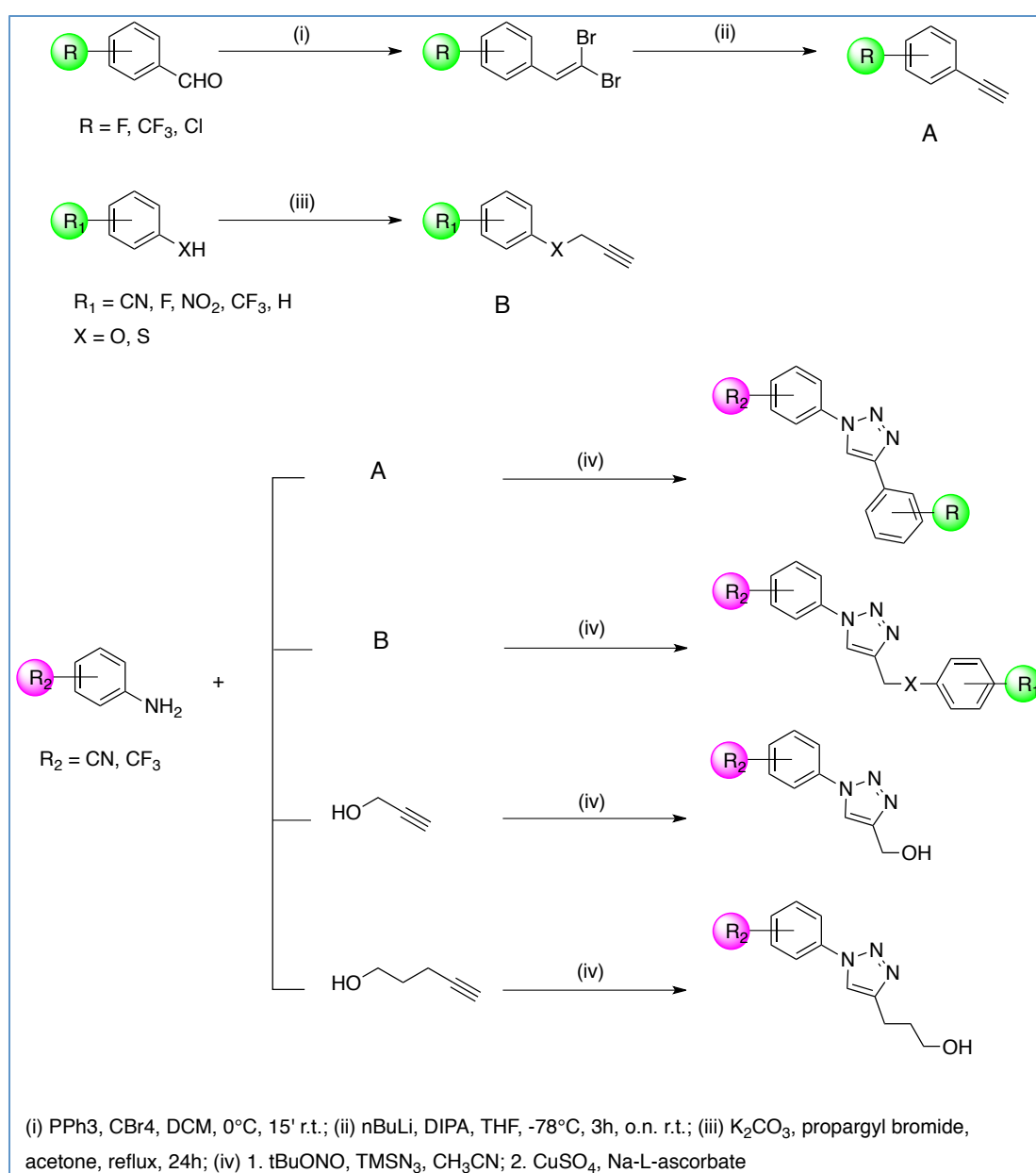
In general, the presence of one or two linkers between the triazole and the aromatic rings, seems to favour antagonistic activity, besides, substituents on to the triazole appear to play a pivotal role on biological outcome, e.g. para- and ortho- positions are preferred and the cyano- and nitro groups increment antagonistic potency.

Additionally, compounds bearing the para-cyano, meta-trifluoromethyl aromatic ring show higher biological activity, while compounds where the triazole is directly linked to the phenyl groups are weakly active or, as seen for 7, behave as agonist.

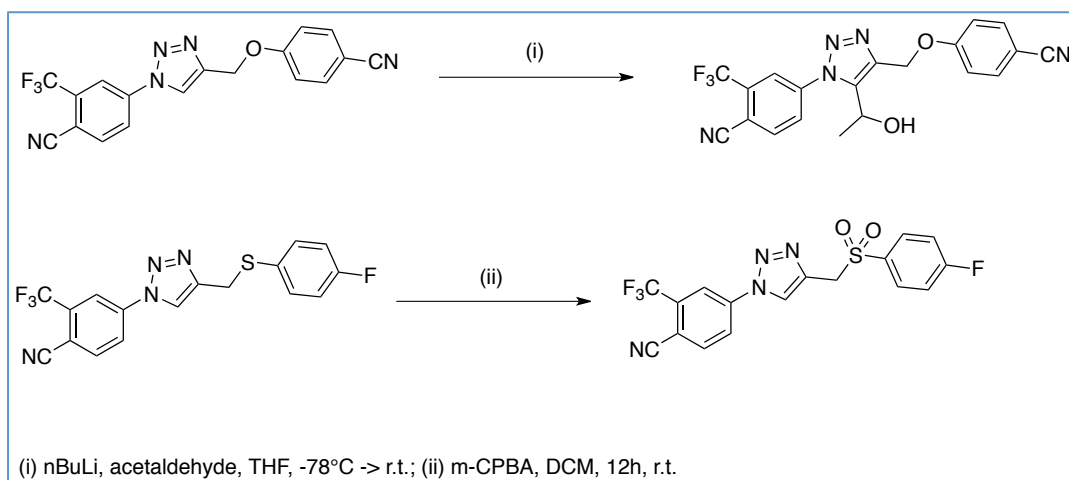
In conclusion, preliminary data suggest that the new molecules reported herein generally decrease the PSA expression, thus they can potentially act as androgen receptor antagonists. On the basis of these promising results, some selected compounds have been chosen for further preclinical studies in order to prove their activity at lower concentrations and to check the anti-androgen effect on other cell lines.

4. Experimental Section

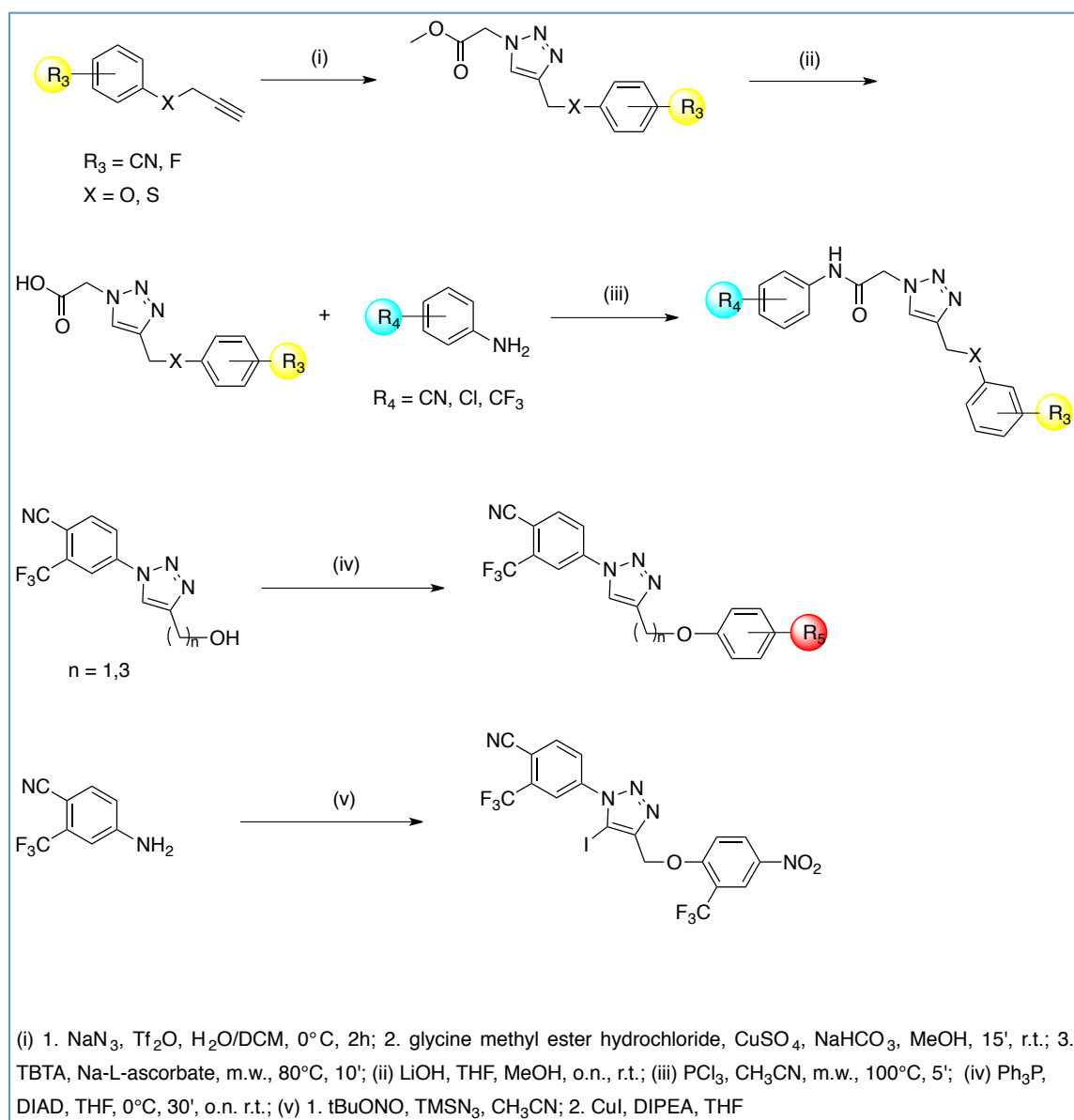
4.1. Schemes of Reaction



Scheme I.



Scheme II.

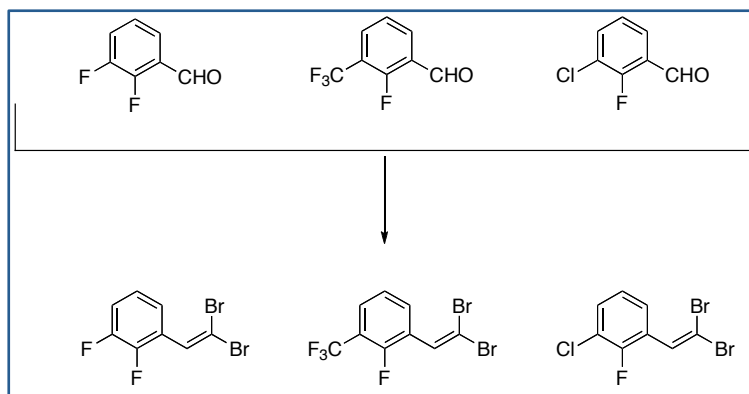


Scheme III.

4.2. Experimental Section

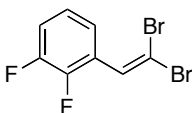
Almost all reactions were performed under an atmosphere of dry nitrogen by using oven-dried glassware. Tetrahydrofuran, toluene, and ethyl ether were distilled from sodium benzophenone ketal. Dichloromethane and acetonitrile were distilled from calcium hydride. All other solvents were HPLC grade. Reactions were magnetically stirred and monitored by thin-layer chromatography (TLC) with E. Merck silica gel 60-F254 plates. Eluted plates were visualized by exposure to ultraviolet light and then by staining with an ethanolic solution of phosphomolybdic acid. The products were isolated and purified using a flash chromatography system, with Merck silica gel (0.04–0.63 μm , 240–400 mesh) under high pressure, with a mixture of hexanes and ethyl acetate as the eluent. Unless otherwise stated, all NMR spectra were measured in CDCl_3 solutions and referenced to the CHCl_3 signal. All ^1H and ^{13}C shifts are given in ppm (s = singlet; d = doublet; t = triplet; dd = quadruplet; dt = doublet of triplets, m = multiplet; br. = broad signal). Coupling constants J are given in Hz. Assignments of proton resonances were confirmed, when possible, by selective homonuclear decoupling experiments or by correlated spectroscopy. High-resolution mass spectra and electrospray (ESI) experiments were performed with a time-of-flight (TOF) mass detector.

4.2.1. Corey Fuchs Reaction



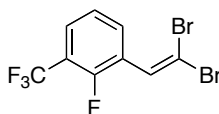
PPh₃ (4 eq.) was added at 0°C to a solution of CBr₄ (4 eq.) in dry CH₂Cl₂. (3 mL x mmol of aldehyde). At the same temperature, aldehyde (1 eq.) dissolved in dry CH₂Cl₂ (2 mL x mmol of aldehyde), was dropped slowly into the reaction mixture. The cooling bath was removed and the progress of the reaction was monitored by TLC. After 15 min, water and CH₂Cl₂ were added and the aqueous phase was extracted twice with CH₂Cl₂. The combined organic phases were dried over Na₂SO₄ and column chromatography (silica gel, CH₂Cl₂) yielded a transparent oil.

1-(2,2-dibromovinyl)-2,3-difluorobenzene



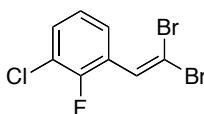
Quantitative yield. ¹H NMR (400 MHz, CDCl₃) δ 7.71 – 7.64 (m, 2H), 7.58 – 7.50 (m, 1H), 7.49 – 7.43 (m, 1H). ¹³C NMR (101 MHz, CDCl₃) δ 152.05 – 151.73 (d, *J* = 12.7 Hz), 149.58 – 149.25 (d, *J* = 12.6 Hz), 149.13 – 148.80 (d, *J* = 13.2 Hz), 146.63 – 146.30 (d, *J* = 13.2 Hz), 125.81 – 125.51 (d, *J* = 10.2 Hz), 124.22 – 123.75 (m), 93.99 – 93.77 (d, *J* = 2.0 Hz).

1-(2,2-dibromovinyl)-2-fluoro-3-(trifluoromethyl)benzene

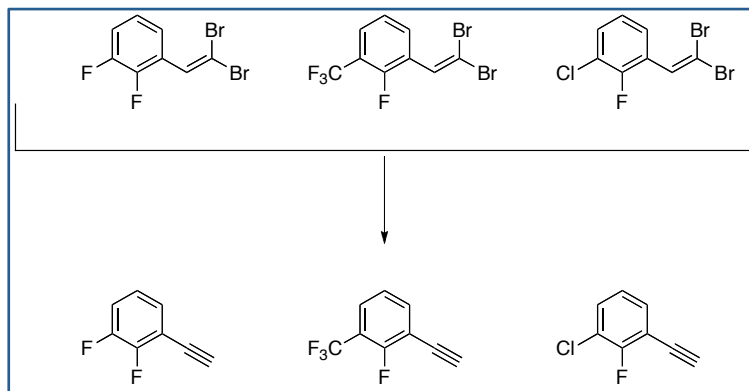


Quantitative yield. ¹H NMR (400 MHz, CDCl₃) δ 7.99 – 7.90 (m, 1H), 7.65 – 7.54 (m, 1H), 7.56 – 7.50 (m, 1H), 7.33 – 7.22 (t, *J* = 7.9 Hz, 1H).

1-chloro-3-(2,2-dibromovinyl)-2-fluorobenzene

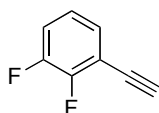


Yield = 89%. ^1H NMR (400 MHz, CDCl_3) δ 7.66 – 7.59 (ddd, J = 8.0, 6.3, 1.7 Hz, 1H), 7.53 – 7.48 (d, J = 1.6 Hz, 1H), 7.43 – 7.35 (ddd, J = 8.6, 7.0, 1.7 Hz, 1H), 7.14 – 7.06 (td, J = 8.0, 1.4 Hz, 1H).



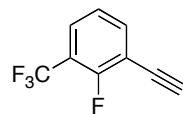
$n\text{BuLi}$ (1.6M in hexanes, 4 eq.) at 0°C was added, via canula, to a solution of diisopropylamine (4 eq.) in dry THF (0.42 mL x mmol of $n\text{BuLi}$) in a three-necked flask. After 1h, the resulting LDA solution was slowly dropped into dibromoalkene (1eq.), dissolved in dry THF (4.5 mL x mmol of dibromoalkene) at -78°C . The temperature was kept at -78°C for 3 h. Then the reaction mixture was allowed to warm slowly to room temperature. The reaction was stirred overnight at rt, then quenched with water and extracted with EtOAc. The combined organic phases were dried over Na_2SO_4 and column chromatography (silica gel, CH_2Cl_2) yielded alkyne.

1-ethynyl-2,3-difluorobenzene



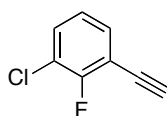
Yield = 24%. ^1H NMR (400 MHz, CDCl_3) δ 7.27 – 7.11 (m, 2H), 7.07 – 6.98 (dtd, J = 8.2, 4.9, 1.6 Hz, 1H), 3.36 – 3.35 (s, 1H). ^{13}C NMR (101 MHz, CDCl_3) δ 153.30 – 151.16 (m), 150.89 – 148.57 (m), 129.45 – 127.74 (d, J = 3.8 Hz), 124.80 – 123.34 (dd, J = 7.2, 5.0 Hz), 119.25 – 117.35 (d, J = 17.2 Hz), 113.41 – 112.53 (dd, J = 12.3, 1.8 Hz), 84.31 – 83.12 (m), 76.15 – 75.57 (dd, J = 4.6, 1.2 Hz).

1-ethynyl-2-fluoro-3-(trifluoromethyl)benzene



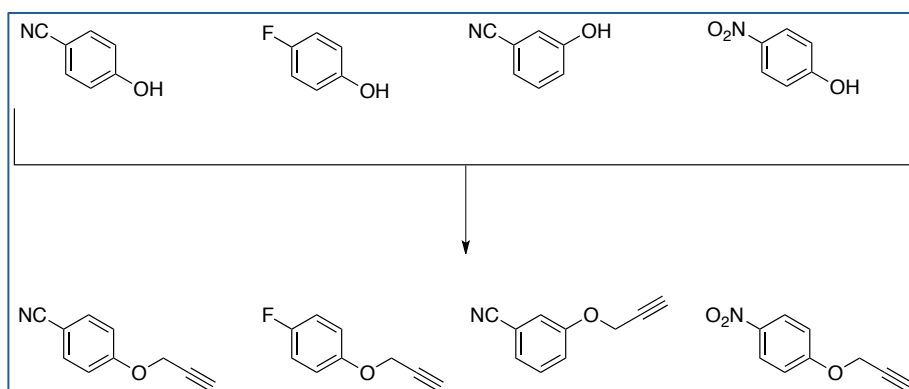
Yield = 10%. ^1H NMR (400 MHz, CDCl_3) δ 7.71 – 7.64 (td, J = 7.2, 6.6, 1.7 Hz, 1H), 7.63 – 7.56 (m, 1H), 7.25 – 7.19 (m, 1H), 3.41 – 3.37 (d, J = 0.8 Hz, 1H). ^{13}C NMR (101 MHz, CDCl_3) δ 163.47 – 157.44 (m), 138.56 – 136.94 (t, J = 1.4 Hz), 127.66 – 127.10 (qd, J = 4.6, 1.6 Hz), 124.05 – 123.70 (d, J = 5.0 Hz), 123.66 – 120.77 (d, J = 272.5 Hz), 119.20 – 118.68 (m), 113.72 – 111.40 (d, J = 15.2 Hz), 85.52 – 83.08 (d, J = 3.8 Hz), 75.79 – 74.63 (s).

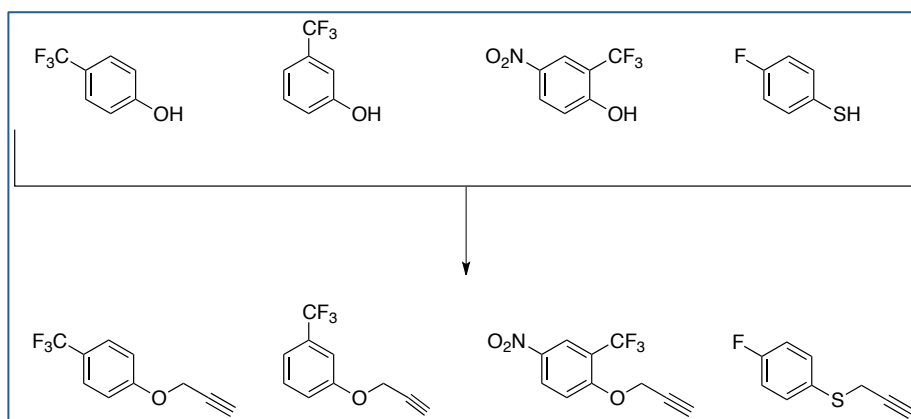
1-chloro-3-ethynyl-2-fluorobenzene



Yield = 51%. ^1H NMR (400 MHz, CDCl_3) δ 7.44 – 7.30 (m, 2H), 7.07 – 6.99 (td, J = 8.0, 1.2 Hz, 1H), 3.37 – 3.33 (s, 1H). ^{13}C NMR (101 MHz, CDCl_3) δ 160.99 – 156.89 (d, J = 254.7 Hz), 132.64 – 131.62 (s), 131.62 – 130.56 (s), 125.04 – 123.79 (d, J = 5.0 Hz), 121.85 – 120.90 (d, J = 17.4 Hz), 112.89 – 111.87 (d, J = 15.7 Hz), 83.93 – 83.12 (m), 76.10 – 75.51 (s).

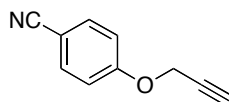
4.2.2. Williamson Reaction





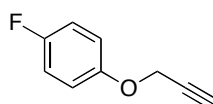
A round bottom flask equipped with a magnetic stir bar was charged with phenol (1 eq.), K_2CO_3 (4 eq.), propargyl bromide (80% wt toluene, 4 eq.) and acetone (2 mL x mmol of phenol). The mixture was heated to reflux for 24h and cooled to rt. The solvent was removed under pressure and water was added. The heterogeneous mixture was extracted twice with EtOAc and the combined organic layers were dried over Na_2SO_4 . The solid didn't need any further purification, quantitative yield.

4-(prop-2-ynyloxy)benzonitrile



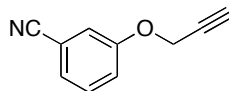
1H NMR (400 MHz, $CDCl_3$) δ 7.66 – 7.55 (d, 2H), 7.08 – 6.99 (d, 2H), 4.78 – 4.71 (d, J = 2.4 Hz, 2H), 2.63 – 2.53 (t, 1H). ^{13}C NMR (101 MHz, $CDCl_3$) δ 159.59 - 133.23 - 133.10 - 133.07 - 133.03 - 132.99 - 132.97 - 132.94 - 132.93 - 132.92 - 132.92 - 132.86 - 132.80 - 132.63 - 117.97 - 114.62 - 114.59 - 114.57 - 103.98 - 103.88 - 64.84 - 54.90 - 54.87.

1-fluoro-4-(prop-2-ynyloxy)benzene



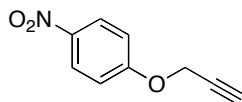
^1H NMR (400 MHz, CD_3OD) δ 7.03 – 6.86 (m, 4H), 4.66 – 4.60 (d, J = 2.5 Hz, 2H), 2.53 – 2.49 (t, J = 2.4 Hz, 1H). ^{13}C NMR (101 MHz, CD_3OD) δ 154.97 - 152.59 - 149.67 - 149.65 - 112.22 - 112.16 - 112.14 - 112.08 - 112.06 - 112.05 - 111.82 - 74.80 - 74.52 - 74.51 - 71.84 - 71.78 - 71.73 - 71.69 - 71.63 - 52.47.

3-(prop-2-ynyloxy)benzonitrile



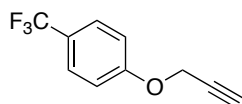
^1H NMR (400 MHz, CDCl_3) δ 7.35 – 7.27 (m, 1H), 7.22 – 7.16 (dd, J = 7.6, 1.2 Hz, 1H), 7.15 – 7.10 (m, 2H), 4.66 – 4.59 (m, 3H), 2.53 – 2.48 (td, J = 2.4, 0.8 Hz, 1H). ^{13}C NMR (101 MHz, CDCl_3) δ 156.42 - 129.42 - 129.39 - 129.35 - 129.09 - 124.52 - 124.27 - 124.22 - 123.95 - 119.07 - 117.52 - 117.30 - 116.98 - 116.67 - 116.62 - 112.14 - 112.13 - 76.46 - 75.59 - 55.06 - 55.03 - 55.01 - 54.94.

1-nitro-4-(prop-2-ynyloxy)benzene



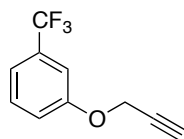
^1H NMR (400 MHz, CDCl_3) δ 8.29 – 8.04 (m, 2H), 7.08 – 6.90 (m, 2H), 4.81 – 4.67 (d, J = 2.4 Hz, 3H), 2.62 – 2.44 (t, J = 2.4 Hz, 1H).

1-(prop-2-yn-1-yloxy)-4-(trifluoromethyl)benzene



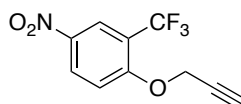
^1H NMR (400 MHz, CDCl_3) δ 2.52 - 2.58 (m, 1 H) 4.69 - 4.77 (m, 2 H) 7.01 - 7.09 (m, 2 H) 7.52 - 7.63 (m, 2 H)

1-(prop-2-yn-1-yloxy)-3-(trifluoromethyl)benzene



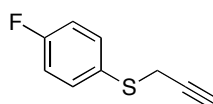
^1H NMR (400 MHz, CDCl_3) δ 2.55 (t, $J=2.47$ Hz, 1 H) 4.72 (d, $J=2.57$ Hz, 2 H) 7.15 (dd, $J=8.25, 2.57$ Hz, 1 H) 7.19 - 7.30 (m, 2 H) 7.35 - 7.46 (m, 1 H)

4-nitro-1-(prop-2-yn-1-yloxy)-2-(trifluoromethyl)benzene



^1H NMR (400 MHz, CDCl_3) δ 2.63 (t, $J=2.38$ Hz, 1 H) 4.93 (d, $J=2.38$ Hz, 2 H) 7.29 (d, $J=9.16$ Hz, 1 H) 8.44 (dd, $J=9.16, 2.75$ Hz, 1 H) 8.52 (d, $J=2.75$ Hz, 1 H)

(4-fluorophenyl)(prop-2-ynyl)sulfane

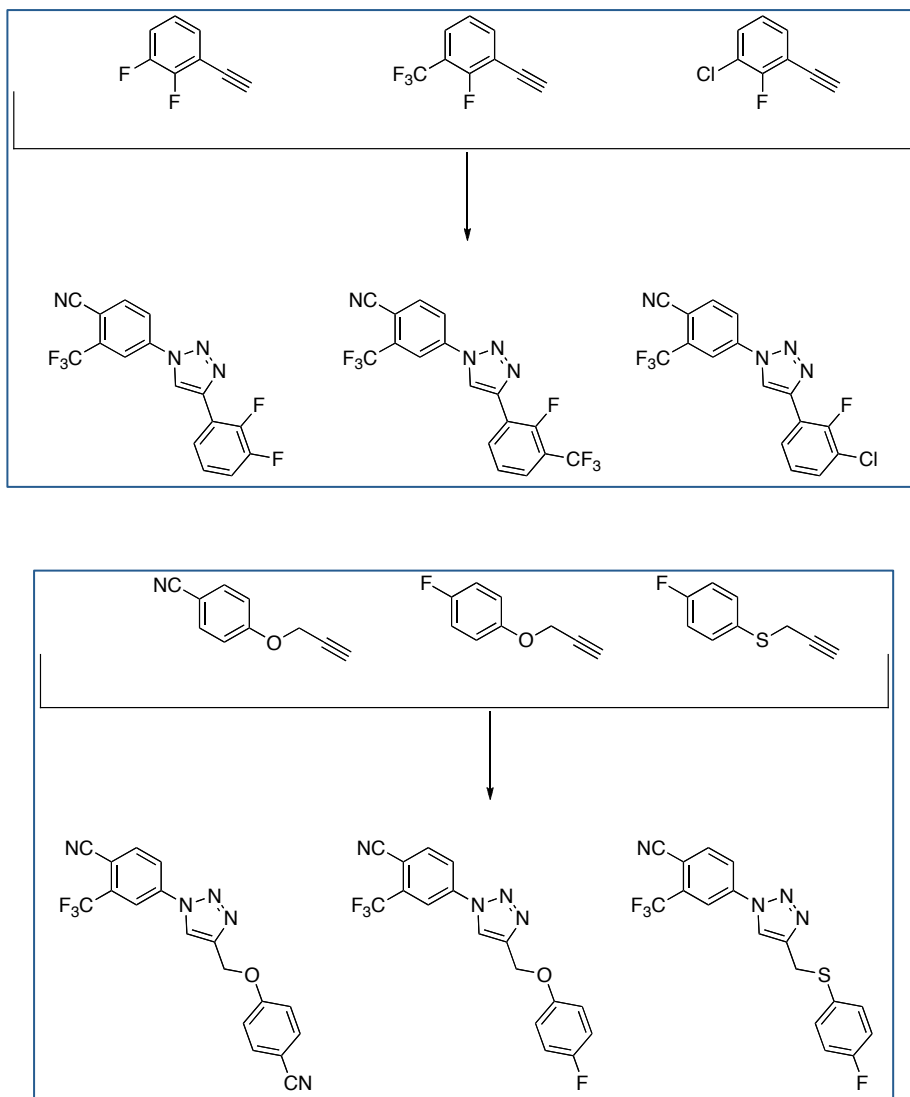


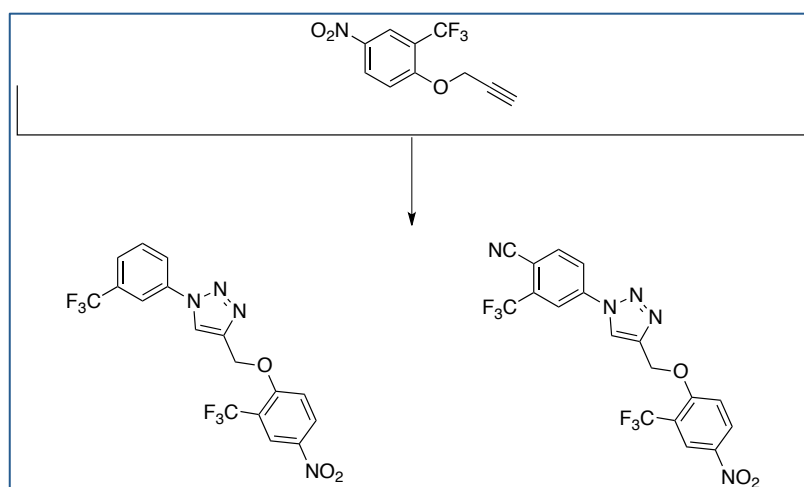
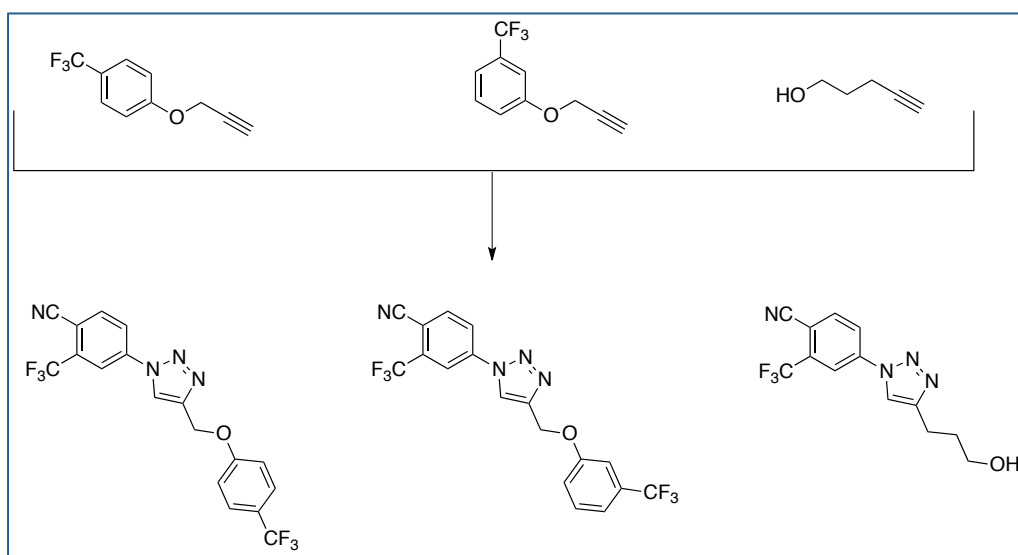
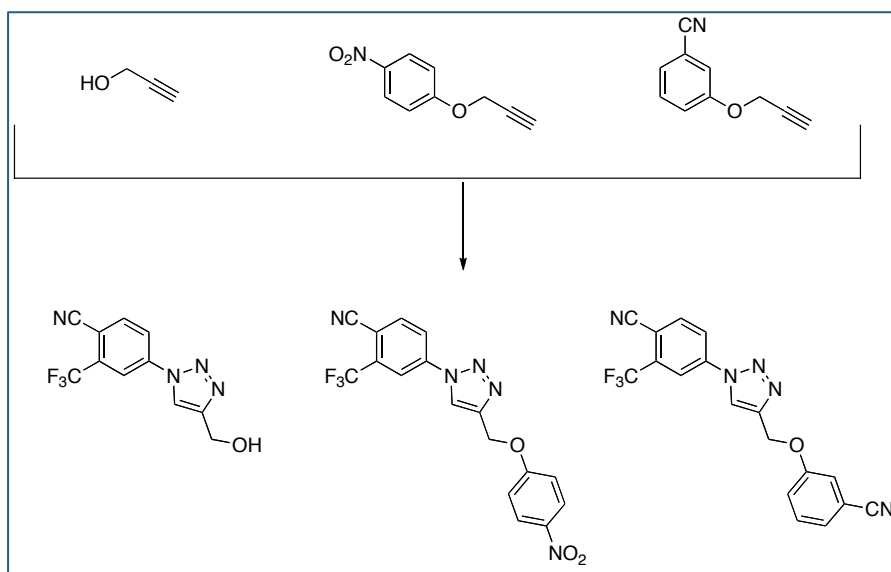
4-Fluorothiophenol (1 eq.) in dry acetone (1,8 mL x mmol of thiophenol) was stirred with anhydrous K_2CO_3 (1 eq.) at rt for 4h. Propargyl bromide (80% wt toluene, 1 eq.) was added under ice-cold condition and the reaction mixture was heated under reflux for 15h and cooled to rt. The solvent was removed under pressure and water was added. The heterogeneous mixture was extracted twice with EtOAc and the combined organic layers were dried over Na_2SO_4 . The residue was purified by column chromatography on silica gel (hexanes), giving a yellow oil (yield = 81%).

^1H NMR (400 MHz, CDCl_3) δ 7.54 - 7.44 (m, 2H), 7.10 - 6.96 (m, 2H), 3.58 - 3.54 (t, $J = 1.3$ Hz, 1H), 2.30 - 2.13 (t, $J = 2.6$ Hz, 1H). ^{13}C NMR (101 MHz, CDCl_3) δ

163.75 – 161.13 (d), 133.80 – 133.52 (d, $J = 8.3$ Hz), 129.70 – 129.47 (d, $J = 3.4$ Hz), 116.38 – 116.13 (s), 116.11 – 115.91 (s), 79.87 – 79.67 (s), 71.93 – 71.73 (s).

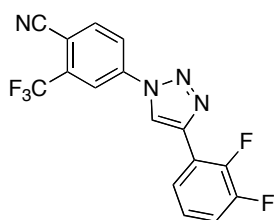
4.2.3. Click Chemistry





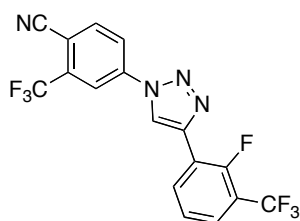
4-amino-2-(trifluoromethyl)benzonitrile (1 eq.) was dissolved in CH₃CN (3.3 mL x mmol of benzonitrile) in a three-necked flask and cooled to 0°C in an ice bath. To this stirred mixture was added tBuONO (1.5 eq.) followed by TMSN₃ (1.2 eq.) dropwise. The resulting solution was stirred at room temperature for 2h. The alkyne (1.5 eq.), an aqueous solution of CuSO₄·5H₂O (0.1 eq.) and sodium L-ascorbate (0.5 eq.) were added and the reaction was stirred overnight at rt. The reaction mixture was diluted with EtOAc and then extracted. The tail solid was purified by preparative TLC Plate or flash chromatography (silica, hexanes/EtOAc: 4/1).

4-(4-(2,3-difluorophenyl)-1H-1,2,3-triazol-1-yl)-2-(trifluoromethyl)benzonitrile (1)



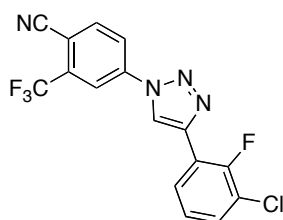
Yield = 32%. MS/ESI m/z calcd for C₁₆H₇F₅N₄ 351.0664 (MH⁺) found 351.0687 (MH⁺). ¹H NMR (400 MHz, CDCl₃) δ 8.54 – 8.49 (d, *J* = 3.0 Hz, 1H), 8.38 – 8.32 (d, *J* = 2.1 Hz, 1H), 8.24 – 8.17 (dd, *J* = 8.4, 2.2 Hz, 1H), 8.17 – 8.11 (ddt, *J* = 7.6, 6.1, 1.9 Hz, 1H), 8.11 – 8.05 (d, *J* = 8.4 Hz, 1H), 7.31 – 7.18 (m, 2H).

4-(4-(2-fluoro-3-(trifluoromethyl)phenyl)-1H-1,2,3-triazol-1-yl)-2-(trifluoromethyl) benzonitrile (2)



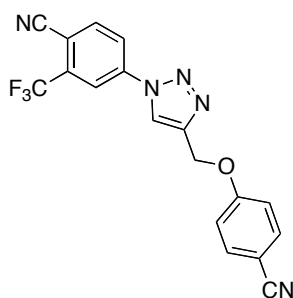
Yield = 24%. MS/ESI m/z calcd for $C_{17}H_7F_7N_4$ 401.0632 (MH^+) found 401.0632 (MH^+). 1H NMR (400 MHz, $CDCl_3$) δ 8.65 – 8.58 (t, J = 7.4 Hz, 1H), 8.58 – 8.54 (d, J = 3.3 Hz, 1H), 8.38 – 8.32 (s, 1H), 8.25 – 8.17 (m, 1H), 8.12 – 8.05 (d, J = 8.4 Hz, 1H), 7.72 – 7.65 (t, J = 7.3 Hz, 1H), 7.48 – 7.41 (t, J = 7.9 Hz, 1H).

4-(4-(3-chloro-2-fluorophenyl)-1H-1,2,3-triazol-1-yl)-2-(trifluoromethyl)benzonitrile (7)



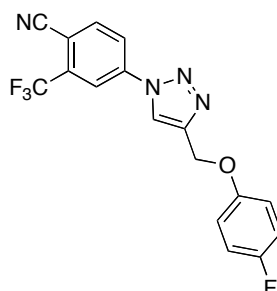
Yield = 30%. MS/ESI m/z calcd for $C_{16}H_7ClF_4N_4$ 367.0368 (MH^+) found 367.0365 (MH^+). 1H NMR (400 MHz, $CDCl_3$) δ 8.60 – 8.46 (d, J = 3.1 Hz, 1H), 8.40 – 8.25 (m, 2H), 8.25 – 8.16 (d, J = 8.3 Hz, 1H), 8.13 – 8.04 (d, J = 8.5 Hz, 1H), 7.53 – 7.40 (t, J = 7.7 Hz, 1H), 7.34 – 7.22 (m, 2H).

4-(4-((4-cyanophenoxy)methyl)-1H-1,2,3-triazol-1-yl)-2-(trifluoromethyl)benzonitrile (4)



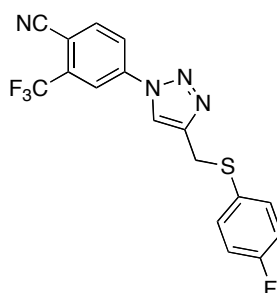
Yield = 43%. MS/ESI m/z calcd for $C_{18}H_{10}F_3N_5O$ 370.0910 (MH^+) found 370.0922 (MH^+). 1H NMR (400 MHz, CD_3OD) δ 8.99 – 8.93 (s, 1H), 8.54 – 8.47 (d, J = 2.1 Hz, 1H), 8.44 – 8.36 (dd, J = 8.6, 2.2 Hz, 1H), 8.27 – 8.20 (d, J = 8.5 Hz, 1H), 7.74 – 7.64 (m, 2H), 7.28 – 7.16 (m, 2H), 5.43 – 5.35 (s, 2H). ^{13}C NMR (101 MHz, $CDCl_3$) δ 161.04 - 145.03 - 139.41 - 136.60 - 135.02 - 134.10 - 123.01 - 121.02 - 118.77 - 118.31 - 118.26 - 115.43 - 114.28 - 104.98 - 65.79.

4-(4-((4-fluorophenoxy)methyl)-1H-1,2,3-triazol-1-yl)-2-(trifluoromethyl)benzonitrile (5)



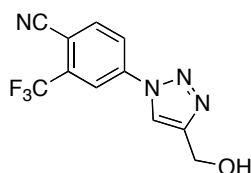
Yield = 48%. MS/ESI m/z calcd for $C_{17}H_{10}F_4N_4O$ 363.0864 (MH^+) found 363.0875 (MH^+). 1H NMR (400 MHz, $CDCl_3$) δ 8.31 – 8.26 (m, 2H), 8.19 – 8.13 (dd, J = 8.5, 2.1 Hz, 1H), 8.07 – 8.02 (m, 1H), 7.04 – 6.91 (m, 4H), 5.29 – 5.26 (s, 2H). ^{13}C NMR (101 MHz, $CDCl_3$) δ 159.20 – 158.47 (s), 156.61 – 155.75 (s), 154.45 – 153.33 (d, J = 2.1 Hz), 146.89 – 145.86 (s), 140.08 – 139.25 (s), 137.09 – 136.26 (s), 135.90 – 134.11 (q, J = 33.7 Hz), 123.69 – 122.39 (d, J = 1.1 Hz), 120.60 – 119.87 (s), 118.64 – 117.61 (q, J = 4.8 Hz), 116.68 – 115.09 (m), 114.62 – 113.99 (s), 110.24 – 109.31 (m).

4-(4-((4-fluorophenylthio)methyl)-1H-1,2,3-triazol-1-yl)-2-(trifluoromethyl)benzonitrile (3)



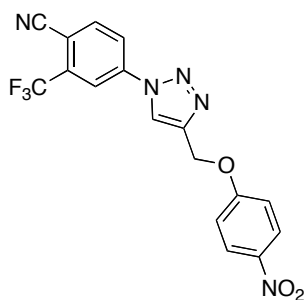
Yield = 72%. MS/ESI m/z calcd for $C_{17}H_{10}F_3N_5O$ 379.0635 (MH^+) found 379.0633 (MH^+). 1H NMR (400 MHz, $CDCl_3$) δ 8.23 – 8.17 (dq, J = 1.4, 0.7 Hz, 1H), 8.08 – 7.97 (m, 2H), 7.91 – 7.86 (t, J = 0.7 Hz, 1H), 7.41 – 7.32 (m, 2H), 7.06 – 6.97 (m, 2H), 4.28 – 4.24 (d, J = 0.7 Hz, 2H).

4-(4-(hydroxymethyl)-1*H*-1,2,3-triazol-1-yl)-2-(trifluoromethyl)benzonitrile (14)



Yield = 89%. MS/ESI *m/z* calcd for C₁₁H₇F₃N₄O 269.0645 (MH⁺) and 291.0464 (MNa⁺) found 269.0658 (MH⁺) and 291.0476 (MNa⁺). ¹H NMR (400 MHz, CD₃OD) δ 8.74 – 8.68 (s, 1H), 8.50 – 8.41 (d, *J* = 2.1 Hz, 1H), 8.37 – 8.30 (dd, *J* = 8.4, 2.2 Hz, 1H), 8.23 – 8.15 (d, *J* = 8.4 Hz, 1H), 4.80 – 4.73 (s, 2H). ¹³C NMR (101 MHz, CD₃OD) δ 149.59 – 149.40 (s), 140.07 – 139.87 (s), 136.94 – 136.74 (s), 134.45 – 134.25 (s), 134.12 – 133.92 (s), 133.79 – 133.59 (s), 123.51 – 123.10 (m), 121.11 – 120.91 (s), 120.79 – 120.59 (s), 118.09 – 117.74 (q, *J* = 5.1 Hz), 114.45 – 114.26 (s), 108.98 – 108.72 (q, *J* = 2.2 Hz), 55.08 – 54.88 (s), 47.70 – 47.51 (s), 47.49 – 47.29 (s), 47.28 – 47.08 (s), 47.07 – 46.87 (s).

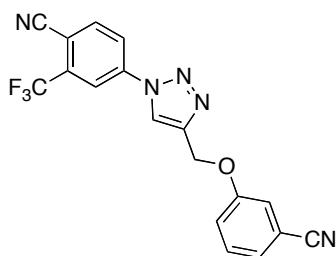
4-(4-((4-nitrophenoxy)methyl)-1*H*-1,2,3-triazol-1-yl)-2-(trifluoromethyl)benzonitrile (19)



Yield = 60%. MS/ESI *m/z* calcd for C₁₇H₁₀F₃N₅O₃ 390.0809 (MH⁺) found 390.0822 (MH⁺). ¹H NMR (400 MHz, CD₃OD) δ 8.57 – 8.49 (t, *J* = 0.8 Hz, 1H), 8.35 – 8.30 (d, *J* = 2.1 Hz, 1H), 8.22 – 8.11 (m, 3H), 8.08 – 8.02 (d, *J* = 8.5 Hz, 1H), 7.13 – 7.05 (m, 2H), 5.38 – 5.32 (d, *J* = 0.7 Hz, 2H). ¹³C NMR (101 MHz, CD₃OD) δ 164.10 – 161.32 (s), 145.05 – 143.75 (s), 143.22 – 141.28 (s), 140.02 – 138.42 (s), 137.88 – 135.94 (s), 135.29 – 133.39 (m), 126.95 – 125.00 (s), 123.52 – 122.68

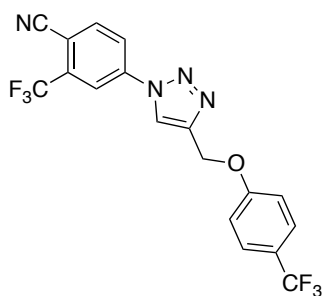
(s), 121.91 – 121.15 (s), 118.60 – 117.30 (d, $J = 4.9$ Hz), 116.01 – 113.76 (s), 110.56 – 107.78 (s), 61.51 – 59.83 (s).

4-(4-((3-cyanophenoxy)methyl)-1H-1,2,3-triazol-1-yl)-2-(trifluoromethyl)benzonitrile (16)



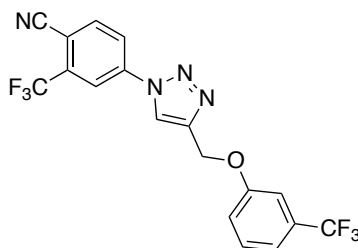
Yield = 64%. MS/ESI m/z calcd for $C_{18}H_{10}F_3N_5O$ 370.0910 (MH^+) found 370.0911 (MH^+). 1H NMR (400 MHz, $CDCl_3$) δ 8.30 – 8.24 (m, 2H), 8.18 – 8.11 (m, 1H), 8.08 – 8.01 (m, 1H), 7.45 – 7.37 (m, 1H), 7.32 – 7.28 (m, 1H), 7.27 – 7.24 (m, 2H), 5.37 – 5.28 (d, $J = 0.7$ Hz, 2H).

2-(trifluoromethyl)-4-(4-((4-(trifluoromethyl)phenoxy)methyl)-1H-1,2,3-triazol-1-yl)benzonitrile (20)



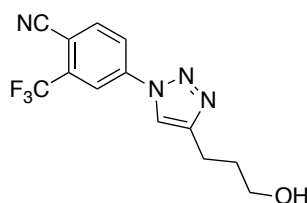
Yield = 67%. 1H NMR (400 MHz, $CDCl_3$) δ 5.37 (s, 2 H) 7.09 (d, $J=8.80$ Hz, 2 H) 7.58 (d, $J=8.80$ Hz, 2 H) 7.99 - 8.19 (m, 2 H) 8.19 - 8.31 (m, 2 H). ^{13}C NMR (101 MHz, $CDCl_3$) δ 160.25 - 145.71 - 139.55 - 136.62 - 123.00 – 120.65 - 135.11 (q, $J = 33.8$ Hz) – 127.15 (m) – 127.08 – 125.56 – 123.86 (q, $J = 33.5$ Hz) - 118.36 (m) – 114.73 – 114.32 – 110.06 – 61.81.

2-(trifluoromethyl)-4-(4-((3-(trifluoromethyl)phenoxy)methyl)-1H-1,2,3-triazol-1-yl)benzonitrile (21)



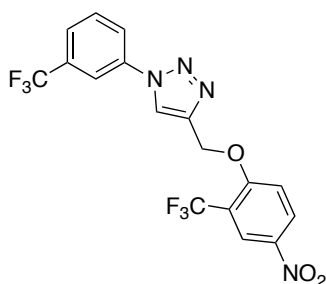
Yield = 73%. ^1H NMR (400 MHz, CDCl_3) δ 5.36 (d, $J=0.55$ Hz, 2 H) 7.20 (dd, $J=8.71$, 1.56 Hz, 1 H) 7.29 (m, 2 H) 7.40 - 7.49 (m, 1 H) 8.02 - 8.08 (m, 1 H) 8.11 - 8.17 (m, 1 H) 8.21 (s, 1 H) 8.27 (d, $J=2.20$ Hz, 1 H)

4-(4-(3-hydroxypropyl)-1H-1,2,3-triazol-1-yl)-2-(trifluoromethyl)benzonitrile (25)



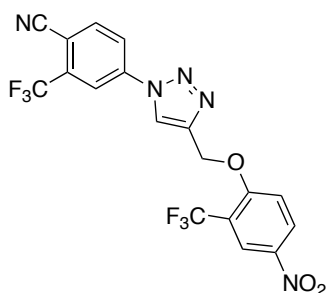
Yield = 69%. ^1H NMR (400 MHz, CDCl_3) δ 2.01 (t, $J=8.0$ Hz, 2 H) 2.95 (t, $J=7.2$ Hz, 2 H) 3.75 (t, $J=6.0$ Hz, 2 H) 7.94 (s, 1 H) 8.01 (d, $J=8.4$ Hz, 1 H) 8.11 (dd, $J=8.4$, 2.0 Hz, 1 H) 8.23 (d, $J=1.6$ Hz, 1 H).

4-((4-nitro-2-(trifluoromethyl)phenoxy)methyl)-1-(3-(trifluoromethyl)phenyl)-1H-1,2,3-triazole (22)



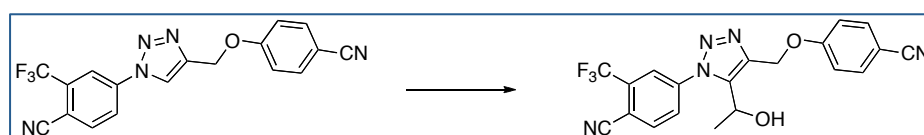
Yield = 62%. ¹H NMR (400 MHz, CDCl₃) δ 5.56 (s, 2 H) 7.44 (d, *J*=9.16 Hz, 1 H) 7.66 - 7.79 (m, 2 H) 7.96 (d, *J*=7.70 Hz, 1 H) 8.04 (s, 1 H) 8.15 (s, 1 H) 8.45 (dd, *J*=9.16, 2.75 Hz, 1 H) 8.52 (d, *J*=2.75 Hz, 1 H)

4-(4-((4-nitro-2-(trifluoromethyl)phenoxy)methyl)-1*H*-1,2,3-triazol-1-yl)-2-(trifluoromethyl)benzonitrile (23**)**



Yield = 65%. ¹H NMR (400 MHz, CDCl₃) δ d ppm 5.56 (s, 2 H) 7.40 (d, *J*=9.35 Hz, 1 H) 8.02 - 8.09 (m, 1 H) 8.09 - 8.15 (m, 1 H) 8.22 (s, 1 H) 8.29 (d, *J*=2.02 Hz, 1 H) 8.47 (dd, *J*=9.16, 2.75 Hz, 1 H) 8.54 (d, *J*=2.75 Hz, 1 H)

4.2.4. Direct Functionalization of 1,4-Triazoles at the 5-Position



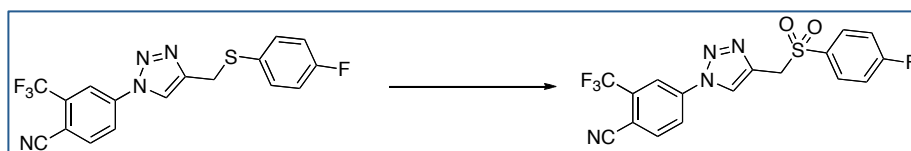
4-(4-((4-cyanophenoxy)methyl)-5-(1-hydroxyethyl)-1*H*-1,2,3-triazol-1-yl)-2-(trifluoromethyl)benzonitrile (8**)**

A solution of triazole (**1** eq.) in dry THF (15 mL x mmol of triazole) was cooled to -78°C before being treated dropwise with *n*BuLi (2.5M in hexanes, 2.2 eq.). The solution was allowed to stir for 5 min at -78°C before being treated with acetaldehyde (3 eq.). The reaction was maintained at -78°C for 5 min then allowed to warm to rt. After being allowed to stir for a further 30 min, the reaction was quenched with CH₂Cl₂. The combined organic extracts were dried over Na₂SO₄ before being concentrated under reduced pressure to furnish the

crude product. Purification by flash chromatography gave a white solid (yield = 44%).

MS/ESI m/z calcd for $C_{20}H_{14}F_3N_5O_2$ 414.1172 (MH^+) and 436.0992 (MNa^+) found 414.1176 (MH^+) and 436.0996 (MNa^+). 1H NMR (400 MHz, $CDCl_3$) δ 8.22 – 8.17 (d, J = 1.9 Hz, 1H), 8.10 – 7.98 (m, 2H), 7.60 – 7.52 (dd, J = 8.7, 1.6 Hz, 2H), 7.14 – 7.07 (dd, J = 8.7, 1.5 Hz, 2H), 5.45 – 5.33 (m, 2H), 5.20 – 5.13 (dd, J = 6.8, 5.0 Hz, 1H), 3.56 – 3.50 (d, J = 5.2 Hz, 1H), 1.54 – 1.49 (dd, J = 6.9, 1.3 Hz, 3H). ^{13}C NMR (101 MHz, $CDCl_3$) δ 161.18, 140.69, 139.97, 139.89, 136.01, 134.19, 134.12, 128.88, 124.09, 124.04, 122.93, 120.20, 118.88, 115.58, 114.30, 111.17, 111.15, 104.72, 61.80, 60.33, 22.46.

4.2.5. Oxidation of Sulfur to Sulfone



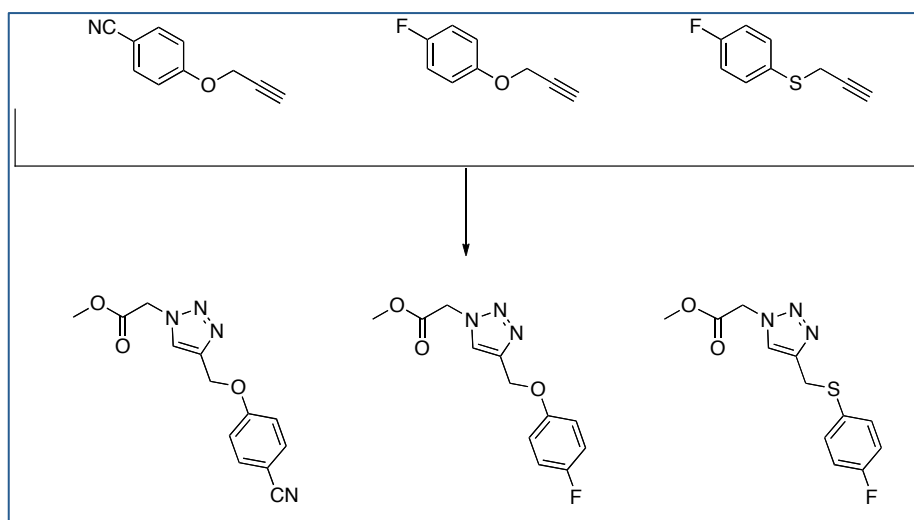
4-((4-((4-fluorophenylsulfonyl)methyl)-1H-1,2,3-triazol-1-yl)-2-(trifluoromethyl)benzonitrile (**6**)

m-Chloroperbenzoic acid (3 eq.) was added to a solution of sulfur (1 eq.) in CH_2Cl_2 (15 mL x mmol of sulfur). The reaction mixture was stirred at rt for 12h. The reaction was then quenched with Na_2SO_3 solution and washed 5 times with saturated $NaHCO_3$ solution. After the removal of solvent under vacuum, the crude solid was washed with diethyl ether and hexanes. A white solid was obtained (Y = 20%).

MS/ESI m/z calcd for $C_{17}H_{10}F_4N_4O_2S$ 411.0533 (MH^+) found 411.0553 (MH^+). 1H NMR (400 MHz, CD_3COCD_3) δ 8.98 – 8.93 (m, 1H), 8.58 – 8.54 (dd, J = 1.6, 0.9 Hz, 1H), 8.54 – 8.49 (dd, J = 8.5, 2.2 Hz, 1H), 8.40 – 8.35 (dt, J = 8.5, 0.7 Hz, 1H), 7.93 – 7.86 (m, 2H), 7.43 – 7.34 (m, 2H), 4.86 – 4.81 (d, J = 0.4 Hz, 2H). ^{13}C NMR (101 MHz, CD_3COCD_3) δ 164.89 – 163.30 (s), 141.34 – 139.06 (s), 138.68 – 137.79 (s), 137.41 – 136.39 (s), 135.12 – 134.42 (d, J = 2.9 Hz), 134.23 – 132.77 (q, J = 33.0 Hz), 132.46 – 130.49 (d, J = 9.9 Hz), 124.40 – 122.81 (m), 121.92 – 119.95 (s),

119.45 – 117.80 (q, $J = 5.0$ Hz), 116.91 – 115.32 (d, $J = 23.0$ Hz), 115.32 – 113.93 (s), 109.61 – 108.21 (q, $J = 2.2$ Hz), 53.44 – 51.47 (s).

4.2.6. Microwave-Assisted Click Chemistry



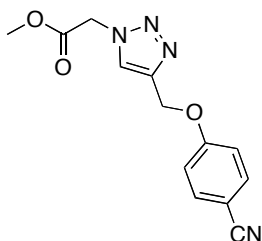
NaN_3 (6 eq.) was dissolved in a minimum volume of water (1 mL x 0.4 g of NaN_3). At 0°C an equal volume of CH_2Cl_2 was added and Tf_2O (3 eq.) was added dropwise to the vigorously stirred solution. After stirring for 2h at 0°C the aqueous phase was once extracted with the same volume of CH_2Cl_2 . The combined organic phase were washed with saturated NaHCO_3 solution and used without further purification.

Glycine methyl ester hydrochloride (1 eq.), $\text{CuSO}_4 \cdot 5\text{H}_2\text{O}$ (2 mol %) and NaHCO_3 (2 eq.) were dissolved in the same volume of water as the volume of the TfN_3 solution to be employed. The TfN_3 solution was added followed by addition of methanol until the solution become homogeneously. The reaction was stirred at rt for 30 min.

Then the alkyne (1 eq.), TBTA (5 mol %) and sodium L-ascorbate (10 mol %) were added and the reaction was heated to 80°C in the microwave for 10 min.

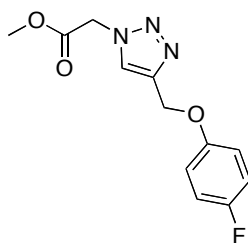
The reaction mixture was diluted with water and then extracted with EtOAc. The crude was purified by flash chromatography (silica, hexanes/EtOAc: 2/1).

methyl 2-(4-((4-cyanophenoxy)methyl)-1H-1,2,3-triazol-1-yl)ethanoate (9)



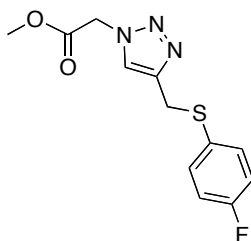
Yield = 92%. MS/ESI m/z calcd for $C_{13}H_{12}N_4O_3$ 273.0982 (MH^+) and 295.0802 (MNa^+) found 273.0986 (MH^+) and 295.0809 (MNa^+). 1H NMR (400 MHz, $CDCl_3$) δ 7.84 – 7.74 (s, 1H), 7.58 – 7.52 (m, 2H), 7.05 – 7.00 (m, 2H), 5.26 – 5.23 (d, J = 0.7 Hz, 2H), 5.21 – 5.16 (s, 2H), 3.81 – 3.74 (s, 3H).

methyl 2-(4-((4-fluorophenoxy)methyl)-1H-1,2,3-triazol-1-yl)ethanoate



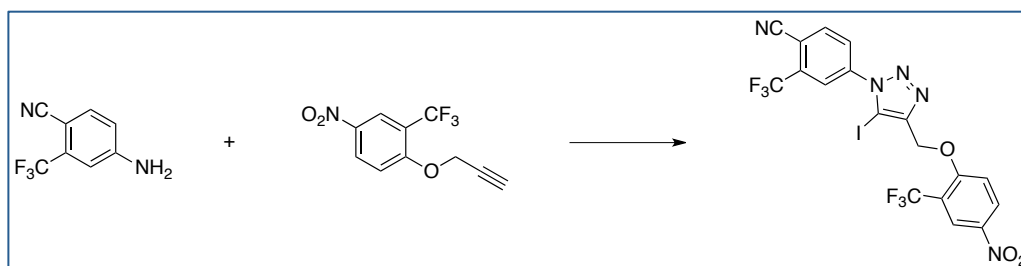
Yield = 84%. MS/ESI m/z calcd for $C_{12}H_{12}FN_3O_3$ 266.0935 (MH^+) and 288.0755 (MNa^+) found 266.0932 (MH^+) and 288.0751 (MNa^+). 1H NMR (400 MHz, $CDCl_3$) δ 7.76 – 7.70 (s, 1H), 6.98 – 6.84 (m, 4H), 5.19 – 5.11 (d, J = 4.7 Hz, 5H), 3.80 – 3.74 (s, 3H). ^{13}C NMR (101 MHz, $CDCl_3$) δ 166.67, 158.64, 156.27, 154.25, 154.23, 144.38, 125.24, 124.24, 115.98, 115.95, 115.92, 115.90, 115.86, 115.82, 115.75, 62.44, 53.05, 50.69.

methyl 2-(4-((4-fluorophenylthio)methyl)-1*H*-1,2,3-triazol-1-yl)ethanoate



Yield = 76%. MS/ESI m/z calcd for $C_{12}H_{12}FN_3O_2S$ 282.0707 (MH^+) and 304.0526 (MNa^+) found 282.0710 (MH^+) and 304.0520 (MNa^+). 1H NMR (400 MHz, $CDCl_3$) δ 7.44 – 7.40 (s, 1H), 7.33 – 7.22 (m, 2H), 6.97 – 6.84 (m, 2H), 5.11 – 5.03 (s, 2H), 4.13 – 4.10 (d, J = 0.7 Hz, 2H), 3.73 – 3.71 (s, 3H). ^{13}C NMR (101 MHz, $CDCl_3$) δ 167.52 – 166.04 (s), 163.90 – 160.04 (m), 146.38 – 143.95 (s), 134.47 – 131.81 (d, J = 8.2 Hz), 130.47 – 129.00 (d, J = 3.3 Hz), 124.19 – 121.90 (s), 116.81 – 114.14 (m), 53.96 – 52.05 (s), 51.53 – 49.82 (s), 30.68 – 29.34 (m).

4.2.7. Click Chemistry with CuI



4-(5-iodo-4-((4-nitro-2-(trifluoromethyl)phenoxy)methyl)-1*H*-1,2,3-triazol-1-yl)-2-(trifluoromethyl)benzonitrile (**24**)

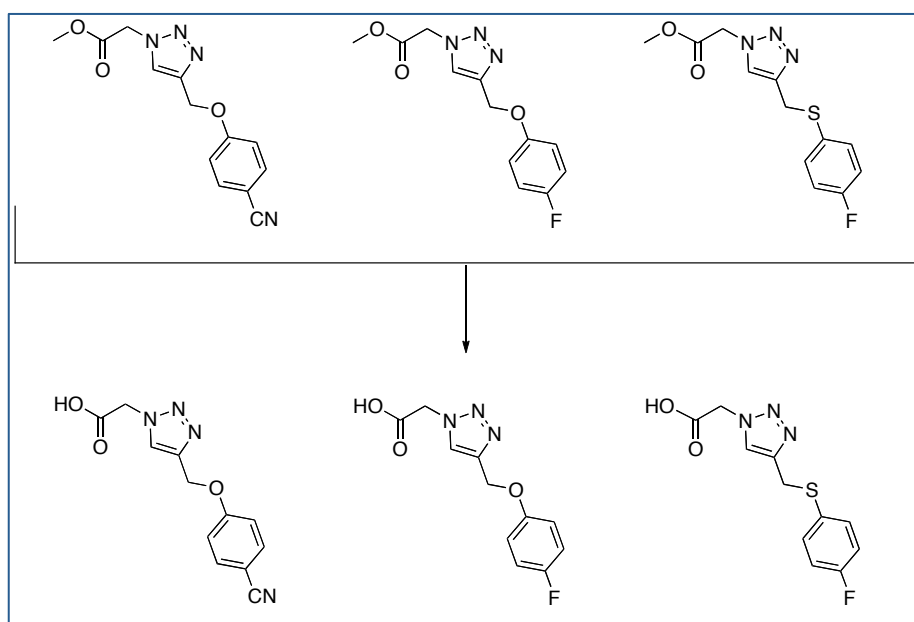
4-amino-2-(trifluoromethyl)benzonitrile (1 eq.) was dissolved in CH_3CN (3.3 mL x mmol of benzonitrile) in a three-necked flask and cooled to $0^\circ C$ in an ice bath. To this stirred mixture was added $tBuONO$ (1.5 eq.) followed by $TMSN_3$ (1.2 eq.) dropwise. The resulting solution was stirred at room temperature for 2h. The solvent was removed in vacuo.

A solution of alkyne (1.0 eq.) in THF was added, followed by CuI (1.2 eq.) and $DIPEA$ (1.2 eq.). NBS (1.2 eq.) in THF was added dropwise. The reaction was stirred at room temperature overnight. The solvent was removed in vacuo.

leaving a brown residue. Purification by flash chromatography, (cyclohexanes: ethyl acetate= 3:1), afforded the target 5-iodo substituted (yield 40%).

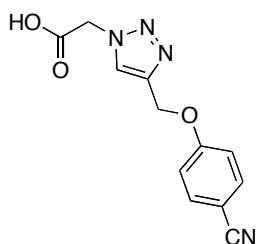
^1H NMR (400 MHz, CDCl_3) δ 5.46 (s, 2 H) 7.92 (d, J = 9.2 Hz, 1 H) 8.01 (dd, J =8.4, 2.0 Hz, 1 H) 8.08 (d, J =8.0 Hz, 1 H) 8.13 (d, J =2.0 Hz, 1 H) 8.44 (dd, J =8.8, 2.4 Hz, 1 H) 8.50 (d, J =2.8 Hz, 1 H).

4.2.8. Deprotection Methyl Ester



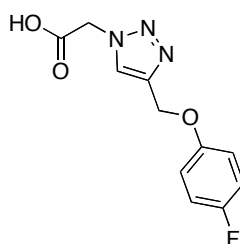
To a solution of methylester (1 eq.) in THF (3.3 mL x mmol of methyl ester) and MeOH (2 mL x mmol of methyl ester) was added an aqueous 1.0 M LiOH solution (2 eq.). The resulting mixture was stirred at rt overnight. The reaction mixture was neutralized with HCl 1N. The aqueous phase was extracted with EtOAc and the combined organics were washed with brine, dried and evaporated. The white solid didn't need any further purification.

2-(4-((4-cyanophenoxy)methyl)-1*H*-1,2,3-triazol-1-yl)ethanoic acid



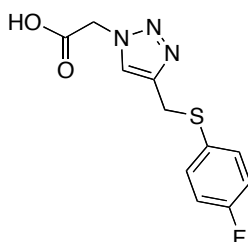
Yield = 96%. ^1H NMR (400 MHz, CD_3OD) δ 8.16 – 8.13 (s, 1H), 7.70 – 7.63 (m, 2H), 7.20 – 7.14 (m, 2H), 5.32 – 5.29 (s, 2H), 5.29 – 5.25 (s, 2H). ^{13}C NMR (101 MHz, CD_3OD) δ 168.25, 161.78, 142.70, 133.80, 125.73, 125.66, 118.55, 115.45, 103.86, 61.16, 50.27.

2-(4-((4-fluorophenoxy)methyl)-1*H*-1,2,3-triazol-1-yl)ethanoic acid



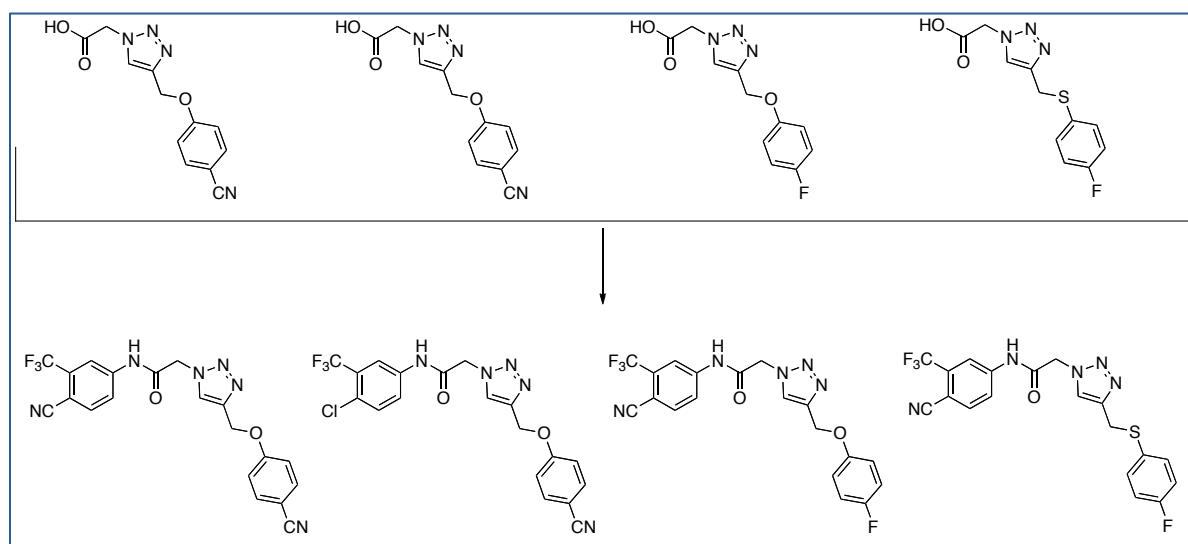
Quantitative yield. MS/ESI m/z calcd for $\text{C}_{11}\text{H}_{10}\text{FN}_3\text{O}_3$ 252.0779 (MH^+) and 274.0598 (MNa^+) found 252.0784 (MH^+) and 274.0599 (MNa^+). ^1H NMR (400 MHz, CD_3OD) δ 8.20 – 8.02 (s, 1H), 7.06 – 6.92 (m, 4H), 5.35 – 5.22 (s, 2H), 5.18 – 5.08 (s, 2H). ^{13}C NMR (101 MHz, CD_3OD) δ 168.25, 158.68, 156.32, 154.53, 154.51, 125.94, 115.85, 115.82, 115.77, 115.45, 115.42, 115.22, 61.76, 50.27.

2-(4-((4-fluorophenylthio)methyl)-1*H*-1,2,3-triazol-1-yl)ethanoic acid



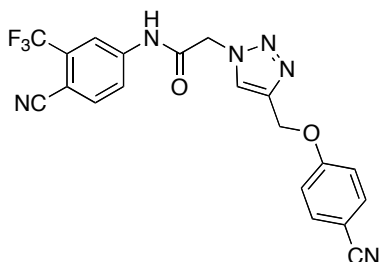
Yield = 88%. MS/ESI m/z calcd for $C_{11}H_{10}FN_3O_2S$ 268.0551 (MH^+) and 290.0370 (MNa^+) found 252.0551 (MH^+) and 290.0364 (MNa^+). 1H NMR (400 MHz, CD_3OD) δ 7.76 – 7.70 (s, 0H), 7.40 – 7.31 (dd, J = 8.6, 5.2 Hz, 1H), 7.06 – 6.97 (t, J = 8.8 Hz, 1H), 5.29 – 5.07 (s, 2H), 5.07 – 4.83 (s, 3H). ^{13}C NMR (101 MHz, CD_3OD) δ 169.49 – 166.04 (s), 164.73 – 158.89 (d, J = 245.6 Hz), 146.37 – 142.92 (s), 135.39 – 132.55 (d, J = 8.3 Hz), 131.24 – 129.55 (s), 125.63 – 120.49 (s), 117.26 – 111.19 (d, J = 22.1 Hz), 51.43 – 48.82 (s), 31.15 – 28.54 (s).

4.2.9. Coupling



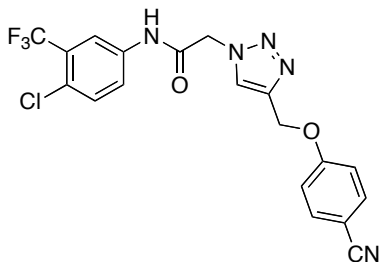
To a solution of aniline (1.01 eq.) and carboxylic acid (1 eq.) in dry CH_3CN (10 mL x mmol of aniline), PCl_3 (1 eq.) was added. The tube was sealed and heated at $100^\circ C$ for 5 min by microwave irradiation (standard method), then mixture was quenched with few drops of water. The reaction mixture was poured on a pre-packed basic alumina column and eluted with $CH_2Cl_2/MeOH$: 97/3. The fractions containing the expected product were collected and evaporated under pressure.

N-(4-cyano-3-(trifluoromethyl)phenyl)-2-(4-((4-cyanophenoxy)methyl)-1H-1,2,3-triazol-1-yl)ethanamide (10**)**



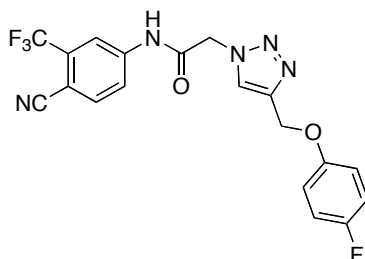
Yield = 68%. MS/ESI m/z calcd for $C_{20}H_{13}F_3N_6O_2$ 427.1125 (MH^+) and 449.0944 (MNa^+) found 427.1140 (MH^+) and 449.0956 (MNa^+). 1H NMR (400 MHz, CD_3OD) δ 8.23 – 8.17 (m, 1H), 8.02 – 7.91 (m, 1H), 7.71 – 7.65 (m, 1H), 7.23 – 7.17 (m, 1H), 5.46 – 5.38 (s, 1H), 5.34 – 5.26 (s, 1H). ^{13}C NMR (101 MHz, CD_3OD) δ 165.22, 161.89, 142.68, 135.88, 133.84, 132.95, 127.35, 127.25, 127.04, 126.08, 123.82, 122.09, 121.98, 118.51, 116.79, 115.37, 103.84, 103.49, 61.17, 52.15.

N-(4-chloro-3-(trifluoromethyl)phenyl)-2-(4-((4-cyanophenoxy)methyl)-1H-1,2,3-triazol-1-yl)ethanamide (11**)**



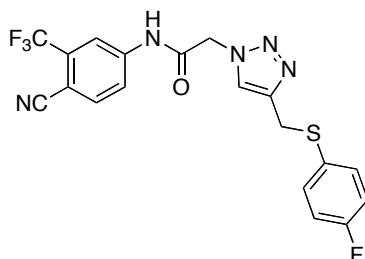
Yield = 72%. MS/ESI m/z calcd for $C_{19}H_{13}ClF_3N_5O_2$ 436.0783 (MH^+) found 486.0786 (MH^+). 1H NMR (400 MHz, CD_3OD) δ 8.21 – 8.18 (s, 1H), 8.10 – 8.04 (d, J = 2.5 Hz, 1H), 7.82 – 7.75 (dd, J = 8.7, 2.6 Hz, 1H), 7.71 – 7.63 (m, 2H), 7.58 – 7.52 (d, J = 8.7 Hz, 1H), 7.22 – 7.14 (m, 2H), 5.41 – 5.36 (s, 3H), 5.32 – 5.28 (s, 3H). ^{13}C NMR (101 MHz, CD_3OD) δ 164.71, 161.80, 142.71, 137.34, 133.79, 131.83, 126.01, 124.03, 123.79, 121.31, 118.52, 118.30, 118.25, 115.43, 103.87, 61.18, 52.08.

N-(4-cyano-3-(trifluoromethyl)phenyl)-2-(4-((4-fluorophenoxy)methyl)-1H-1,2,3-triazol-1-yl)ethanamide (13)



Yield = 56%. MS/ESI m/z calcd for $C_{19}H_{13}F_4N_5O_2$ 420.1078 (MH^+) found 420.1170 (MH^+). 1H NMR (400 MHz, CD_3OD) δ 8.21 – 8.16 (d, J = 2.1 Hz, 1H), 8.15 – 8.12 (s, 1H), 8.01 – 7.94 (m, 1H), 7.94 – 7.88 (m, 1H), 7.05 – 6.94 (d, J = 6.3 Hz, 4H), 5.45 – 5.39 (s, 2H), 5.21 – 5.12 (s, 2H). ^{13}C NMR (101 MHz, CD_3OD) δ 158.68, 156.32, 154.55, 154.53, 143.58, 142.70, 135.96, 133.17, 132.85, 132.52, 125.76, 121.99, 121.03, 116.88, 116.83, 116.78, 116.73, 115.82, 115.75, 115.44, 115.21, 115.08, 103.53, 103.51, 61.57, 52.16.

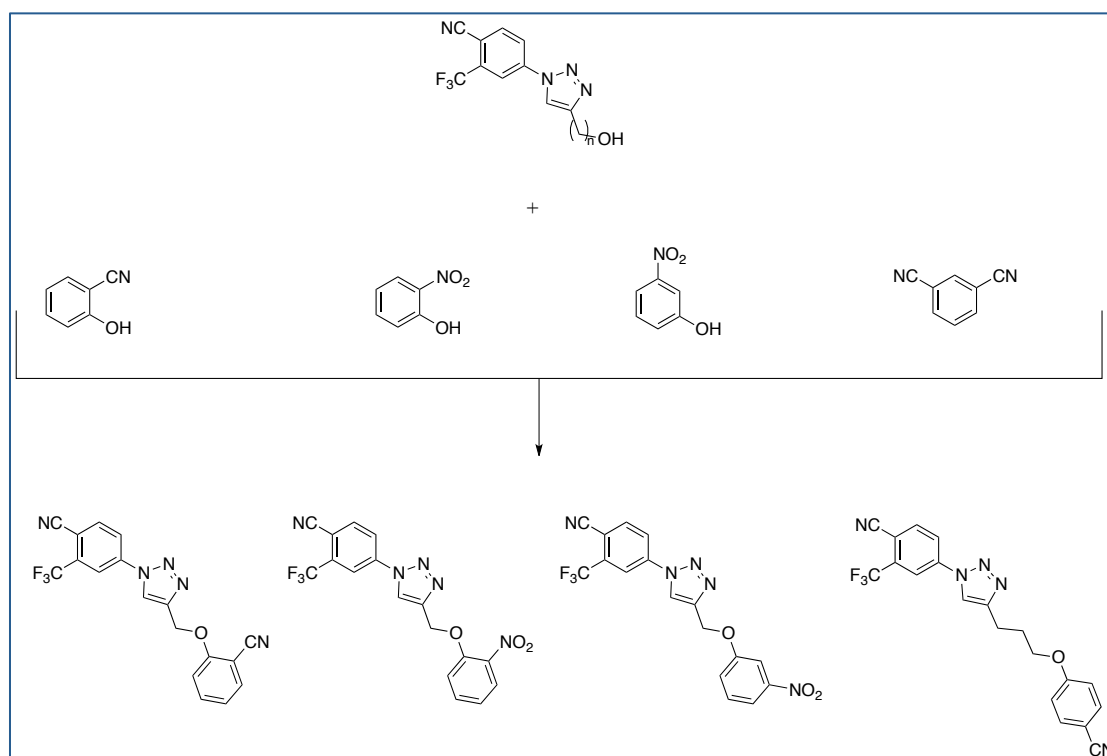
N-(4-cyano-3-(trifluoromethyl)phenyl)-2-(4-((4-fluorophenylthio)methyl)-1H-1,2,3-triazol-1-yl)ethanamide (12)



Yield = 71%. MS/ESI m/z calcd for $C_{19}H_{13}F_4N_5OS$ 436.0850 (MH^+) found 436.0930 (MH^+). 1H NMR (400 MHz, CD_3OD) δ 8.19 – 8.09 (d, J = 2.0 Hz, 1H), 7.98 – 7.91 (m, 1H), 7.91 – 7.85 (m, 1H), 7.81 – 7.77 (s, 1H), 7.39 – 7.30 (td, J = 5.5, 1.9 Hz, 2H), 7.04 – 6.93 (t, J = 8.7 Hz, 2H), 5.38 – 5.29 (s, 2H), 4.20 – 4.11 (s, 2H). ^{13}C NMR (101 MHz, CD_3OD) δ 166.38 – 164.47 (s), 163.69 – 159.92 (m), 145.36 – 143.96 (s), 143.17 – 141.59 (s), 136.70 – 134.96 (s), 133.82 – 133.29 (d, J = 8.2 Hz), 133.24 – 132.94 (s), 132.94 – 132.53 (s), 130.50 – 129.15 (d, J = 3.4 Hz),

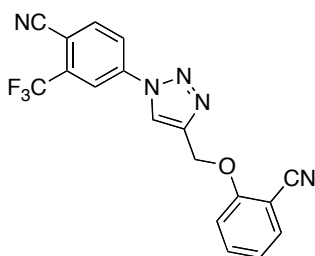
122.28 – 121.73 (s), 117.07 – 116.49 (q, $J = 5.1$ Hz), 115.88 – 115.27 (d, $J = 22.1$ Hz), 115.27 – 114.77 (s), 103.83 – 103.08 (d, $J = 2.3$ Hz), 53.03 – 51.20 (s), 29.90 – 27.97 (s).

4.2.10. Mitsunobu Reaction



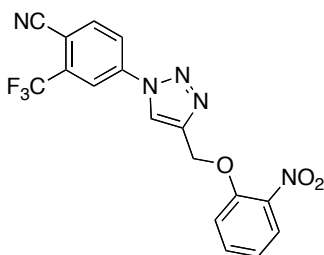
A solution of phenol (1 eq.), Ph_3P (1.1 eq.) and alcohol (1.1 eq.) in anhydrous THF (7.5 mL x mmol of phenol) was cooled in an ice bath under nitrogen. Diisopropylazodicarboxylate (DIAD, 1.1 eq.) was added dropwise and the solution was stirred for 30 min at 0°C and then at room temperature overnight. The solvent was evaporated under pressure. The crude was purified by flash chromatography.

4-(4-((2-cyanophenoxy)methyl)-1H-1,2,3-triazol-1-yl)-2-(trifluoromethyl)benzonitrile (15)



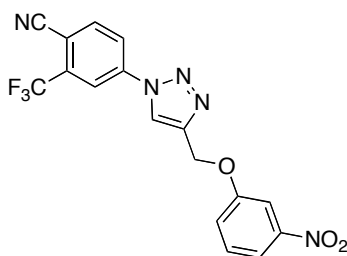
Yield = 77%. MS/ESI m/z calcd for $C_{18}H_{10}F_3N_5O$ 370.0910 (MH^+) and 392.0730 (MNa^+) found 370.0895 (MH^+) and 392.0716 (MNa^+). 1H NMR (400 MHz, CD_3OD) δ 9.00 – 8.87 (s, 1H), 8.54 – 8.47 (d, J = 2.2 Hz, 1H), 8.43 – 8.30 (dd, J = 8.5, 2.3 Hz, 1H), 8.24 – 8.15 (d, J = 8.4 Hz, 1H), 7.70 – 7.57 (m, 2H), 7.43 – 7.32 (d, J = 8.5 Hz, 1H), 7.17 – 6.97 (t, J = 7.6 Hz, 1H), 5.51 – 5.39 (s, 2H). ^{13}C NMR (101 MHz, CD_3OD) δ 159.76, 144.41, 139.85, 136.86, 134.65, 134.29, 133.62, 123.44, 122.78, 121.44, 118.29, 118.24, 115.89, 114.35, 112.86, 101.60.

4-(4-((2-nitrophenoxy)methyl)-1H-1,2,3-triazol-1-yl)-2-(trifluoromethyl)benzonitrile (17)



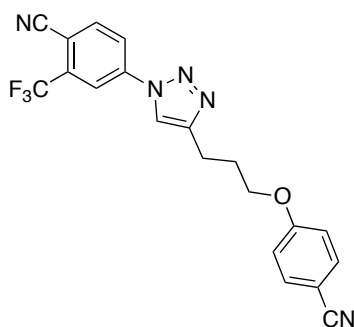
Yield = 57%. MS/ESI m/z calcd for $C_{17}H_{10}F_3N_5O_3$ 390.0809 (MH^+) found 390.0855 (MH^+). 1H NMR (400 MHz, $CDCl_3$) δ 8.37 – 8.31 (m, 1H), 8.16 – 8.10 (m, 1H), 8.10 – 8.04 (m, 0H), 7.94 – 7.87 (dt, J = 8.1, 1.6 Hz, 0H), 7.65 – 7.56 (ddt, J = 8.9, 7.4, 1.6 Hz, 0H), 7.34 – 7.24 (m, 1H), 7.17 – 7.09 (tt, J = 8.1, 1.4 Hz, 0H), 5.52 – 5.43 (d, J = 1.6 Hz, 1H). ^{13}C NMR (101 MHz, $CDCl_3$) δ 151.23, 145.49, 139.52, 136.60, 135.26, 134.86, 134.55, 125.95, 122.95, 121.62, 120.93, 120.18, 118.57, 118.53, 118.48, 115.15, 114.40, 110.02, 63.57.

4-(4-((3-nitrophenoxy)methyl)-1*H*-1,2,3-triazol-1-yl)-2-(trifluoromethyl)benzonitrile (18)



Yield = 35%. MS/ESI m/z calcd for $C_{17}H_{10}F_3N_5O_3$ 390.0809 (MH^+) found 390.0878 (MH^+). 1H NMR (400 MHz, DMSO) δ 9.43 – 9.26 (s, 1H), 8.66 – 8.36 (m, 3H), 7.97 – 7.78 (m, 2H), 7.66 – 7.42 (m, 2H), 5.51 – 5.33 (s, 2H). ^{13}C NMR (101 MHz, DMSO) δ 158.81, 149.19, 144.45, 140.03, 137.94, 133.30, 132.92, 131.27, 124.45, 124.25, 122.66, 118.93, 118.88, 116.52, 115.43, 109.70, 108.43, 62.10.

4-(4-(3-(4-cyanophenoxy)propyl)-1*H*-1,2,3-triazol-1-yl)-2-(trifluoromethyl)benzonitrile (26)



Yield = 65%. 1H NMR (400 MHz, $CDCl_3$) δ 2.21 - 2.39 (m, 2 H) 3.04 (t, $J=7.52$ Hz, 2 H) 4.03 - 4.18 (m, 2 H) 6.90 - 7.01 (m, 2 H) 7.51 - 7.63 (m, 2 H) 7.88 - 7.95 (m, 1 H) 7.98 - 8.06 (m, 1 H) 8.06 - 8.15 (m, 1 H) 8.22 (d, $J=2.02$ Hz, 1 H)

5. References

1. Lu, N. Z.; Wardell, S. E.; Burnstein, K. L.; Defranco, D.; Fuller, P. J.; Giguere, V.; Hochberg, R. B.; McKay, L.; Renoir, J. M.; Weigel, N. L.; Wilson, E. M.; McDonnell, D. P.; Cidlowski, J. A., International Union of Pharmacology. LXV. The pharmacology and classification of the nuclear receptor superfamily: glucocorticoid, mineralocorticoid, progesterone, and androgen receptors. *Pharmacol Rev* **2006**, *58* (4), 782-97.
2. Verrijdt, G.; Haelens, A.; Claessens, F., Selective DNA recognition by the androgen receptor as a mechanism for hormone-specific regulation of gene expression. *Mol Genet Metab* **2003**, *78* (3), 175-85.
3. Gao, T.; Marcelli, M.; McPhaul, M. J., Transcriptional activation and transient expression of the human androgen receptor. *J Steroid Biochem Mol Biol* **1996**, *59* (1), 9-20.
4. Ylikomi, T.; Bocquel, M. T.; Berry, M.; Gronemeyer, H.; Chambon, P., Cooperation of proto-signals for nuclear accumulation of estrogen and progesterone receptors. *EMBO J* **1992**, *11* (10), 3681-94.
5. Feldman, B. J.; Feldman, D., The development of androgen-independent prostate cancer. *Nat Rev Cancer* **2001**, *1* (1), 34-45.
6. Narayanan, R.; Mohler, M. L.; Bohl, C. E.; Miller, D. D.; Dalton, J. T., Selective androgen receptor modulators in preclinical and clinical development. *Nucl Recept Signal* **2008**, *6*, e010.
7. Gelmann, E. P., Molecular biology of the androgen receptor. *Journal of Clinical Oncology* **2002**, *20* (13), 3001-3015.
8. Heinlein, C. A.; Chang, C. S., Androgen receptor in prostate cancer. *Endocrine Reviews* **2004**, *25* (2), 276-308.
9. Chen, Y.; Clegg, N. J.; Scher, H. I., Anti-androgens and androgen-depleting therapies in prostate cancer: new agents for an established target. *Lancet Oncol* **2009**, *10* (10), 981-91.
10. Yin, D. H.; Gao, W. Q.; Kearbey, J. D.; Xu, H. P.; Chung, K. W.; He, Y. L.; Marhefka, C. A.; Veverka, K. A.; Miller, D. D.; Dalton, J. T., Pharmacodynamics of

selective androgen receptor modulators. *Journal of Pharmacology and Experimental Therapeutics* **2003**, *304* (3), 1334-1340.

11. Fujii, S.; Hashimoto, Y.; Suzuki, T.; Ohta, S.; Endo, Y., A new class of androgen receptor antagonists bearing carborane in place of a steroidal skeleton. *Bioorganic & Medicinal Chemistry Letters* **2005**, *15* (1), 227-230.

12. Miller, D. C.; Hafez, K. S.; Stewart, A.; Montie, J. E.; Wei, J. T., Prostate carcinoma presentation, diagnosis, and staging: an update from the National Cancer Data Base. *Cancer* **2003**, *98* (6), 1169-78.

13. van der Crujsen-Koeter, I. W.; Vis, A. N.; Roobol, M. J.; Wildhagen, M. F.; de Koning, H. J.; van der Kwast, T. H.; Schröder, F. H., Comparison of screen detected and clinically diagnosed prostate cancer in the European randomized study of screening for prostate cancer, section rotterdam. *J Urol* **2005**, *174* (1), 121-5.

14. Hoffman, R. M.; Gilliland, F. D.; Eley, J. W.; Harlan, L. C.; Stephenson, R. A.; Stanford, J. L.; Albertson, P. C.; Hamilton, A. S.; Hunt, W. C.; Potosky, A. L., Racial and ethnic differences in advanced-stage prostate cancer: the Prostate Cancer Outcomes Study. *J Natl Cancer Inst* **2001**, *93* (5), 388-95.

15. Jemal, A.; Murray, T.; Ward, E.; Samuels, A.; Tiwari, R. C.; Ghafoor, A.; Feuer, E. J.; Thun, M. J., Cancer statistics, 2005. *CA Cancer J Clin* **2005**, *55* (1), 10-30.

16. Venkateswaran, V.; Klotz, L. H., Diet and prostate cancer: mechanisms of action and implications for chemoprevention. *Nat Rev Urol* **2010**, *7* (8), 442-53.

17. Nelson, W. G.; De Marzo, A. M.; DeWeese, T. L.; Isaacs, W. B., The role of inflammation in the pathogenesis of prostate cancer. *J Urol* **2004**, *172* (5 Pt 2), S6-11; discussion S11-2.

18. De Marzo, A. M.; Marchi, V. L.; Epstein, J. I.; Nelson, W. G., Proliferative inflammatory atrophy of the prostate: implications for prostatic carcinogenesis. *Am J Pathol* **1999**, *155* (6), 1985-92.

19. De Marzo, A. M.; Meeker, A. K.; Zha, S.; Luo, J.; Nakayama, M.; Platz, E. A.; Isaacs, W. B.; Nelson, W. G., Human prostate cancer precursors and pathobiology. *Urology* **2003**, *62* (5 Suppl 1), 55-62.

20. Putzi, M. J.; De Marzo, A. M., Morphologic transitions between proliferative inflammatory atrophy and high-grade prostatic intraepithelial neoplasia. *Urology* **2000**, *56* (5), 828-32.

21. Valdman, A.; Jonmarker, S.; Ekman, P.; Egevad, L., Cytological features of prostatic intraepithelial neoplasia. *Diagn Cytopathol* **2006**, *34* (5), 317-22.
22. Hanahan, D.; Weinberg, R. A., The hallmarks of cancer. *Cell* **2000**, *100* (1), 57-70.
23. Folkman, J., Fundamental concepts of the angiogenic process. *Curr Mol Med* **2003**, *3* (7), 643-51.
24. Gottlieb, B.; Trifiro, M.; Lumbroso, R.; Vasiliou, D. M.; Pinsky, L., The androgen receptor gene mutations database. *Nucleic Acids Res* **1996**, *24* (1), 151-4.
25. Veldscholte, J.; Berrevoets, C. A.; Ris-Stalpers, C.; Kuiper, G. G.; Jenster, G.; Trapman, J.; Brinkmann, A. O.; Mulder, E., The androgen receptor in LNCaP cells contains a mutation in the ligand binding domain which affects steroid binding characteristics and response to antiandrogens. *J Steroid Biochem Mol Biol* **1992**, *41* (3-8), 665-9.
26. Culig, Z.; Hoffmann, J.; Erdel, M.; Eder, I. E.; Hobisch, A.; Hittmair, A.; Bartsch, G.; Utermann, G.; Schneider, M. R.; Parczyk, K.; Klocker, H., Switch from antagonist to agonist of the androgen receptor blocker bicalutamide is associated with prostate tumour progression in a new model system. *British Journal of Cancer* **1999**, *81* (2), 242-251.
27. Hara, T.; Miyazaki, J.; Araki, H.; Yamaoka, M.; Kanzaki, N.; Kusaka, M.; Miyamoto, M., Novel mutations of androgen receptor: a possible mechanism of bicalutamide withdrawal syndrome. *Cancer Res* **2003**, *63* (1), 149-53.
28. Chen, C. D.; Welsbie, D. S.; Tran, C.; Baek, S. H.; Chen, R.; Vessella, R.; Rosenfeld, M. G.; Sawyers, C. L., Molecular determinants of resistance to antiandrogen therapy. *Nature Medicine* **2004**, *10* (1), 33-39.
29. Isaacs, J. T.; Isaacs, W. B., Androgen receptor outwits prostate cancer drugs. *Nature Medicine* **2004**, *10* (1), 26-27.
30. Kirby, R. S., Recent advances in the medical management of prostate cancer. *British Journal of Clinical Practice* **1996**, *50* (2), 88-93.
31. Labrie, F.; Dupont, A.; Belanger, A.; Cusan, L.; Lacourciere, Y.; Monfette, G.; Laberge, J. G.; Emond, J. P.; Fazekas, A. T. A.; Raynaud, J. P.; Husson, J. M., New hormonal-therapy in prostatic carcinoma-combined treatment with an LHRH

agonist and an anti-androgen. *Clinical and Investigative Medicine-Medecine Clinique Et Experimentale* **1982**, 5 (4), 267-275.

32. Diaz, M.; Patterson, S. G., Management of androgen-independent prostate cancer. *Cancer Control* **2004**, 11 (6), 364-73.

33. Gaillardmoguilewsky, M., Pharmacology of antiandrogens and value of combining androgen suppression with antiandrogen therapy. *Urology* **1991**, 37 (2), 5-12.

34. Tucker, H.; Crook, J. W.; Chesterson, G. J., Nonsteroidal antiandrogens-Synthesis and Structure Activity Relationships of 3-substitued derivatives of 2-hydroxypropionanilides. *Journal of Medicinal Chemistry* **1988**, 31 (5), 954-959.

35. Gao, W.; Dalton, J. T., Expanding the therapeutic use of androgens via selective androgen receptor modulators (SARMs). *Drug Discovery Today* **2007**, 12 (5-6), 241-248.

36. Scher, H. I.; Kolvenbag, G., The antiandrogen withdrawal syndrome in relapsed prostate cancer. *European Urology* **1997**, 31, 3-7.

37. Matias, P. M.; Donner, P.; Coelho, R.; Thomaz, M.; Peixoto, C.; Macedo, S.; Otto, N.; Joschko, S.; Scholz, P.; Wegg, A.; Bäsler, S.; Schäfer, M.; Egner, U.; Carrondo, M. A., Structural evidence for ligand specificity in the binding domain of the human androgen receptor. Implications for pathogenic gene mutations. *J Biol Chem* **2000**, 275 (34), 26164-71.

38. Sack, J. S.; Kish, K. F.; Wang, C.; Attar, R. M.; Kiefer, S. E.; An, Y.; Wu, G. Y.; Scheffler, J. E.; Salvati, M. E.; Krystek, S. R.; Weinmann, R.; Einspahr, H. M., Crystallographic structures of the ligand-binding domains of the androgen receptor and its T877A mutant complexed with the natural agonist dihydrotestosterone. *Proc Natl Acad Sci U S A* **2001**, 98 (9), 4904-9.

39. Hur, E.; Pfaff, S. J.; Payne, E. S.; Grøn, H.; Buehrer, B. M.; Fletterick, R. J., Recognition and accommodation at the androgen receptor coactivator binding interface. *PLoS Biol* **2004**, 2 (9), E274.

40. Estébanez-Perpiñá, E.; Moore, J. M.; Mar, E.; Delgado-Rodrigues, E.; Nguyen, P.; Baxter, J. D.; Buehrer, B. M.; Webb, P.; Fletterick, R. J.; Guy, R. K., The molecular mechanisms of coactivator utilization in ligand-dependent transactivation by the androgen receptor. *J Biol Chem* **2005**, 280 (9), 8060-8.

41. Ostrowski, J.; Kuhns, J. E.; Lupisella, J. A.; Manfredi, M. C.; Beehler, B. C.; Krystek, S. R.; Bi, Y.; Sun, C.; Seethala, R.; Golla, R.; Sleph, P. G.; Fura, A.; An, Y.; Kish, K. F.; Sack, J. S.; Mookhtiar, K. A.; Grover, G. J.; Hamann, L. G., Pharmacological and x-ray structural characterization of a novel selective androgen receptor modulator: potent hyperanabolic stimulation of skeletal muscle with hypostimulation of prostate in rats. *Endocrinology* **2007**, *148* (1), 4-12.
42. Osguthorpe, D. J.; Hagler, A. T., Mechanism of androgen receptor antagonism by bicalutamide in the treatment of prostate cancer. *Biochemistry* **2011**, *50* (19), 4105-13.
43. McGinley, P. L.; Koh, J. T., Circumventing anti-androgen resistance by molecular design. *J Am Chem Soc* **2007**, *129* (13), 3822-3.
44. Bohl, C. E.; Gao, W.; Miller, D. D.; Bell, C. E.; Dalton, J. T., Structural basis for antagonism and resistance of bicalutamide in prostate cancer. *Proc Natl Acad Sci USA* **2005**, *102* (17), 6201-6.
45. Tran, C.; Ouk, S.; Clegg, N. J.; Chen, Y.; Watson, P. A.; Arora, V.; Wongvipat, J.; Smith-Jones, P. M.; Yoo, D.; Kwon, A.; Wasielewska, T.; Welsbie, D.; Chen, C. D.; Higano, C. S.; Beer, T. M.; Hung, D. T.; Scher, H. I.; Jung, M. E.; Sawyers, C. L., Development of a second-generation antiandrogen for treatment of advanced prostate cancer. *Science* **2009**, *324* (5928), 787-90.
46. Jung, M. E.; Ouk, S.; Yoo, D.; Sawyers, C. L.; Chen, C.; Tran, C.; Wongvipat, J., Structure-activity relationship for thiohydantoin androgen receptor antagonists for castration-resistant prostate cancer (CRPC). *J Med Chem* **2010**, *53* (7), 2779-96.
47. Scher, H. I.; Beer, T. M.; Higano, C. S.; Anand, A.; Taplin, M. E.; Efstathiou, E.; Rathkopf, D.; Shelkey, J.; Yu, E. Y.; Alumkal, J.; Hung, D.; Hirmand, M.; Seely, L.; Morris, M. J.; Danila, D. C.; Humm, J.; Larson, S.; Fleisher, M.; Sawyers, C. L.; Consortium, P. C. F. D. o. D. P. C. C. T., Antitumour activity of MDV3100 in castration-resistant prostate cancer: a phase 1-2 study. *Lancet* **2010**, *375* (9724), 1437-46.
48. Mohler, M. L.; Bohl, C. E.; Jones, A.; Coss, C. C.; Narayanan, R.; He, Y.; Hwang, D. J.; Dalton, J. T.; Miller, D. D., Nonsteroidal selective androgen receptor

modulators (SARMs): dissociating the anabolic and androgenic activities of the androgen receptor for therapeutic benefit. *J Med Chem* **2009**, *52* (12), 3597-617.

49. Miller, C. P.; Shomali, M.; Lyttle, C. R.; O'Dea, L. S. L.; Herendeen, H.; Gallacher, K.; Paquin, D.; Compton, D. R.; Sahoo, B.; Kerrigan, S. A.; Burge, M. S.; Nickels, M.; Green, J. L.; Katzenellenbogen, J. A.; Tchesnokov, A.; Hattersley, G., Design, Synthesis, and Preclinical Characterization of the Selective Androgen Receptor Modulator (SARM) RAD140. *ACS Medicinal Chemistry Letters* **2011**, *2* (2), 124-129.